RE(I) TRI-CARBONYL BASED RADIOPHARMACEUTICALS; SYNTHESIS, IN VITRO STUDIES, AND PROTEIN COMPLEXATION

A Dissertation

Presented to

The Graduate Faculty of The University of Akron

In Partial Fulfillment

Of the Requirements for the Degree

Doctor of Philosophy

Sarah L. Binkley

August ,2016

RE(I) TRI-CARBONYL BASED RADIOPHARMACEUTICALS; SYNTHESIS, IN VITRO STUDIES, AND PROTEIN COMPLEXATION

Sarah L. Binkley

Dissertation

Approved:

_____
Advisor
Christopher J. Ziegler, Ph.D.

_____
Committee Member
Thomas C. Leeper, Ph.D.

_____
Committee Member
Sailaja Paruchuri, Ph.D.

_____
Committee Member
Leah Shriver, Ph.D.

_____
Committee Member
Todd Blackledge, Ph.D.

Accepted:

_____
Department Chair
Kim C. Calvo, Ph.D.

_____
Dean of the College
John Green, Ph.D.

_____
Dean of the Graduate School
Chand K. Midha, Ph.D

_____
Date

ABSTRACT

^{99m}Tc is the most used radionuclide in diagnostic nuclear medicine. Technetium small molecule imaging agents are being used to image almost every tissue in the body, from heart and bones, to the difficult imaging of brain tissue. Though there are many ^{99m}Tc complexes currently in use, the search for an ideal technetium radiopharmaceutical is ongoing. Ideal imaging agents must be robust enough to withstand complex biological conditions and ensure clearance from the body, yet selective enough to reach their target tissues for successful scanning. Recent work has shown that compounds based on the *fac*-^{99m}Tc(I)$(CO)_3^+$ core exhibit increased stability and resistance to decomposition. The chemistry and pharmacokinetics of these complexes can be safely explored using the non-radioactive, isoelectronic Re(I)$(CO)_3^+$ species. Medically useful isotopes of rhenium, ^{188}Re and ^{186}Re, add to the potential applications of this chemistry.

In this dissertation we describe the synthesis and metathesis of $[Re(CO)_3(TAME)]X$ (where X= Br^-, Cl^-, NO_3^-, ClO_4^-, and PF_6^-), and it's toxicity in both primary and secondary cell culture lines. The toxicity of the parent molecule, $[Re(CO)_3(OH_2)_3]Br$, in HeLa-S3 cell culture is explored. The preparation and characterization of a $Re(CO)_3^+$-lysozyme adduct is discussed. Additional studies of the efficacy of $[Re(CO)_3(OH_2)_3]Br$ and as an X-ray contrast agent and the preparation and partial characterization of an $Re(CO)_3^+$-insulin adduct is also described herein.

DEDICATION

To my mom and my brother; because they would be so proud of me if they were here today.

To my husband, David, my siblings, parents, grandparents, and all my family who have helped me, supported me, prodded me, and loved me; to the people who are proud of me every day.

To Declan and Josie May, who don't yet understand; so that they might be proud of me someday.

ACKNOWLEDGEMENTS

This work would not have been possible without the help of a great many people. The first person to thank has to be my advisor, Christopher Ziegler, who took a risk (or possibly assumed a pedagogical responsibility) in accepting me into his research group as a non-traditional student. I truly enjoyed learning from you and working with you. Your leadership was the only reason I got to this point and I greatly appreciate all the guidance, assistance, and consideration you have given me. When people ask me what my research advisor was like, I tell them about the zeal and enthusiasm you have for science. The same zeal that told me about my first publication being accepted in the receiving line at my wedding. I strive to emulate your enthusiasm and to impart it to the students that I teach. Thank you for all your support.

I would also like to thank Amy Milsted, now retired, for her amazing support throughout my research. Whenever I had a question, you were there and you made me feel welcome in your lab and your life. Your warmth helped me through the experiments when nothing seemed to go right and your guidance was invaluable in the creation of this work. I strive to emulate your leadership style in my interaction with the students that I teach and mentor. Thank you for all your support.

I would like to thank our collaborators, Rick Herrick, Roger Rowlett, and Thomas Leeper for all of their support, expertise, and assistance. I want to thank all the UA

chemistry department, faculty and staff, for all the support and services they offer stressed out graduate students- whether that be training on an instrument or a willing ear. You are all a blessing to all of the students that you serve and I hope to emulate your dedication in my professional life.

I would like to thank my committee members, Dr. Thomas Leeper, Dr. Sailaja Paruchuri, Dr. Leah Shriver, Ph.D., and Dr. Todd Blackledge. Thank you for giving of your valuable time to be on my committee. I would like to thank my former group members: Natalie Weingart, Dr. Saovalak Sripothongnak, Dr. Roshinee Costa, James Engle, Dr. Ingrid-Suzy Tamgho, Chris Belock, Hira Qayyum, Goran Martic, Tien-Hao Chen, Francesca DiSanto, and all the other Ziegler group students for creating such an enjoyable work environment and for all your support.

The biggest thank you has to go to my family, especially my husband, David Binkley. Graduate school was where we met and there is no better person in the world to have been on this journey with. You have run with me, walked with me, supported my stumbles, sat with me when I fell, picked me up, brushed me off, and helped me to walk again over and over. Neither of us could have anticipated the crazy route we arrived by, but it was because of you that we got here. You simultaneously managed to be a great husband, a best friend, and a great dad. Thank you. I love you. I thank my children, Josie May and Declan, for the inspiration to try to complete my degree. I want you to live your lives with strength of conviction, humility, courage, and perseverance. This is just one of the personal battles I will take on to live an example for you. I love you both.

This work would not have been possible without the blessings of my extended family. I thank my father for inspiring me to love science, while teaching me how to love

and lead my family (along with my mom and Chris). You were my best and most rigorous science teacher, you were the one that taught me that science is fun, interesting, and a worthwhile life goal, along with teaching me about experimental design and the genus name for butterflies. Thank you to all my siblings for your support and love. In addition to that: Julie- thank you for proofreading a document that had to be a very boring read. Katie, thank you for always being there to listen to me vent. Libby, thank you for the Starbucks, prayers, and musical inspiration. Sarah Liz and Carolyn, thank you for being such amazing academic achievers; your example inspires me every day. Ricky, thank you for letting me mother you and letting me tell you about the science I find interesting without telling me that it's really not. Rachel, I cannot thank you enough for the care you have given both my special babies; it gave me the peace of mind I needed to go work to support them. A special thank you to my grandparents, especially Denny and Jo Clunk, for their encouragement, love, and financial support (and cookies) given freely throughout my life and graduate school experience.

Last, but by no means least, I thank my brother, John, in heaven, for teaching me so much about what is important in life, even in your death. I thank my mother, in heaven, who would not have understood one word of this work, but who would have been so proud of the effort; I thank you for teaching me so much about how to be a good student, teacher, and most importantly, mother. I know this is the way you taught me to live and I hope I am making you proud. It's through you that I know God's unconditional love and it's through His love that I am still standing today. I thank God for watching over my family in heaven, my family on earth, and for all of His continued blessings in my life.

TABLE OF CONTENTS

Page

LIST OF TABLES

LIST OF FIGURES

LIST OF SCHEMES

LIST OF ABBREVIATIONS

1D – one dimensional

2D – two dimensional

α-MSH - α-melanocyte stimulating hormone

BBN – bombesin

BFCA - bi-functional chelating agent

CECT- contrast enhanced computed tomography

Cisplatin - *cis*-diamminedichloroplatinum(II)

CO – carbonyl

CORM – carbon monoxide releasing molecule

DMEM - Dulbecco's modified eagle medium

DMSA - dimercaptocsuccinic acid

DNA – deoxyribonucleic acid

Dpr – diaminopropionic

DTMA - 2-(N,N'-bis(tertbutoxycarbonyl)diethylenetri-amine acetic acid

DTPA – diethylenetriaminepentaacetate

ESI-TOF – electrospray ionization time of flight

FBS – fetal bovine serum

FDA – Food and drug administration

FT- Fourier transform

GABA – gamma aminobutyric acid

GRPR - gastrin-releasing peptide receptor

H_2xbsms - 1,2-bis(4-mercapto-3,3-dimethyl-2-thiabutyl)benzene)

HEDP – hydroxyethylidenediphosphonate

HEPES - 4-(2-hydroxyethyl)-1-piperazineethanesulfonic acid

HEWL – hen egg white lysozyme

HH – head to head

HOMO - highest occupied molecular orbital

HSQC – heteronuclear single quantum coherence spectroscopy

HT – head to tail

ICP-OES – inductively coupled plasma optical emission spectroscopy

im - imidazole

IR – infrared

L - ligand

LD_{50} – lethal dose for 50% of population

LUMO - lowest unoccupied molecular orbital

M – metal

MAG_3 - mercaptoacetylglycylglycyl-glycine

MALDI-TOF – Matrix-assisted laser desorption/ionization time of flight

MES - 2-(N-morpholino)ethanesulfonic acid

MDR – Multidrug resistance

MO – molecular orbital

MS – mass spectrometry

MTT - (3-(4, 5-dimethylthiazolyl-2)-2, 5-diphenyltetrazolium bromide)

NIH – National Institute of Health

NMR – nuclear magnetic resonance

P – Partition coefficient

pa – pyridine-2-carboxylic acid

PADA-AVA - 2-picolylamine-N,N-diacetic acid and an aminovaleric acid spacer

PBS – phosphate buffer solution

PDB – Protein Data Bank

PEG - Poly(ethyleneglycol)

PET - Positron emission tomography

RTC – rhenium (I) tri-carbonyl

SAAC - single amino acid chelate

SHR – Spontaneously hypertensive rats

SPECT - Single photon emission computed tomography

TAME - 1,1,1-tris(aminomethyl)ethane

TFCA - tri-functional chelating agent

CHAPTER I

INTRODUCTION AND BACKGROUND

1.1 The role of radiopharmaceuticals in nuclear medicine

Cancer is the second leading cause of death in the United States, and this disease accounted for 7.6 million deaths in 2008, according to the World Health Organization.[1] Early detection is essential for the successful treatment of cancer and many other diseases.[2] The importance of early detection has led to the development of multiple imaging techniques, each with its own benefits and limitations. Single photon emission computed tomography (SPECT)[3] and positron emission tomography (PET)[3] imaging techniques offer the advantages of non-invasive, whole body imaging.

These well-established, clinical imaging tools rely on the administration of a radiopharmaceutical containing a gamma (γ) or positron (β^+) emitting isotope. In the case of SPECT imaging, γ emission is collected by a gamma camera, allowing reconstruction of the emission source in the patient.[4] In β^+ emission, the β^+ particle emitted from an isotope collides with an electron, producing two 511 keV γ photons that travel in opposite directions from each other and are detected by a circular array of gamma cameras. The source of the decay is computed by following the line of coincidence of the two photons and mathematically reconstructed into a PET image.[5] Because two γ photons are emitted for each β^+ decay, PET offers higher image resolution compared to SPECT images.[5] Traditional SPECT and PET scanners were only able to image with millimeter resolution.

However, with improved technologies, such as disease/organ specific cameras and targeted radionuclides, resolution using these techniques is approaching the molecular level.[6] SPECT is used more often in the clinic because of the comparatively low cost of γ emission isotopes. The isotope source often dictates the type of imaging technique used as well; clinics not within range of a nuclear reactor or cyclotron source are limited to nuclides that can be produced in on site generators.[7, 8]

As a necessary part of the evolution of imaging agents, the development and improvement of radiopharmaceuticals is an active area of research.[7, 9-13] Radiopharmaceuticals can be divided into two classes: diagnostic and therapeutic. Diagnostic radiopharmaceuticals use low energy γ or β^+ emitting isotopes and are administered in low concentrations as they should not have any pharmacological effects. Diagnosis and interpretation of a disease state can be facilitated by studying the accumulation of the radiopharmaceutical in the tissue or organ of interest. Therapeutic radiopharmaceuticals use isotopes that are Auger electron, α particle, or β^- particle emitters to deliver ionizing radiation via external beam irradiation, brachytherapy, or systemic administration.[4] Accumulation of therapeutic radiopharmaceuticals at a disease site results in a cascade of events, including the modification of cellular DNA caused by the ionizing radiation, which results in apoptotic cell death.[14] A list of medically relevant isotopes and their properties is given in Table 1.1 below.

Table 1.1 : Physical properties of relevant radionuclides for clinical applications.[4, 9]

Isotope	Half-life	Mode of Decay (%)	Production Method	Application
^{11}C	20.3 min	β^+	$^{14}N(p,a)-^{11}C$/ cyclotron	PET
^{18}F	109.8 min	β^+ (97), EC (3)	$^{18}O(p,n)-^{18}F$/ cyclotron	PET
^{61}Cu	3.3 h	β^+ (62), EC (38)	$^{59}Co(a, 2n)-^{61}Cu$/ nuclear reactor	PET
^{62}Cu	0.16 h	β^+ (98), EC (2)	$^{62}Zn/^{62}Cu$ generator	PET
^{64}Cu	12.7 h	β^- (40), β^+ (19), EC (41)	$^{64}Ni(p.n)-^{64}Cu$/ cyclotron	PET/Therapy
^{67}Cu	61.8 h	β^- (100)		Therapy
^{67}Ga	3.26 d	EC (100)	$^{68}Zn(p,2n)-^{67}Ga$/ cyclotron	SPECT
^{68}Ga	67.8 min	EC (100)	$^{68}Ge/^{68}Ga$ generator	SPECT
^{86}Y	14.7 h	β^+ (33), EC (66)	$^{86}Sr(p,n)-^{86}Y$/ cyclotron	PET
^{90}Y	64.1 h	β^- (100)	$^{90}Sr/^{90}Y$ generator	Therapy
^{89}Zr	78.5 h	β^+ (22.7), EC (77)	$^{89}Y(p,n)-^{89}Zr$/ cyclotron	PET
^{94m}Tc	52 min	β^+ (72%)	$^{94}Mo(p,n)-^{94m}Tc$/ nuclear reactor	PET
^{99m}Tc	6 h	IT (100)	$^{99}Mo/^{99}mTc$ generator	SPECT
^{111}In	67.4 h	EC (100)	$^{111}Cd(p,n)-^{111m,g}In$ cyclotron	SPECT
^{123}I	13.2 h	EC (100)		SPECT
^{131}I	8.02 d	β^- (100)		Therapy
^{153}Sm	46.3 d	β^- (100)	$^{152}Sm(n,\gamma)-^{153}Sm$/ nuclear reactor	Therapy
^{166}Ho	26.8 d	β^- (100)	$^{165}Ho(n, c)-^{166}Ho$/ nuclear reactor	Therapy
^{177}Lu	6.73 d	β^- (100)	$^{176}Lu(n,\gamma)-^{177}Lu$/ nuclear reactor	Therapy
^{186}Re	89.2 h	β^- (92), EC (8)	$^{185}Re(n,\gamma)-^{186}Re$/ nuclear reactor	Therapy
^{188}Re	17 h	β^- (100)	$^{188}W/^{188}Re$ generator	Therapy

Diagnostic and therapeutic radiopharmaceuticals can further be divided into two categories: metal essential and target specific.[10] The biodistribution of metal essential radiopharmaceuticals depends on the charge of the metal, the size of the metal complex, and the lipophilicity of the metal chelator for distribution in the body. Lipophilicity is traditionally predicted by the partition coefficient (P) by measuring the ratio of a radiopharmaceutical that dissolves in 1-octantol versus water.[15] The solvent 1-octanol is used to mimic the phospholipid bilayer of a cell. Drugs with a positive P value are more lipophilic, however, as P becomes large, the drug becomes so lipophilic that it will remain trapped in the lipid bilayer. For example, the log P value for many drugs that are able to cross the blood-brain barrier is 2, suggesting that drugs that act on the brain with different log P values, do so via other mechanisms.[16] Adjusting the log P value of a radiopharmaceutical is one way to optimize the elimination route for that radiopharmaceutical.[17] The ability to adjust the log P values of a specific radiopharmaceutical is necessary to allow researchers to optimize the pharmacokinetic profile of the drug.[2, 17]

Many radiopharmaceuticals are of the metal-essential type and include such well known entities as ^{99m}Tc-sestamibi[18, 19] for myocardial perfusion imaging and ^{99m}Tc-Bicisate[20] for cerebral perfusion imaging.[4] These metal essential radiopharmaceuticals are desired for imaging large areas and high capacity systems, such as the vascularization of the heart and associated vessels or the vasculature of the brain as is the case with ^{99m}Tc-sestamibi[3] and ^{99m}Tc-Bicisate[20], respectively. These molecules are shown in Figure 1.1a and 1.1b. Examples of other high capacity systems suitable for imaging by metal essential ^{99m}Tc imaging agents are phagocytosis, hepatocyte clearance, glomerular function, and

multidrug resistance (MDR) imaging, among others.[2] Current research in the area of metal essential imaging agents focuses on the development of next-generation versions of radiopharmaceuticals to image these systems.[21, 22] For example, a next-generation version of ^{99m}Tc-Sestamibi would have better myocardial uptake and faster clearance from the liver and lungs. Because metal essential agents are used to image a wide variety of systems and disease states, their development is still an active area of research.

Target specific radiopharmaceuticals use a targeting moiety to concentrate at the site of a disease.[6] These targeting moieties can bind to receptors, antibodies, or other cellular structures within the tissue of interest.[9] The drug ^{111}In-DTPA-octreotide (OctreoScan®), shown in Figure 1.1c, uses a chelating moiety, DTPA (diethylenetriaminepentaacetate), to chelate the ^{111}In isotope and connect the metal to the small peptide octreotide, which is an analog of the human hormone, somatostatin. This allows the ^{111}In isotope to localize at the site of neuroendocrine tumors that over-express the somatostatin receptor.[23] These target specific radiopharmaceuticals are desired when the goal is imaging a small area that is difficult to access by traditional methods or delivering therapeutic radiation to a specific disease site while limiting radiation exposure to healthy tissue. Much of the recent research in the literature has focused on the development of target specific radiopharmaceuticals. However this research has resulted in comparatively few clinically available target specific radiopharmaceuticals, which some reviewers attribute to the high cost of radiopharmaceutical development and clinical trials and the smaller patient populations served by some target specific radiopharmaceuticals.[22]

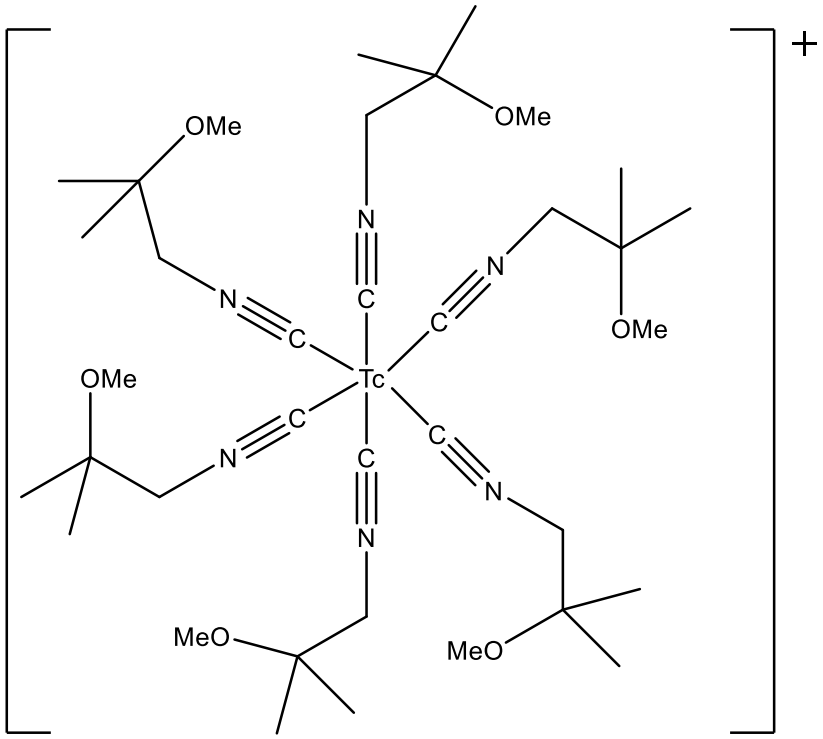

(a)

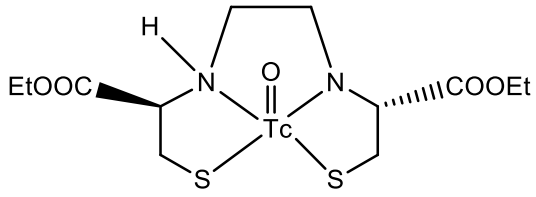

(b)

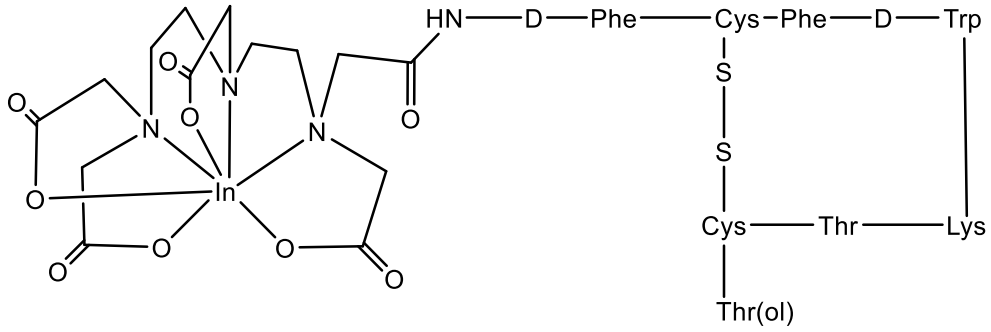

(c)

Figure 1.1: Examples of metal essential radiopharmaceuticals: (a) ^{99m}Tc-sestamibi (Cardiolite®), (b) ^{99m}Tc-bicisate (Neurolite®) and target specific radiopharmaceuticals: (c) ^{111}In-DTPA-octreotide (OctreoScan®).[18-20, 23]

Drugs incorporating radionuclides have specific requirements.[3] For diagnostic purposes, the radiopharmaceuticals should incorporate isotopes that emit radiation in the range suitable for detection by SPECT or PET. Diagnostic radiopharmaceuticals should possess a long enough half-life to reach their target tissue and accomplish the imaging modality but short enough to limit radiation exposure to the patient.[3, 24] The isotope should decay into a stable, daughter nucleus to limit radiation exposure while the radiopharmaceutical is eliminated from the patient.[17] Additionally, the drug should be non-toxic at the concentrations required for imaging purposes (10^{-8} M to 10^{-6} M).[25] The low concentration is also a consideration in the synthesis of target specific diagnostic radiopharmaceuticals as excess biomolecule used in synthesis could flood the receptor *in vivo* and prevent high amounts of radiopharmaceutical binding.

Ideal therapeutic radiopharmaceuticals should incorporate isotopes with a high specific activity and with half-life constraints similar to those of ideal diagnostic radiopharmaceuticals.[22, 26] The half-life should be long enough for the radiopharmaceutical to be synthesized, administered to the patient, and reach its target to deliver a cytotoxic dose of radiation, but short enough to limit radiation exposure to healthy tissue.[26] Some requirements apply to ideal radiopharmaceuticals of both the diagnostic and therapeutic type. Commercial considerations dictate that the isotope used should be relatively inexpensive and easy to obtain. The radiopharmaceutical itself should be synthesized quickly in high yields, in low concentrations, under aqueous conditions, forming a single, stable product. The radiopharmaceutical synthesis should be simple and utilize synthetic pathway amenable to a "kit-chemistry" preparative method.[27] Radiopharmaceuticals of

both types should be stable and resistant to decomposition in the body, as metal binding to biomolecules can complicate the elimination of the drug.[22]

Radiopharmaceuticals based on the medically relevant isotopes of technetium have already proved to be excellent imaging agents, as can be seen by the number of commercially available radiopharmaceuticals that incorporate these nuclides as shown in Table 1.2.[4, 7, 22, 28] Radiopharmaceuticals based on the medically relevant isotopes of rhenium are not as prevalent, as just a single example of a metal-essential rhenium therapeutic agent, ^{188}Re-HEDP, has reached the clinic in Europe.[4, 29] However, the properties of these isotopes, along with new drug synthesis strategies, make the production of new radiopharmaceuticals based on these isotopes a prevalent topic in the literature. These isotopes have the potential to make ideal diagnostic and therapeutic radiopharmaceuticals, of both the metal-essential and target-specific types, and they will be the focus of this work.

Table 1.2 ^{99m}Tc and $^{188/186}$Re based radiopharmaceuticals.[4, 7, 22, 28, 29]

Radiopharmaceutical	Trade Name	Primary Use
^{99m}Tc-Sestamibi	Cardiolite®	Myocardial perfusion imaging, multidrug resistant (MDR) tumor imaging
	Miraluna®	Breast cancer imaging
^{99m}Tc-Tetrafosmin	Myoview®	Myocardial perfusion imaging, MDR tumor imaging
^{99m}Tc-Exametazine (HMPAO)	Ceretec®	Cerebral perfusion imaging
^{99m}Tc-Gluceptate	Glucoscan®	Renal Imaging
^{99m}Tc-Pentetate (DTPA)	Technescan®	Renal imaging and function studies
^{99m}Tc-Bicisate (ECD)	Neurolite®	Cerebral perfusion imaging
^{99m}Tc-Oxidronate (HDP)	Osteoscan® HDP	Bone imaging
^{99m}Tc-MDP	Medronate®	Skeletal scintigraphy
^{99m}Tc-Teboroxime	Cardiotec®	Myocardial perfusion imaging
^{99m}Tc-Depreotide	Neo Tect®	Evaluation of certain lung lesions (somatostatin receptor-bearing)
^{99m}Tc-Apcitide	AcuTect®	Synthetic peptide based probe for DVT imaging
^{99m}Tc-Arcitumumab	CEA-Scan®	Monoclonal antibody for colorectal cancer imaging
^{188}Re-HEDP	-	Treatment of metastatic bone pain (therapy)
^{99m}Tc-LeuTech	Leukoscan®	Infection imaging (appendicitis)
^{99m}Tc-Disofenin (DISIDA)	Hepatolite®	Hepatobiliary imaging
^{99m}Tc-Succimer (DMSA)	Tc-DMSA®	Renal cortical imaging and medullary thyroid cancer
^{99m}Tc-Albumin nanocolloids	Nanocoll®	Bone marrow imaging, inflammation scintigraphy and lymphoscintigraphy
^{99m}Tc-ciproflaxin	Infecton®	Infection imaging

1.2 ^{99m}Tc-based Radiopharmaceuticals

Element 43, technetium, was first observed in 1936 and a small amount of this element can be found in uranium and molybdenum ores.[19] More than 80% of the radiopharmaceuticals used in diagnostic nuclear medicine incorporate the ^{99m}Tc isotope.[30] In the United States, ^{99m}Tc based radiopharmaceuticals account for more than 15 million doses a year.[30] Technetium-99m radiopharmaceuticals are attractive because they can be produced on site with a ^{99}Mo-^{99m}Tc generator, first produced by Brookhaven National Labs in 1959.[31] A typical ^{99}Mo-^{99m}Tc generator is composed of $^{99}MoO_4^{2-}$ absorbed onto an alumina column. The half-life of ^{99}Mo, 66 hours, allows shipment to the clinical setting. In the clinic, $^{99m}TcO_4^-$ can then be eluted from the column with saline. The chloride in the saline displaces the monoanionic pertechnetate ions containing the ^{99m}Tc isotope and a small amount of the ^{99}Tc isotope from the column, leaving the dianionic molybdenate in place.[25] The decay scheme of ^{99}Mo can be seen below in Scheme 1.1.[22]

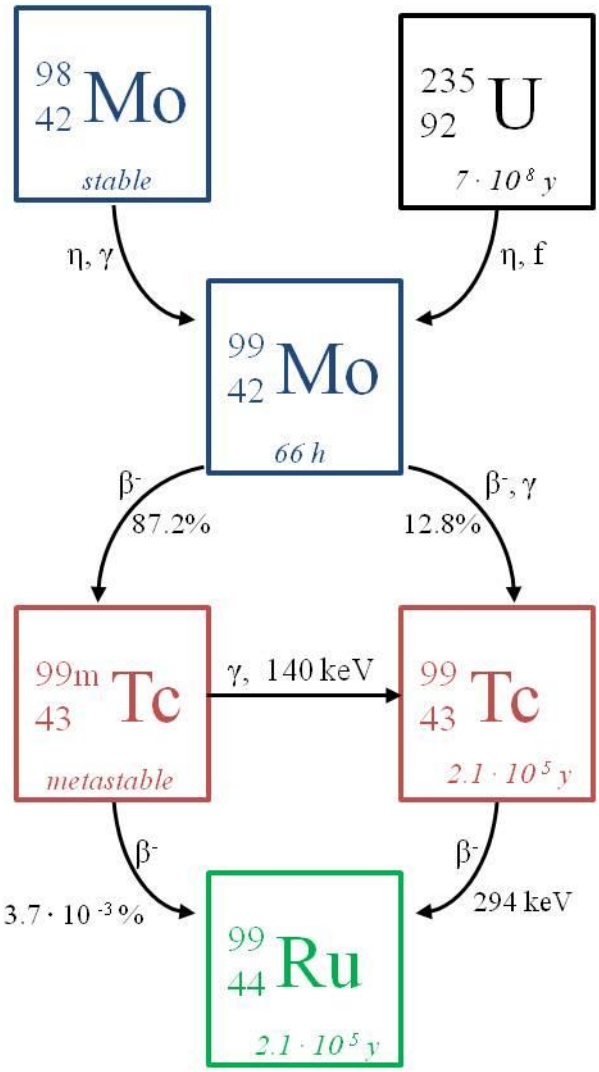

Scheme 1.1: Synthesis and decay pathways of ^{99}Mo.[22]

The 140.5 keV γ ray released by the decay of ^{99m}Tc to ^{99}Tc is too weak to cause cellular damage,[25] but strong enough to be easily detected by SPECT cameras.[32] SPECT, incorporating ^{99m}Tc based radiopharmaceuticals, has been used to image, assess and help diagnose a wide range of disease states. A partial list of those states is included in Table 1.2. In addition, the short half-life of the ^{99m}Tc, combined with the low concentration of imaging agent used, limits the radiation exposure for a patient to that of a single X-ray

radiograph.[25] Imaging agents containing ^{99m}Tc are designed to resist biological degradation and be cleared rapidly from the body.[22] Thus, the daughter nuclei, ^{99}Tc, which is a β^- emitter with a long half-life (2.14×10^5 years) does not add significantly to a patient's radiation exposure at low concentrations.[25] The six hour half-life of ^{99m}Tc allows for synthesis of the radiopharmaceutical from a kit. ^{99m}Tc-Sestamibi, which is among the most well-known of the ^{99m}Tc radiopharmaceuticals, can be produced from kits sold under the brand names Cardiolite™ (for cardiac perfusion imaging) or Miraluna™ (for breast tumor imaging), from $^{99m}TcO_4^-$ in approximately 30 minutes, with >90% yield.[11, 17]

While each kit can contain different final complexes, depending on the target tissue for the ^{99m}Tc, the +7 oxidation state of the pertechnetate ion requires that each kit contain a reducing agent to allow complexation. The most common reducing agent used is $SnCl_2$.[22] The reduced ^{99m}Tc can then be reacted with ligands to produce an imaging complex. This presents a challenge in producing a product with a high enough concentration of the desired radiopharmaceutical, since the ^{99m}Tc eluted from the generator is not carrier free; approximately 12.8% of the eluted pertechnetate will be of the ^{99}Tc instead of the desired ^{99m}Tc variety.[25] Additionally, the short half-life of ^{99m}Tc makes any type of chromatographic purification impossible.[25]

Researchers who design ^{99m}Tc based radiopharmaceuticals have traditionally developed the chemistry using ^{99}Tc, which can be purchased in milligram quantities.[18] An HPLC instrument with a γ detector can then be used to compare the retention times of imaging agents made with both isotopes.[18] With the kit-chemistry approach, and the variety of oxidation states/ coordination geometries available to technetium, many ^{99m}Tc cores have been developed. Several examples of these core structures are shown in Figure 1.2.[22]

Additional modification of a targeting moiety and a linking moiety allows these cores to be incorporated into target-specific radiopharmaceuticals, which will be discussed later in this chapter.

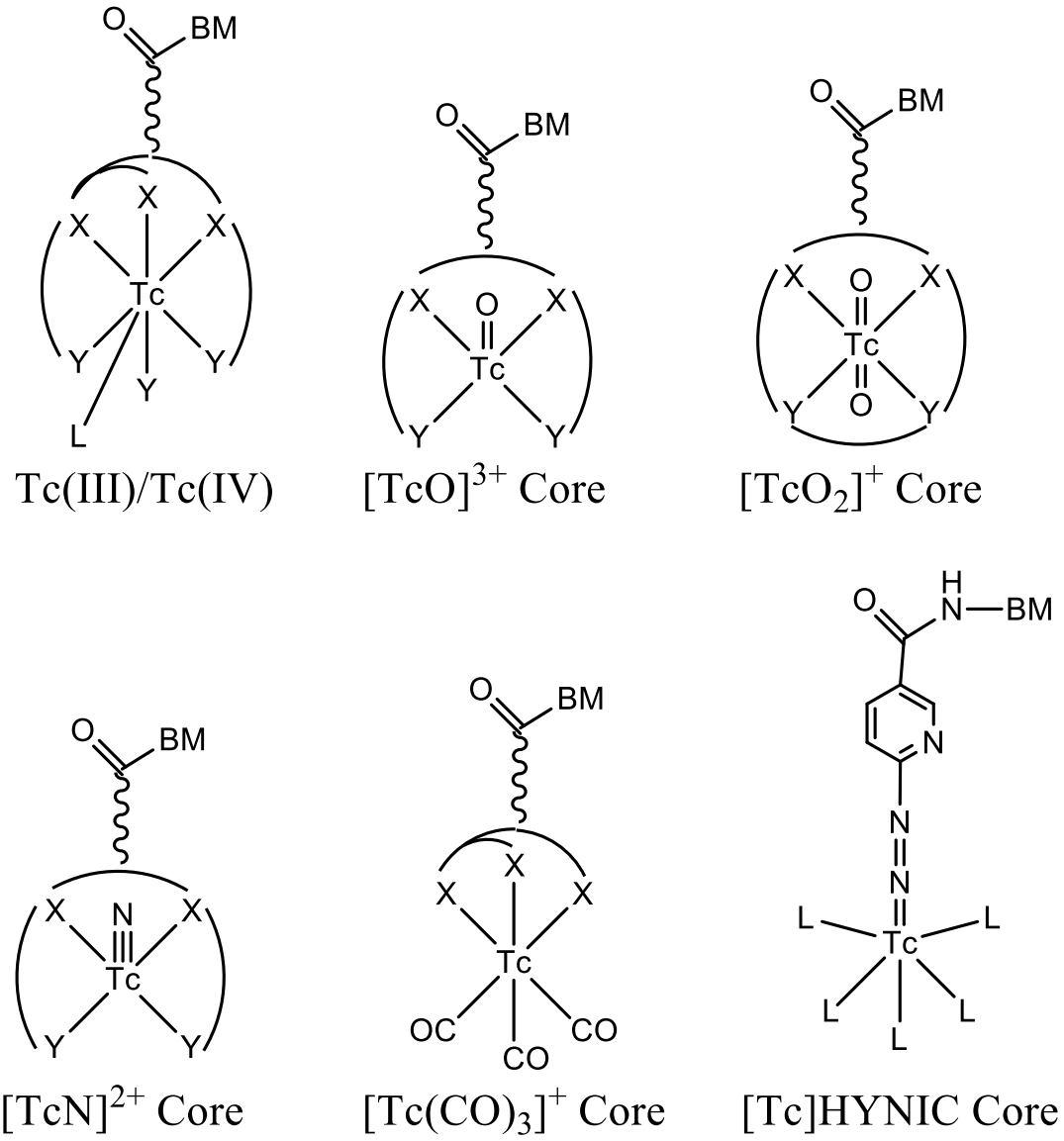

Figure 1.2: Examples of ^{99m}Tc cores available for radiopharmaceutical development.[22]

A lesser used, but medically relevant, isotope of technetium is ^{94m}Tc. This isotope has a half-life of 52 minutes and decays via a 2.47 MeV positron emission. It is produced in a cyclotron from a number of decay products, however the ^{94}Mo(p, n)/^{94m}Tc reaction is the reaction with the highest yield of ^{94m}Tc. Access to the pertechnetate form of ^{94m}Tc allows the use of the same kits used to make the more widely available ^{99m}Tc based radiopharmaceuticals. The positron emission of the ^{94m}Tc makes it a suitable isotope for use with PET. Since PET methods generally offer higher resolution, use of imaging agents containing both ^{94m}Tc and ^{99m}Tc isotopes gives researchers and clinicians with access to cyclotron produced nuclides the ability to combine the strengths of these two imaging techniques.[33]

1.3 $^{186/188}$Re radiopharmaceuticals

Rhenium was first isolated in 1925 and occurs naturally as a mixture of the non-radioactive isotopes ^{185}Re and ^{187}Re.[18] There are two isotopes of rhenium that are useful for incorporation into therapeutic radiopharmaceuticals.[25] ^{186}Re is a reactor-produced nuclide (^{185}Re(n,γ) ^{186}Re) with a half-life of 3.68 days. This isotope decays with a beta emission and a γ photon in the range for imaging by SPECT, which would allow monitoring of therapy.[9] However, because ^{186}Re is a reactor-produced nuclide, it is somewhat more expensive and less available for general use. Additionally, the natural abundances of the two isotopes of rhenium (^{185}Re 37.4% and ^{187}Re, 62.6%) ensure that reactor produced ^{186}Re will be contaminated with a significant amount of ^{188}Re. The shorter half-life of ^{188}Re allows it to be removed by decay but not without a corresponding loss of

^{186}Re activity.[34] Higher purity ^{186}Re can be achieved using isotopically enriched ^{185}Re instead of naturally occurring rhenium, however, this isotope is currently not available in a carrier-free form.[34] The emission range of ^{186}Re in tissue is 5 mm, making this nuclide useful for the treatment of smaller tumors.[18] The long half-life of this isotope makes it useful for incorporation into large biomolecules that are not rapidly cleared from the blood-stream.[34] Rhenium-188 has a shorter half-life of 17 hours with a β^- of 2.1 MeV and a γ emission of 155 keV. This isotope can be produced in a clinical setting from a ^{188}W/^{186}Re generator, which can last from 2 to 6 months and produce enough doses of $[^{188}ReO_4]^-$ to make >100 therapeutic radiopharmaceutical doses. The generator makes this nuclide relatively inexpensive and widely available. The generator produced ^{188}Re is carrier free with a high specific activity and has a range in tissue of 11 mm.[18] The chemistry of rhenium is similar to technetium, however, rhenium complexes are more chemically inert, and thus harder to reduce, than their technetium counterparts.[18] A similar variety of oxidation states of rhenium are available, from +7 to -1.[34] The ^{186}Re or ^{188}Re is supplied directly to the clinical setting or produced from the ^{188}W generator, respectively, as perrhenate which is then reduced with stannous chloride and reacted with a ligand system to produce the therapeutic radiopharmaceutical.[25]

The therapeutic β^- emission of ^{186}Re and ^{188}Re, along with their gamma emission in the range detectable by SPECT have allowed these isotopes to be incorporated into a wide variety of both metal essential and target specific radiopharmaceuticals, some of which are pictured in Figure 1.3. Reaction of the reduced perrhenate with 1-hydroxyethylidenediphosphonate (HEDP) ligand, shown below in Figure 1.3a, produces a complex that will localize in areas of bone damage caused by metastatic bone cancer.[35]

Either ^{186}Re or ^{188}Re can be used in this complex, which is employed primarily to provide bone pain relief often in conjunction with other chemotherapeutics.[18, 25] The structure of the active complex has not been elucidated and is thought to be a mixture of polymers.[36] Rhenium-188 is currently being studied for the treatment of medullary thyroid carcinoma as the radiopharmaceutical ^{188}Re-dimercaptocsuccinic acid (DMSA).[37] Instead of only being able to image the cancer using SPECT, this rhenium analog of ^{99m}Tc(V)DMSA, shown below in Figure 1.3b, is taken up by the tumor cells, then disrupts the uncontrolled mitosis with βemission. Target specific examples of rhenium radiopharmaceuticals are also in development.[18, 25] One example of these target specific radiopharmaceuticals are the Re labeled peptide analogs of the α-melanocyte stimulating hormone (α-MSH) being developed by Correia and co-workers.[9] Rhenium coordinates to the sulfydryls and amide nitrogens of the cysteine residues of an α-MSH analog, which then binds to melanocortin receptors which are overexpressed on human melanoma cells. One of these complexes, Re-[Cys^{3,4,10},$_{D}$Phe^{7}]-α-MSH, is shown in Figure 1.3 (C) below.[9] A ^{188}Re complex incorporating a α-MSH with high receptor affinity would allow simultaneous imaging and treatment of melanoma tumors.[9] Non-radioactive rhenium isotopes are also used to model the chemistry of ^{99m}Tc and $^{186/188}$Re in the laboratory setting as will be discussed elsewhere in this work.[38]

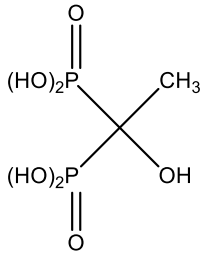

A

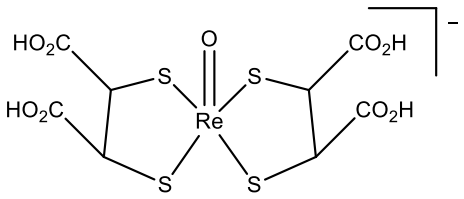

B

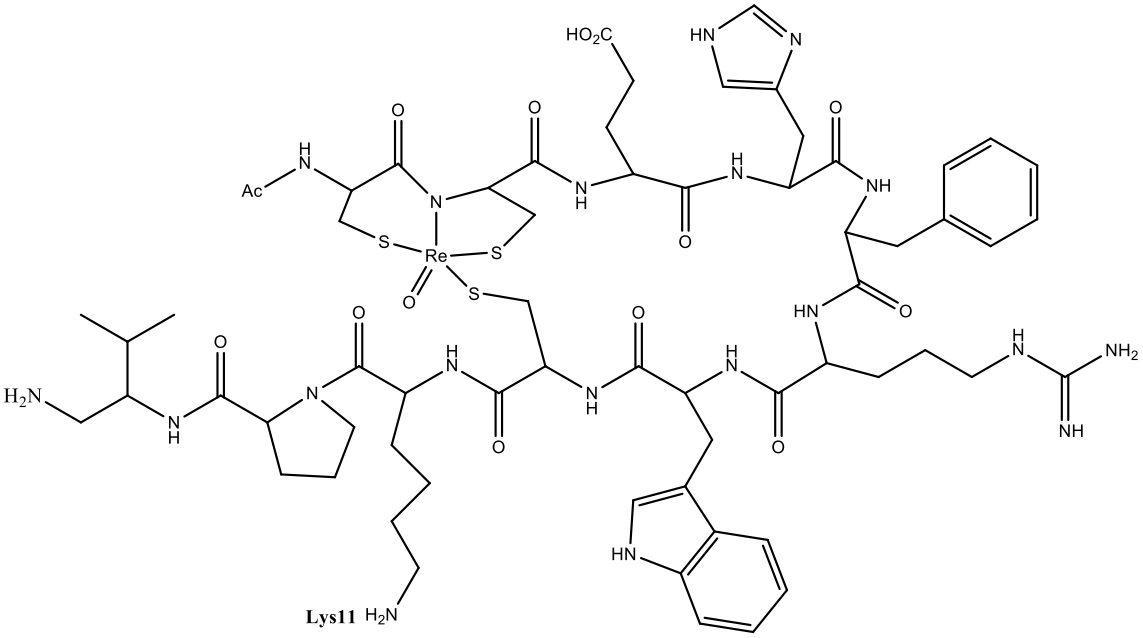

C

Figure 1.3: Rhenium based radiopharmaceuticals. (A) the HEDP ligand used to make the $^{186/188}$Re[HEDP] complexes used to alleviate metastatic bone pain,[36] (B) Re(V)DMSA for the treatment of medullary thyroid carcinoma,[37] and (C) Re-[Cys^{3,4,10},$_{D}$Phe^{7}]-α-MSH for melanoma therapy.[9]

1.4 Targeted radiopharmaceutical development; Several distinct approaches

Since over 80% of radiopharmaceutical injections in the US utilize ^{99m}Tc, and approximately half of those are perfusion scans, the popularity of metal essential radiopharmaceuticals like the ^{99m}Tc-sestamibi (Cardiolite) complex, among other complexes listed in Table 1.2, is obvious.[17] However, metal essential radiopharmaceuticals are not without drawbacks. Background uptake of a perfusion agent can limit resolution of the tissue/organ of interest. For example, ^{99m}Tc-sestamibi has an ideal imaging window of 1-2 hours after injection. Before the one hour point, cardiac imaging is impaired by uptake in the lung and ribs and, after the two hour point, imaging suffers from washout due to the high concentration of the drug in the liver and kidney during breakdown of the radiopharmaceutical.[3] Because of these drawbacks, attention in recent years has turned towards the development of target specific radiopharmaceuticals. Table 1.2 contains three examples of FDA approved, target specific, and ^{99m}Tc based radiopharmaceuticals sold under the respective names AcuTect®, CEA-Scan®, and Neotect®, currently in clinical use.[39-41] These imaging agents use peptides to selectively reach their target tissue

Throughout the literature, several approaches appear that can be applied to radiopharmaceutical development in general and development of targeted ^{188}Re/^{99m}Tc based radiopharmaceuticals specifically. The first approach is to use a bi-functional chelating agent (BFCA) to tightly chelate the metal and to attach it covalently to a biomolecule of interest. The BFCA approach can be seen in Figure 1.4.[22] A number of considerations are necessary when developing a target specific radiopharmaceutical via the BFCA approach. Development starts with a clinical need for a specific type of

radiopharmaceutical to image or treat a specific disease/disease state. Next, researchers must select a receptor system and a peptide receptor ligand for that disease/disease state. After the identification and synthesis of the peptide targeting moiety, researchers must select an appropriate BFCA, produce the radiopharmaceutical, and optimize its pharmacokinetics, first *in vitro* then *in vivo* with animal models. Synthesis of an optimized radiopharmaceutical must then be adapted to a kit formulation before it can undergo phase I through phase III clinical trials and be submitted to the FDA.[23]

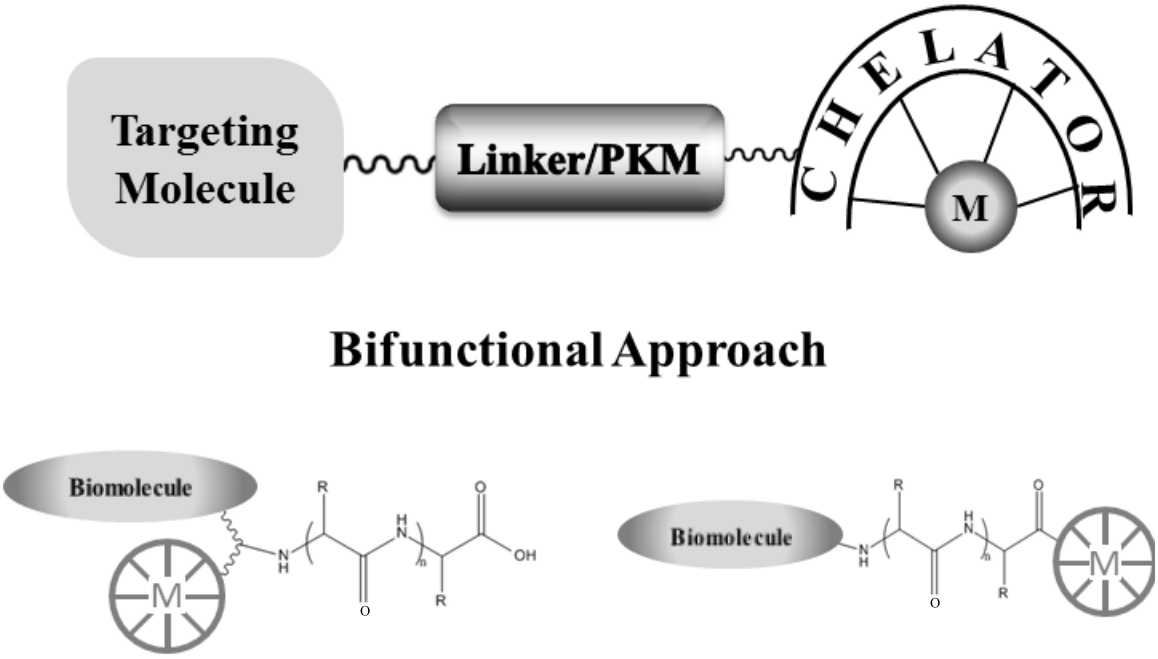

Figure 1.4: The BFCA approach to target specific radiopharmaceutical development. The biomolecule, linker, or metal chelate can be modified to improve pharmacokinetics.[22]

An advantage of the BFCA approach is that it allows the molecule to be tuned to specifically interact with the tissue of interest through linker and targeting moiety selection. The linker moiety serves to separate the chelator from the targeting molecule to ensure that the size and charge of the metal chelate does not interfere with binding of the targeting

moiety with the tissue of interest. Thus, the selection of the linker can be specific to the targeting molecule and metal chelate being used.[42] Even beyond this selection criteria, the linker moiety can be modified to improve the pharmacokinetics of the radiopharmaceutical. Hydrocarbon linkers of various lengths can be used to modify the lipophilicity of the molecule. Simple peptide linkers, such as polyglycine, can be used to modify the hydrophilicity and renal clearance of the radiopharmaceutical. Poly(ethyleneglycol), or PEG, linking moieties can be used to slow liver extraction for imaging methods needing longer imaging times.[6, 23, 42] A variety of cationic, anionic, neutral and cleavable linkers have been reported to modify the absorption, distribution, metabolism, and elimination of a BFCA. A sample of these is shown in Figure 1.5.[23]

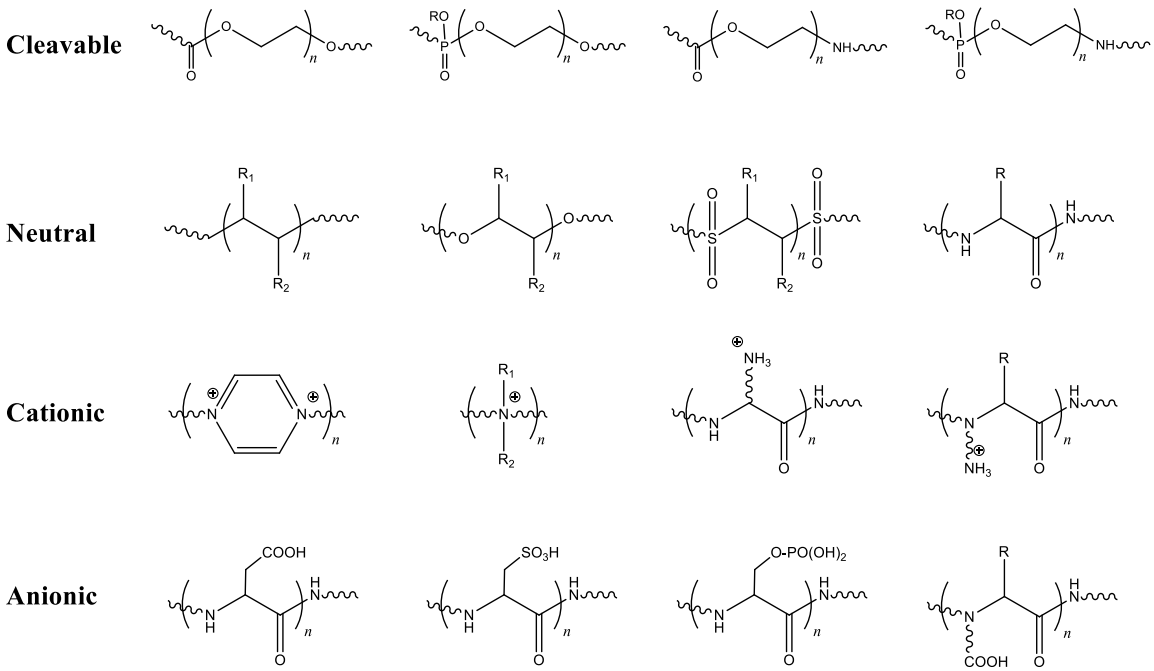

Figure 1.5: Example of linkers for incorporation into and pharmacokinetic modification of a BFCA.[23]

More recently, Alberto and co-workers have developed a tri-functional chelating agent (TFCA) approach to deliver radionuclides directly to the nucleus of a cell to deliver therapeutic radiation.[43-46] This approach takes advantage of the Auger emission of ^{99m}Tc. The Auger effect occurs when a core electron is removed and a higher energy level electron falls to the vacated core electron space. The energy released from this transition can be emitted as a photon or transferred to another electron, ejecting it from the atom as an Auger electron.[44] The Auger emission of ^{99m}Tc is normally not a factor in the dosing of ^{99m}Tc based imaging agents, since most ^{99m}Tc imaging agents accumulate in the extracellular spaces or on cytoplasmic receptors.[44, 47] The low penetration of Auger electrons (>10 μm) ensures that Auger emitting agents are relatively non-toxic if located outside a cell nucleus.[47] However, if the ^{99m}Tc complex can enter the cell and bind to nuclear DNA, the Auger emission of ^{99m}Tc can produce toxic effects from the double-strand cleavage of DNA.[44, 46, 47]

To target the nucleus, the TFCA is composed of a three parts, a targeting moiety, the metal chelate, and an intercalating agent.[43] The targeting moiety is designed to interact with a specific cell type, i.e. with a receptor that is overexpressed by cancer cells.[43] Once inside the cell, the targeting moiety would be cleaved, allowing the metal chelate and intercalating agent to be attracted to the nucleus. Once inside the nucleus, the intercalating agent interacts with the DNA allowing the α, or Auger electron, emitting isotope to selectively deliver a toxic radiation dose resulting in DNA cleavage.[43] This approach can be seen in Figure 1.6.[43]

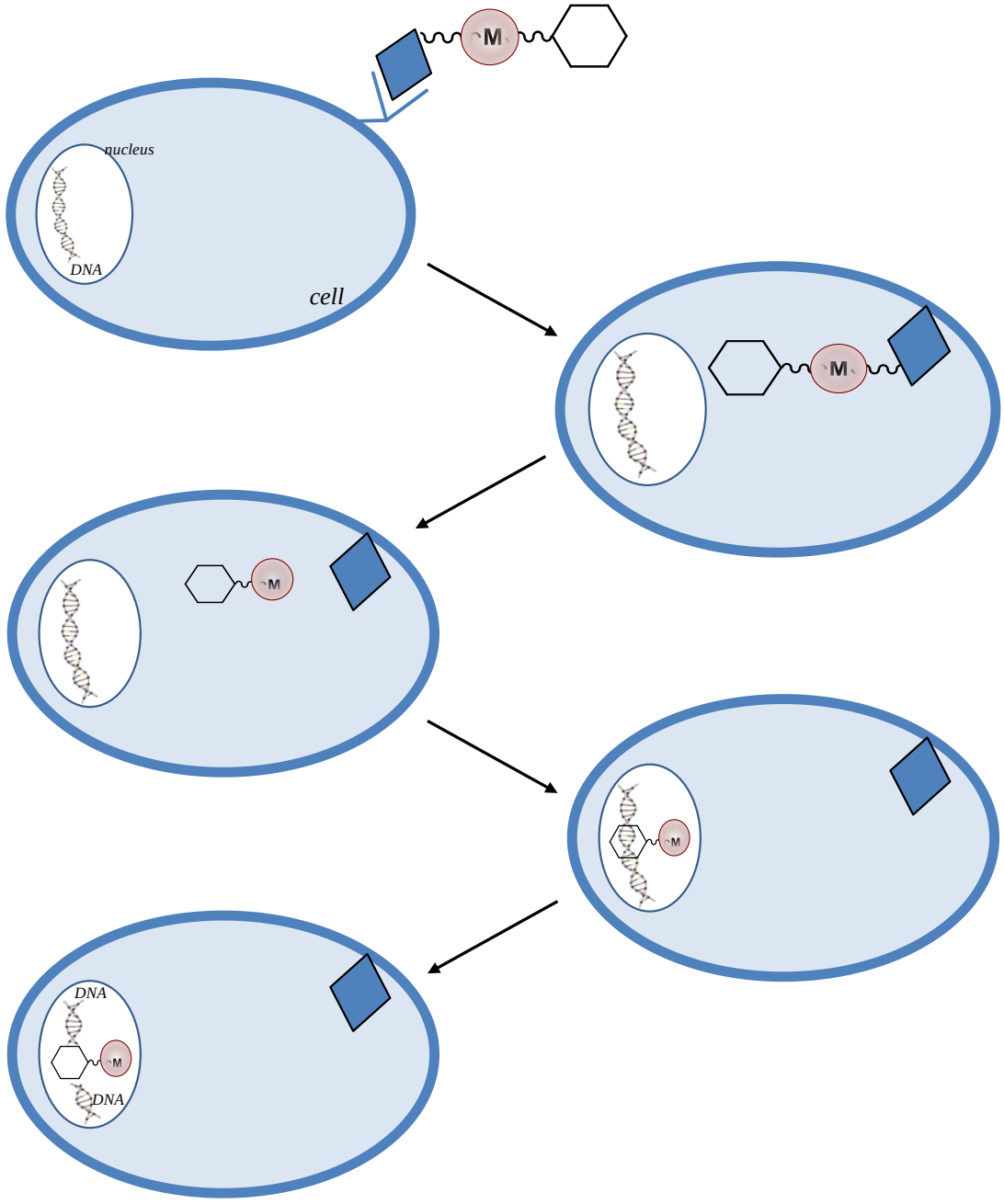

Figure 1.6: The TFCA approach to radiopharmaceutical development. First the radiopharmaceutical binds to a receptor and is transported to the cytoplasm. Then the cell targeting moiety is cleaved from the radiopharmaceutical allowing the nuclear targeting moiety to transport the metal to the nucleus to deliver cytotoxic radiation, often resulting in DNA strand sission, as shown.[43]

The challenge of the BFCA and TFCA approaches to radiopharmaceutical development is that the artificial attachment of the biomolecule to the radionuclide can lead to instability of the bioconjugate *in vivo* and affect the binding of the biomolecule to its target.[34] Another approach to creating target specific radiopharmaceuticals is to integrate the metal chelate directly into a biomolecule.[18] This so-called integrated approach has to be done carefully so that the replacement of part of the biomolecule with the artificial metal chelate does not significantly change the affinity of the biomolecule for its receptor.[4] Although the size, conformation, and lipophilicity of the biomolecule can all be altered, and thus tuned to ideally interact with the receptor of interest, while incorporating the metal chelate,[26] there are few examples of radiopharmaceuticals created via the integrated approach. One such example can be seen in Figure 1.7. Estradiol binds to the estrogen receptor, which is overexpressed in certain tumors (such as breast tumors).[48] A rhenium analog of estradiol, also shown in Figure 1.7 exhibits a very low receptor affinity, in spite of its similar size to estradiol, possibly because the rhenium metal is part of its binding motif.[48] A rhenium cyclopentadienyltricarbonyl appended estradiol molecule, created using the BFCA approach with an acetylene linker, has a contrastingly high receptor affinity.[49] The authors of this study attribute this high affinity to the location of the rhenium complex, which is slightly behind the steroid molecule, allowing it to be out of the way of receptor binding.[18, 49]

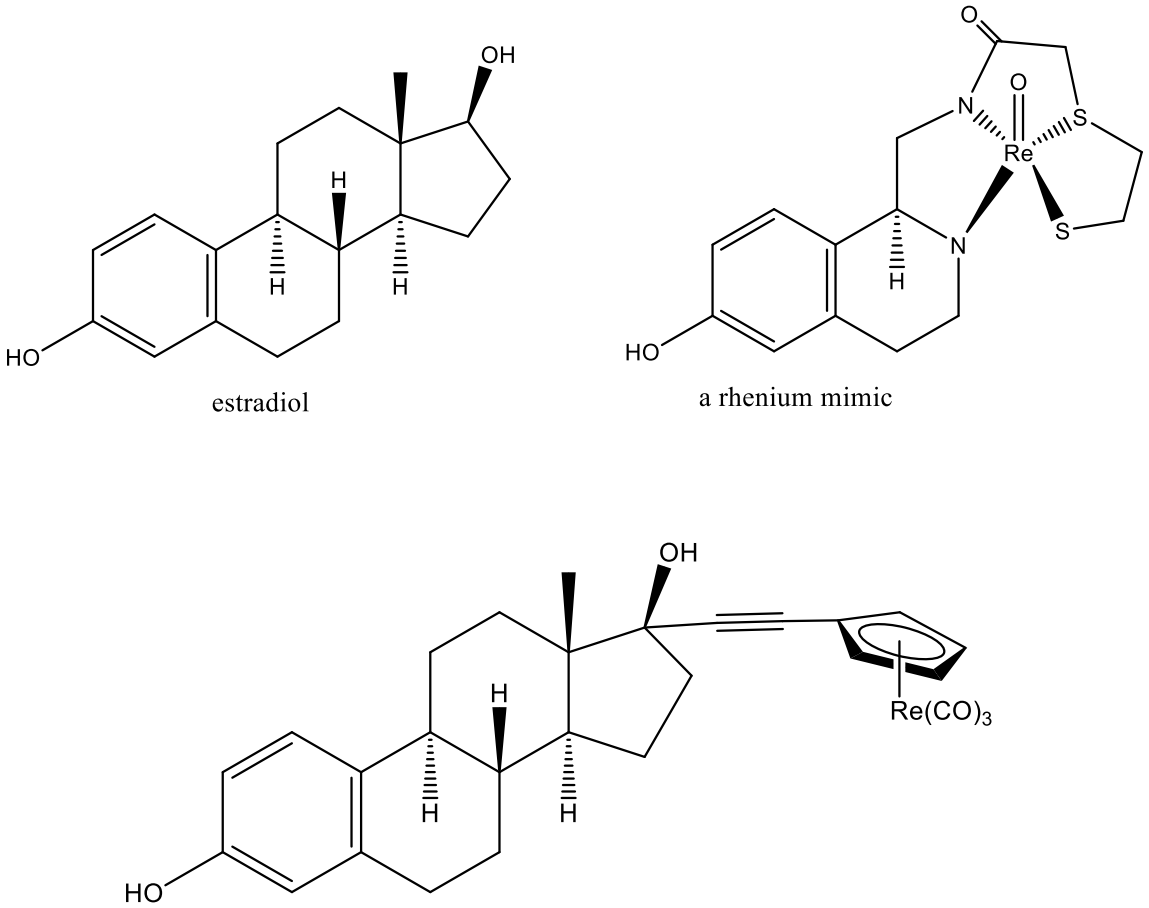

Figure 1.7: An integrated approach to radiopharmaceutical development.[48, 49]

As the size of the biomolecule increases, the size and charge contributions of the metal chelator to it decrease.[4] There are many examples in the literature of molecular imaging agents derived from the human insulin protein, as well as radioimaging studies of the many insulin disregulation diseases using these radiopharmaceuticals.[13, 50-56] Radiopharmaceuticals have been produced by directly labeling insulin with metal complexes using isotopes such as iodine-123,[50] iodine-124,[51] iodine-125,[52] fluorine-18,[53] gallium-67,[54] and technetium-99m.[13, 55] Specifically, ^{123}I-insulin has been used for insulin distribution studies in diabetic patients and for the detection of human hepatocellular

carcinoma.[56] The ^{99m}Tc-insulin was produced by treating the hormone directly with pertectnetate in the presence of $SnCl_2$ and it resulted in a multiply labeled product. While non-specific, this insulin mimic still showed high receptor affinity and stability, as shown by chromatographic and SPECT animal studies.[13, 55] The metal interaction of technetium and rhenium with specific components of proteins will be discussed elsewhere in this manuscript, however, possible bindings sites are highlighted on the insulin backbone shown below in Figure 1.7 and include the side chains of the amino acids glutamic acid (Glu), tyrosine (Tyr), cysteine (Cys), histidine (His), arginine (Arg), Lysine (Lys), and methionine (Met), along with the amino termini, carboxylic acid termini, backbone amide nitrogens and carbonyl oxygens.[55] There are a similar number of insulin radiopharmaceuticals developed using the BFCA approach in the literature.[13, 55, 56] An example of a ^{99m}Tc-insulin mimic designed via the BFCA approach is also shown below in Figure 1.8.[13] The use of this ^{99m}Tc-insulin mimic was supported by the analogous Re-insulin mimic which had an affinity for the insulin receptor that was similar in magnitude to native insulin.[13]

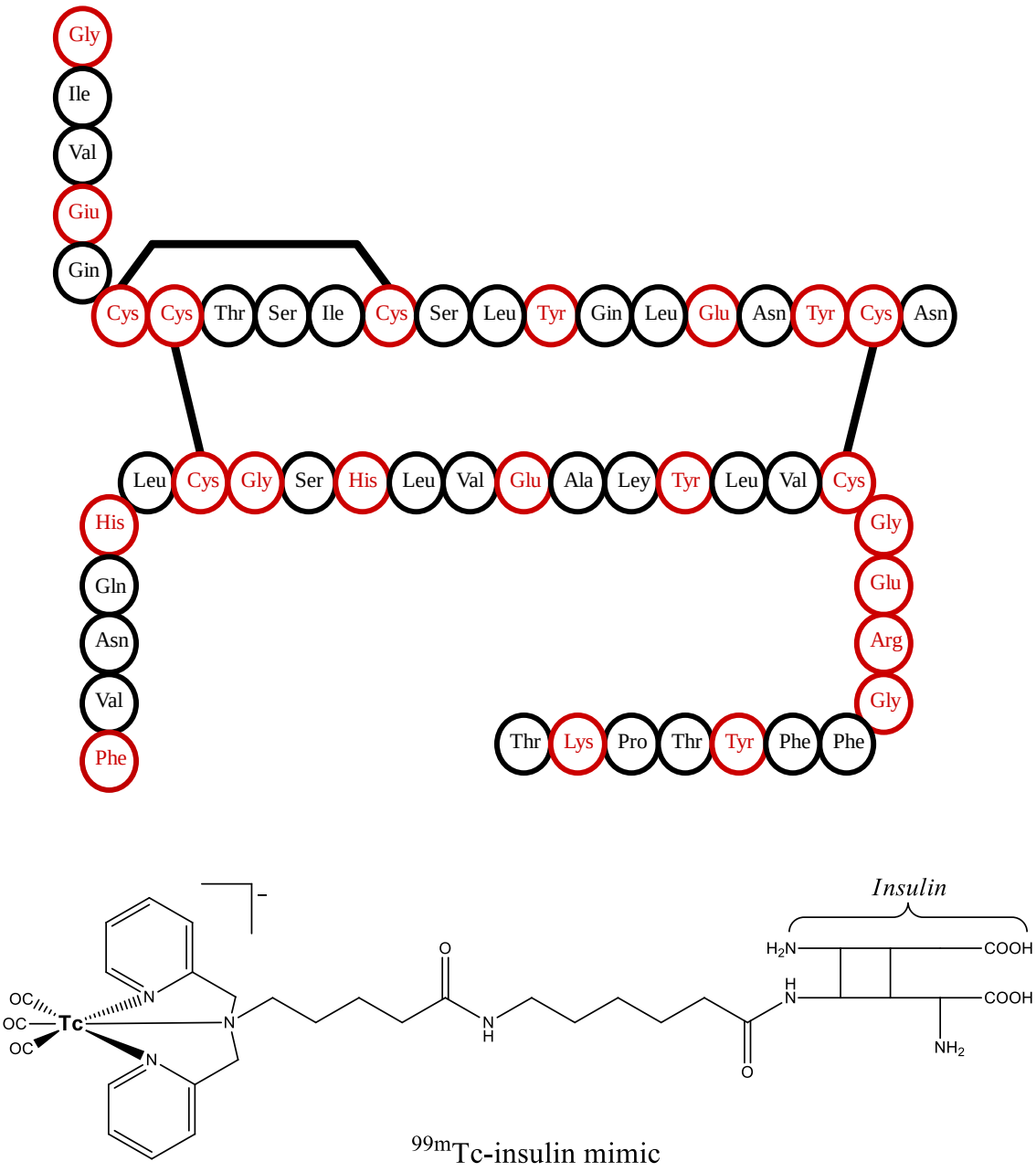

^{99m}Tc-insulin mimic

Figure 1.8: Insulin with highlighted transition metal binding sites and a ^{99m}Tc-insulin mimic created via the BFCA approach.[13]

1.5 The $M(CO)_3^+$ (M= ^{99m}Tc, $^{186/188}Re$) core: Basic inorganic chemistry

This section will focus on the contributions of ^{99m}Tc and $^{186/188}Re$ based radiopharmaceuticals of the $M(CO)_3^+$ (M= ^{99m}Tc, $^{186/188}Re$) type. The tricarbonyl metal core is a particularly attractive core for radiopharmaceutical development for a number of reasons, including its size, stability, ease of preparation, organometallic nature (which gives its chelation more covalent character), and lipophilicity.[2] The sizes of the technetium and rhenium tricarbonyl cores are considerably smaller than many of the other cores,[10] such as those listed in Figure 1.2. This is significant as smaller metal complexes are less likely to interfere with the biological activity of a targeting moiety in radiopharmaceutical development.[10] Figure 1.9 compares the size of the technetium tricarbonyl core with an example of a widely used technetium (V) core, $TcMAG_3$.[10, 22]

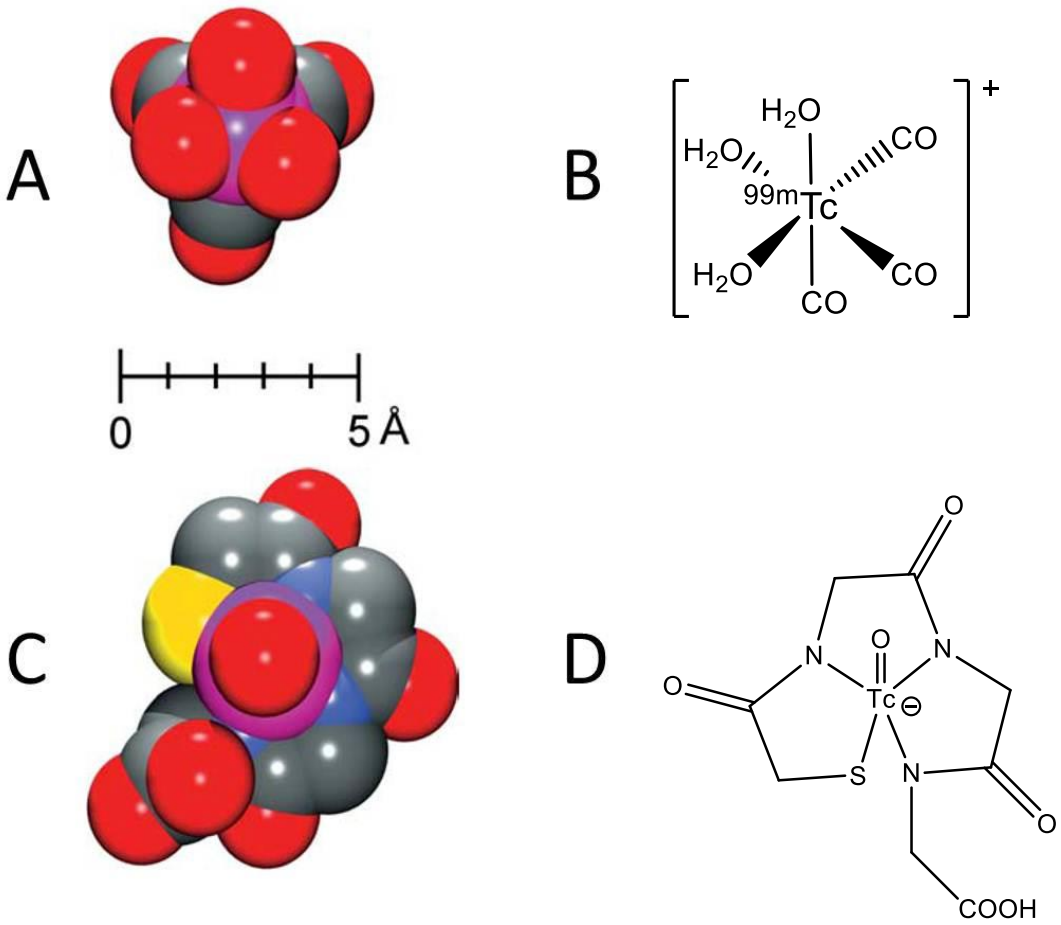

Figure 1.9: Size comparison of Tc cores for radiopharmaceutical development: $[Tc(H_2O)_3(CO)_3]^+$ (a) and (b) and Tc-MAG_3 (c) and (d)[22, 57]

Additionally, as the labile waters are replaced by an appropriate ligand system during radiopharmaceutical synthesis, the octahedral coordination sphere of the metal will be compact and protected from ligand attack or re-oxidation.[10] Ligand attack has historically been an issue for metal centers in the more open square pyramidal structure of the technetium (V) complexes, and, because of increased metal diameter, is even more prevalent in rhenium (V) species.[10] This is an undesirable property for radiopharmaceutical development as ligand attack leads to decomposition of the original complex, which can

lead to metabolism and elimination issues *in vivo*.[22] A variety of ligand systems are appropriate for the $M(CO)_3^+$ core, some of which will be described elsewhere in this thesis.

Adding to the desirable chemical stability of the tricarbonyl cores is their kinetic inertness as they incorporate technetium and rhenium in their low-spin, +1 oxidation states.[10] The kinetic inertness of the metal tricarbonyl complex can be explained by crystal and ligand field theory. When the metal is surrounded by anions, an electrostatic field is created which splits the energies of the d orbitals of the metal ion.[58] The d orbitals aimed in the direction of the surrounding ligands, $d_{x^2-y^2}$, and d_{z^2}, are thus raised in energy while the remaining d_{xy}, d_{xz}, and d_{yz} orbitals are unaffected by the field as they are directed between the octahedral ligands.[58] The energy difference between the orbitals is described by Δ_0.[58] In the case of a technetium or rhenium, low-spin, d^6 metal complex, the electrons reside in the lower energy orbitals and the large Δ_0 results in the kinetic inertness indicative of these complexes, as shown in Figure 1.10 below.[58]

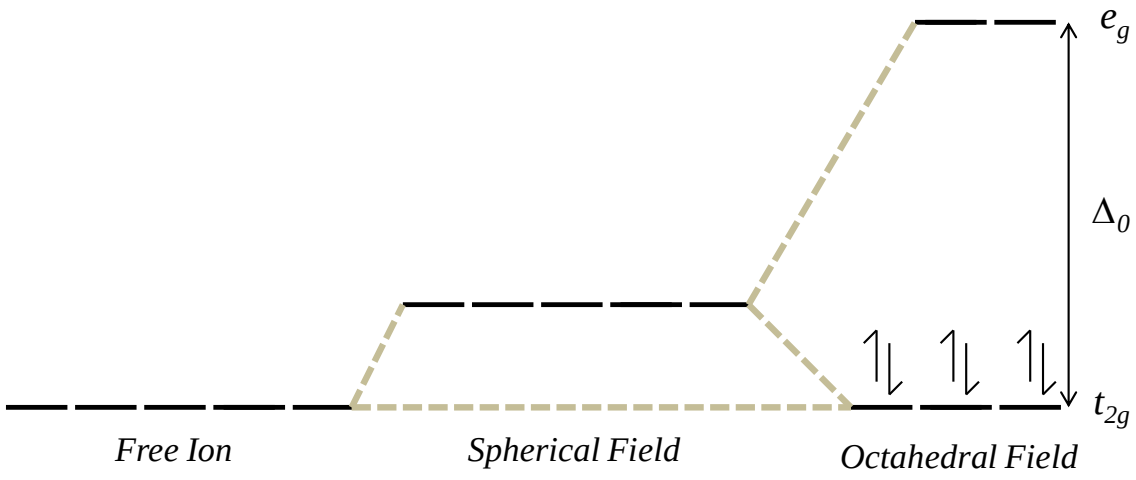

Figure 1.10 The energy difference of the d orbitals in an octahedral field, shown for $[M(H_2O)_3(CO)_3]^+$ (M= ^{99m}Tc, $^{186/188}$Re)[58]

The inert nature of tricarbonyl technetium and rhenium complexes is further emphasized upon consideration of the three carbonyl ligands. The molecular orbital diagram of CO can be seen in Figure 1.11 below.[58] The highest occupied molecular orbital (HOMO) of the carbonyl donates electron density to an unfilled d orbital on the metal in a σ–donor type interaction.[58] The lowest unoccupied molecular orbital (LUMO) of the carbonyl consists of two empty π* orbitals, which allow the metal to donate electron density to the carbonyl from metal orbitals of appropriate symmetry.[58] The metal-carbonyl σ and π interactions can also be seen in Figure 1.11.[58] The sum of the σ–donor and π–acceptor interactions results in a strong interaction between the metal and the carbonyls thus designating the carbonyls as strong field ligands.[58] The presence of the strong field ligands contributes to the tendency of these complexes to be low-spin as the magnitude Δ_o is comparatively large, as can be appreciated from Figure 1.11.[58] Combining the metal orbitals for technetium or rhenium with six, σ–donor ligands results in an MO diagram similar to one shown in Figure 1.12.[58] The molecules that make up the body of this work are similar to this type.

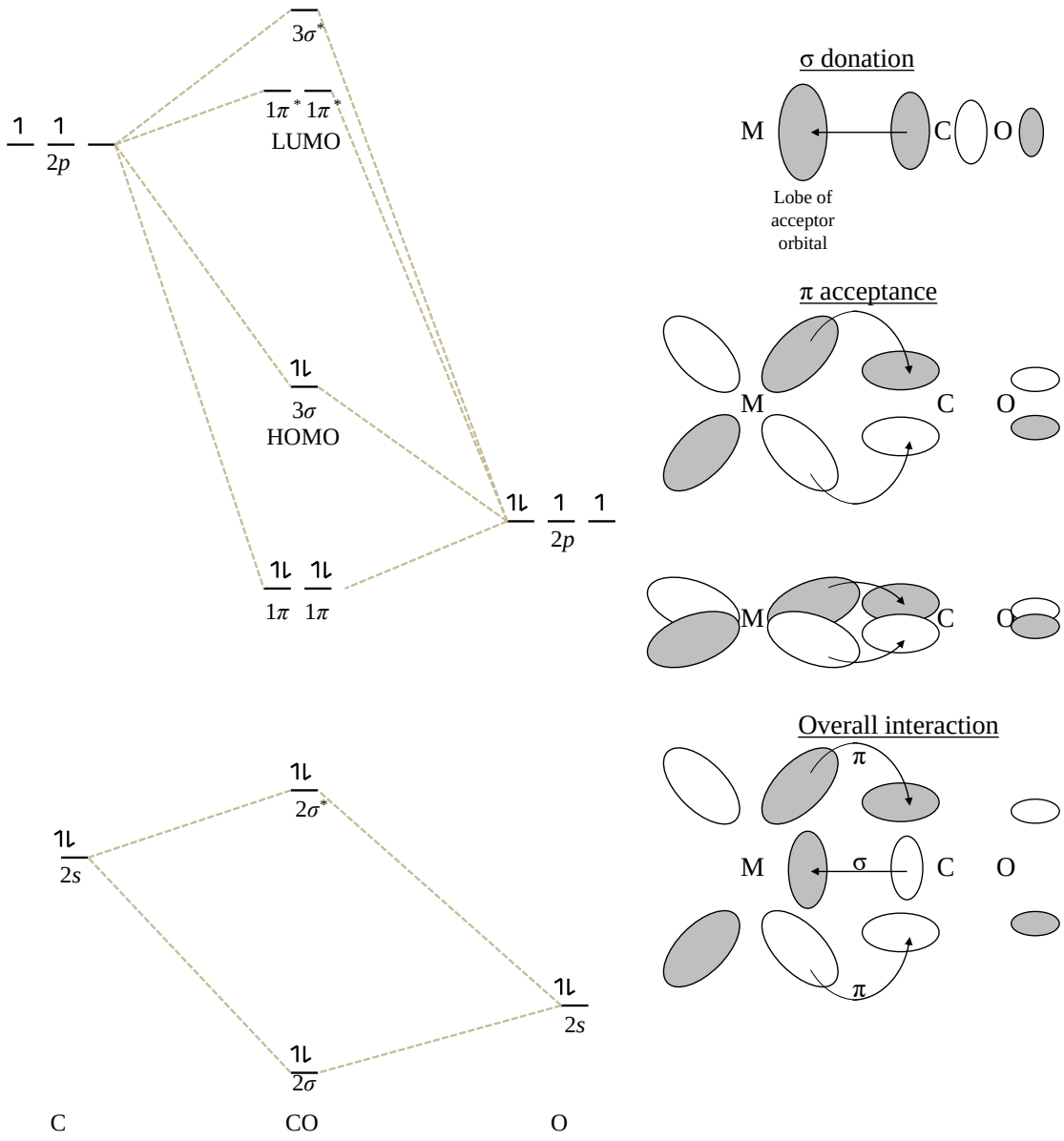

Figure 1.11: The molecular orbital diagram of the carbonyl ligand and an illustration of the σ–donor and π–acceptor metal-carbonyl interactions.[58]

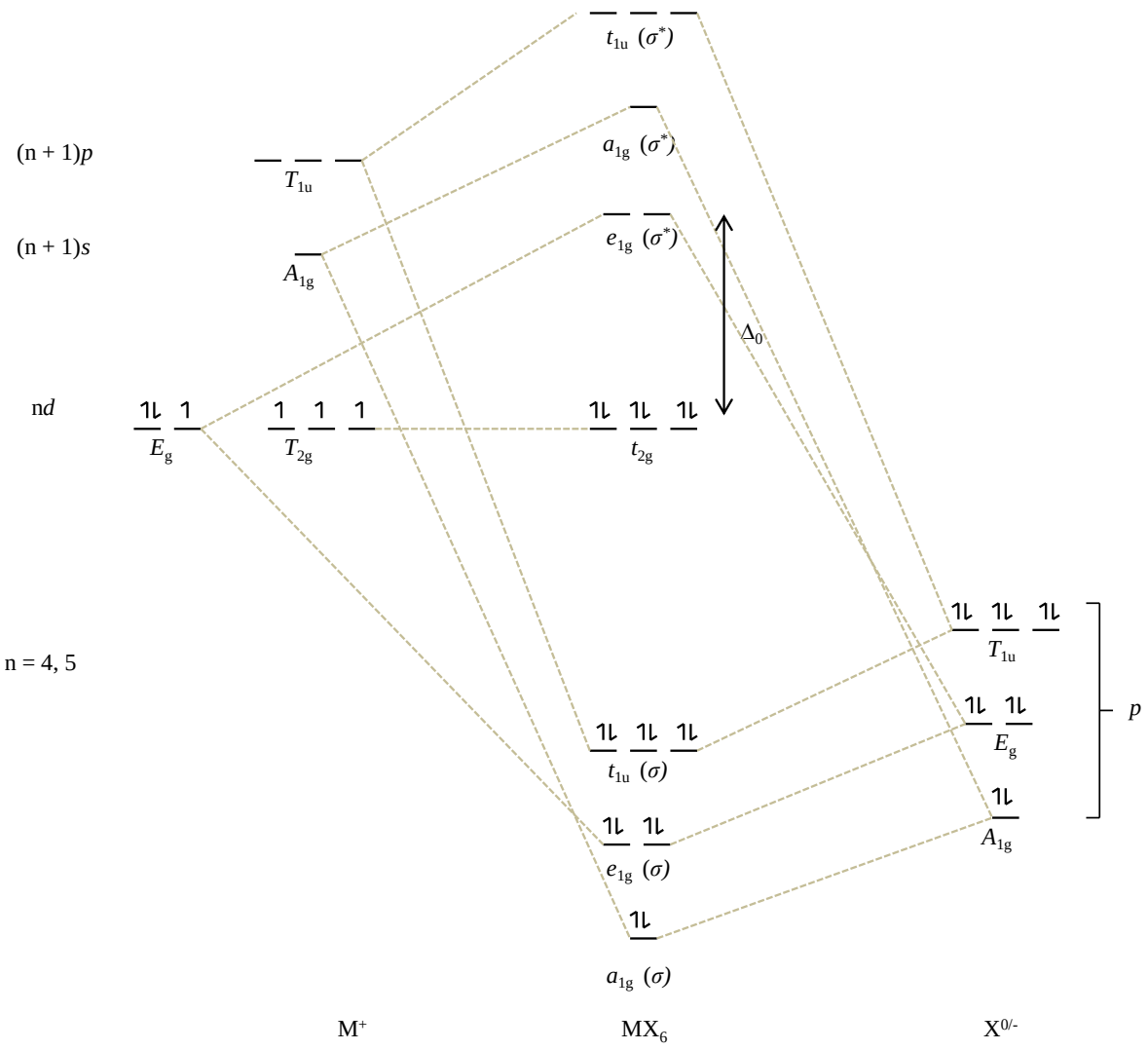

Figure 1.12: Molecular orbital diagram of an octahedral technetium(I) or rhenium(I) complex with sigma donor/pi acceptor ligands.[58]

Another reason that the technetium(I) and rhenium(I) tricarbonyl cores are attractive for radiopharmaceutical development is the ease with which they can be produced in the clinical setting. Alberto and co-workers first reported a method to reduce the pertechnetate eluted from the molybdenum generators in the clinic; using sodium borohydride in the presence of carbon monoxide to produce the $[^{99m}Tc(H_2O)_3(CO)_3]^+$ complex in solution.[59] This complex could then be further modified with a ligand system

to replace one or more of the highly labile waters.[60] Soon after, Alberto and co-workers developed a method to produce the carbon monoxide *in situ* using $K_2[H_3BCO_2]$.[59] This chemistry, shown below in Scheme 1.2 was so straightforward that it was developed into a kit for clinical use by Covidien (Tyco-Mallinckrodt, Inc.), known as the IsoLink® kit. Each reaction vial contains sodium boranocarbonate, used both as a reducing agent and as a source of CO, hydrous sodium tartrate, used as a weak chelating agent to inhibit MO_2 production, and hydrous sodium tetraborate, and sodium carbonate, which are used to control solution pH.[11] These components convert the pertechnetate supplied from a molybdenum generator to the desired $[^{99m}Tc(H_2O)_3(CO)_3]^+$ species in aqueous solution in 20 minutes with a greater than 95% yield.[61]

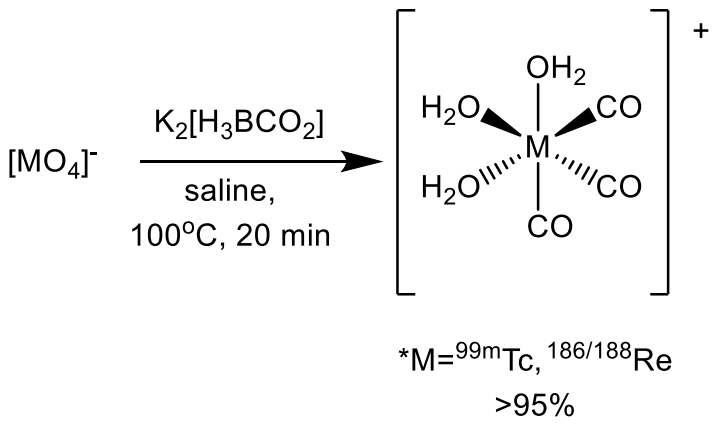

Scheme 1.2: Production of $[^{99m}Tc(H_2O)_3(CO)_3]^+$ via the Isolink® kit and the structure of the $Re(H_2O)_3(CO)_3^+$ cation.[62]

The $[^{188}Re(H_2O)_3(CO)_3]^+$ complex can also be produced from the IsoLink® kit, by first acidifying the perrhenate eluted from the tungsten column mentioned previously with phosphoric acid.[57, 61] The acidified perrhenate is then added to a pre-reduction kit vial containing an NH_3BH_3 complex, γ-cyclodextrin and sodium ascorbate, before being

transferred to the IsoLink® vial.[57, 61] Cold analogs of $[^{188}Re(H_2O)_3(CO)_3]^+$ can be produced in the laboratory setting by refluxing pentacarbonyl rhenium(I) bromide in water for 24-72 hrs.[63] It can be produced in gram quantities without the expense and radiation exposure risks which make it an ideal test model for the development of radiopharmaceuticals based on the $^{99m}Tc(CO)_3^+$ or $^{186/188}Re(CO)_3^+$ cores.[22]

The non-radioactive rhenium(I) tricarbonyl core has an additional use as an *in vitro* fluorescent microscopy probe, as complexes of $Re(CO)_3^+$ with aromatic donor ligands are often fluorescent.[2] Luminescent probes based on the $Re(CO)_3^+$ core have a long excited state lifetime, polarized emission, and a large Stokes shift.[8] Molecules incorporating the $^{99m}Tc(CO)_3^+$ fragment have been shown to have similar fluorescent properties, however, the lack of availability of non-radioactive isotopes, and the larger concentrations of complexes required for fluorescent microscopy, make them less than ideal candidates for this application. Those considerations notwithstanding, the similar chemistry of the $Re(CO)_3^+$ and $^{99m}Tc(CO)_3^+$ cores make them ideal models for the design of complementary fluorescent and radiodiagnostic probes, respectively.[2, 8] An example of one such complex utilizes a lysine residue that has been modified with bisquinoline ligands, as shown in Figure 1.13.[2] The modified lysine residue can then be incorporated via solid phase synthesis methods into a targeting peptide. The single lysine residue is modified to act as the BFCA for this complex in an approach that the authors call the single amino acid chelate (SAAC) approach to radiopharmaceutical development.[2] The resulting rhenium complex displays the desired fluorescence and the resulting ^{99m}Tc complex is stable in aqueous solution, demonstrating the feasibility of this approach in the development of complementary *in vitro* fluorescent and *in vivo* radiodiagnostic probes.[2, 8]

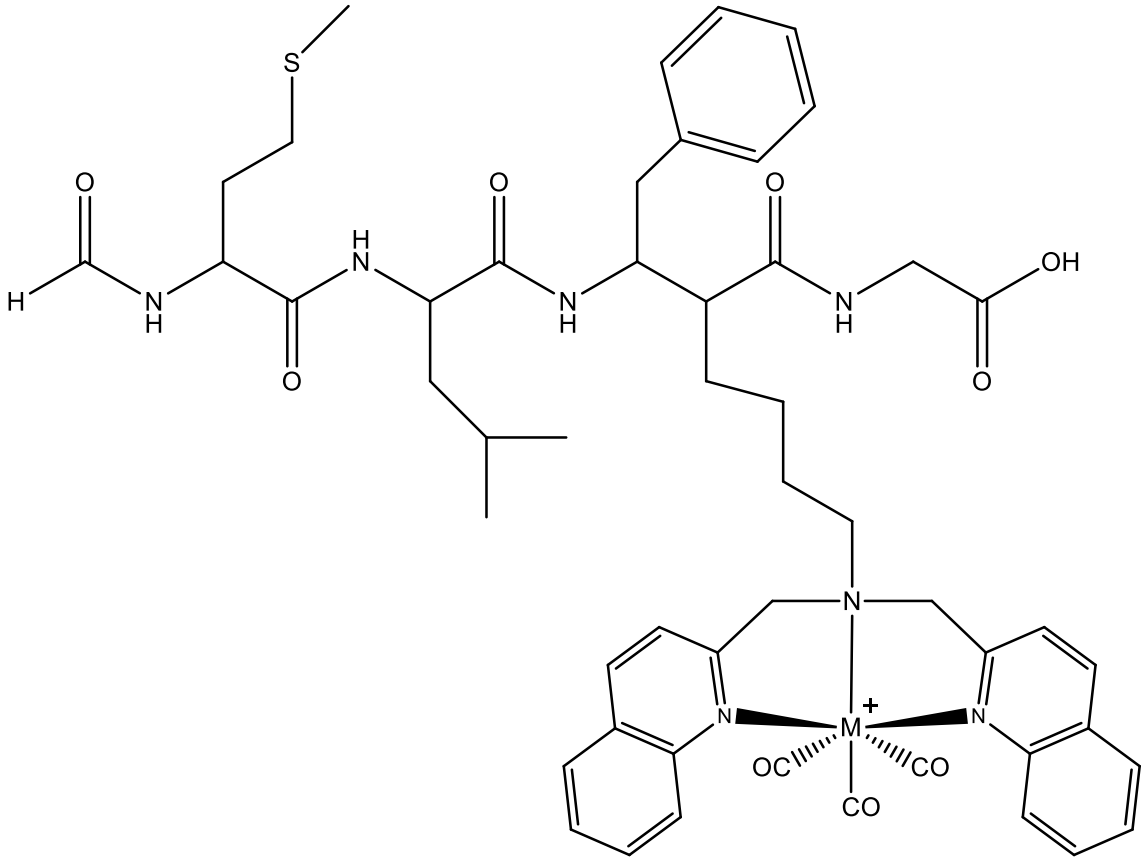

Figure 1.13: Peptide labeled with the $Re(CO)_3^+$ core for fluorescent imaging or with $^{99m}Tc(CO)_3^+$ for diagnostic imaging.[2]

1.6 Ligand systems for the $M(CO)_3^+$ (M= Tc, Re) fragment

Unlike the Cardiolite® kit that produces ^{99m}Tc sestamibi, the IsoLink® kit does not produce a radiopharmaceutical suitable for patient administration. Current research in this area has focused on ligand and/or BFCA development for the $M(CO)_3^+$ (M= Tc, Re) core. Many ligand systems are suitable for the functionalization of this core. Histidine, methionine, amines, imidazoles, pyridines, pyrazoles, amides, thioethers, thiols, phosphines, carboxylic acids, and N-heterocycles containing combinations of these are all

examples of ligand systems that have been used with the $M(CO)_3^+$ core.[17, 64] Complexes formed from the $M(CO)_3^+$ core and mondentate or bidentate ligand systems traditionally show lower *in vivo* stability.[10, 65] The extra bonding groups in the bidentate and tridentate ligand systems lead to stronger chelate effects.[65] Additionally, chelation with monodentate or bidentate ligand systems only displaces one or two of the highly labile waters of the $[M(CO)_3(OH_2)_3]^+$ core. Exchange of the remaining water, or chloride, could lead to aggregation or undesired bonding to plasma proteins *in vivo*, which would slow elimination of the final product.[65] This is an undesirable characteristic for a radiopharmaceutical not meant for the direct labeling of proteins or whose target organ is not an elimination organ, such as the kidney or the liver.

Ideal ligand systems are those which chelate in a tridentate fashion.[10, 65, 66] $M(CO)_3^+$ complexes with a tridentate chelating system have historically high stability in human plasma or in solutions containing an excess of biological competing ligands, such as cysteine, histidine, or glutathione.[65] The complexes with tridentate chelating systems also trend towards better blood and tissue/organ clearance *in vivo*.[10, 65, 66] Tridentate ligands can be separated into two groups; linear and tripodal. N-heterocyclic amine and amine groups incorporated into tripodal ligands represent some of the strongest binding chelate systems. Many examples of tripodal ligand systems are relatively simple to produce synthetically or commercially available such as the 1,1,1-tris(aminomethyl)ethane shown in Figure 1.14 below.[67] The aromatic amine ligand systems display rapid metal complexation, which is a necessary property for radiopharmaceutical syntheses, as they must be accomplished in a short period of time.[24, 34] The combination of aromatic amines with aliphatic amines or carboxylate groups in ligand systems also gives rise to ligands with fast complex formation

and high aqueous stability.[24, 34] The tridentate chelator used in the (SAAC) approach to radiopharmaceutical development, discussed previously and shown in Figure 1.13, is a good example of a stable ligand system incorporating aromatic and aliphatic amines.[2] A single drawback to these ligand systems is that they tend to be somewhat bulky and lipophilic, which can increase their hepatobiliary retention.[38] The amino acids methionine, cysteine, and histidine are examples of naturally occurring tridentate ligands for the $M(CO)_3^+$ center.[10, 65, 66] The amino acid tripodal ligands are soluble, stable and have good clearance *in vivo* along with a lower incidence of immunogenic effects as compared typical tridentate ligands.[38] These ligands along with several other examples of tridentate ligands suitable for complexation to the $M(CO)_3^+$ core can be seen in Figure 1.14 below. In general, all tridentate ligands display similarities in donor atoms (N, O, P, and S being most popular) and coordination sphere size (5-6 atoms).[68]

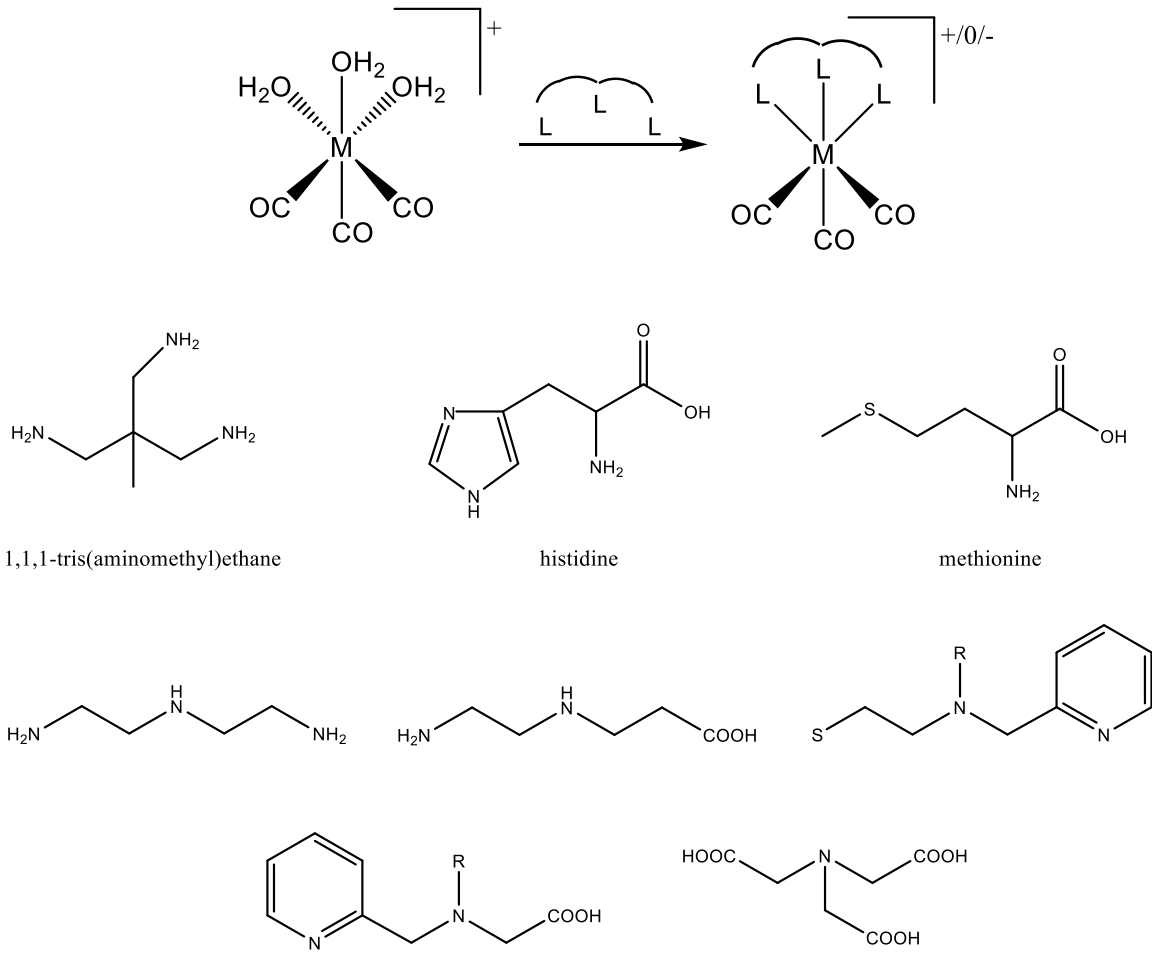

Figure 1.14: Selected examples of tridentate chelators for the $M(CO)_3^+$ (M= Tc, Re) core.[10, 43, 65, 66]

While the tridentate ligand systems have superior stability *in vivo*, the need to incorporate a suitable functional group for covalent coupling to a targeting biomolecule can make their development a synthetic challenge, often involving protecting group chemistry.[66] Histidine is a unique exception in that the $Re(CO)_3^+$ core can serve as the protecting group for the functionalization of histidine's Nε position, as illustrated in Scheme 1.3 below.[64-66] Histidine is a strong binding tridentate chelator that forms complexes with $Tc(CO)_3^+$ and $Re(CO)_3^+$ cores at stoichiometric ratios even at very low

(>10^{-6} M) concentrations.[64-66] [Re(His)$(CO)_3$] forms in one step by combining histidine and $[Re(CO)_3(OH_2)_3]^+$ in solution. This allows alkylation only at the Nε position of the histidine. After a targeting moiety, such as a peptide, is coupled, the $Re(CO)_3^+$ core can be cleaved from the histidine at low pH with an oxidizing agent like H_2O_2 to form the complete histidine BFCA. Subsequent addition of the $[^{99m}Tc(CO)_3(OH_2)_3]^+$ in solution will form the active radiopharmaceutical.[64-66]

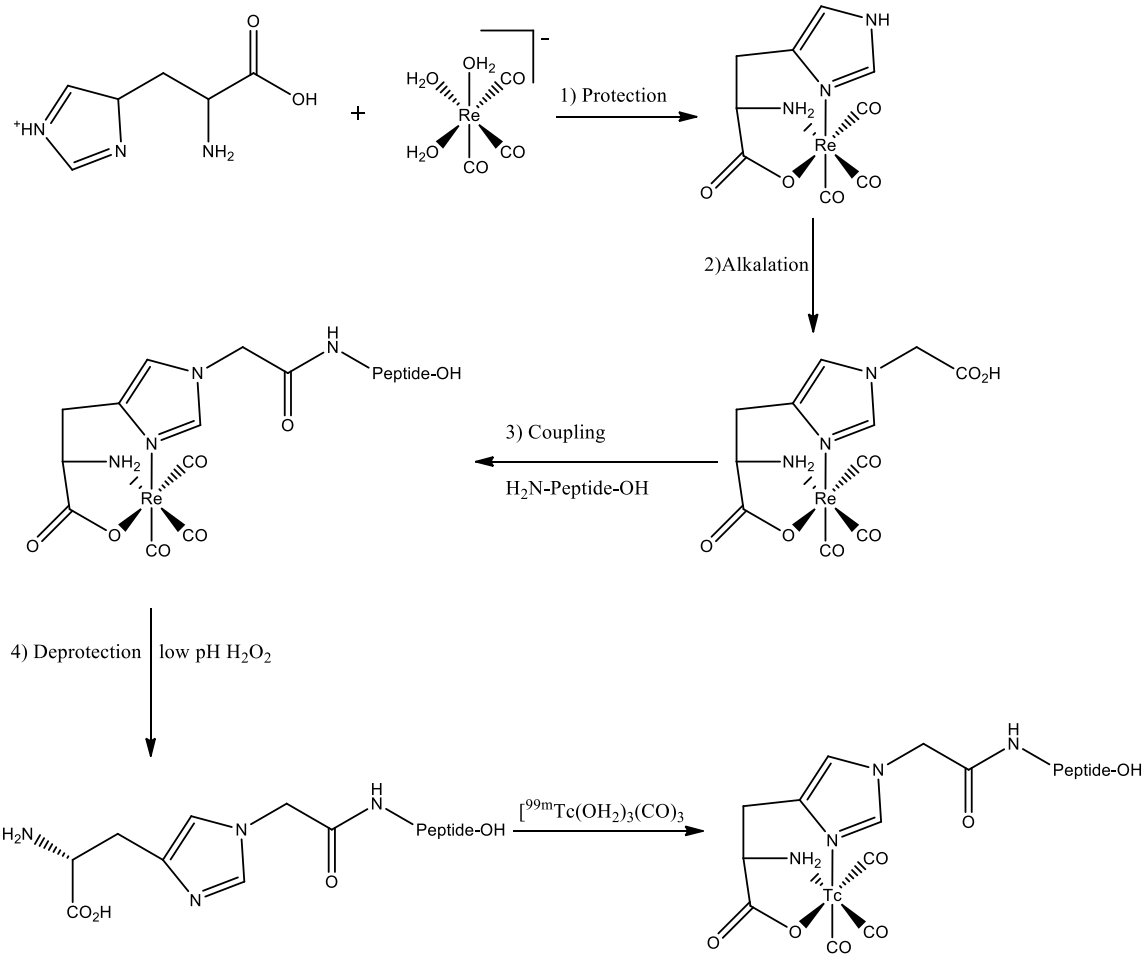

Scheme 1.3: The protection, N-alkylation, peptide coupling, deprotection, and synthesis of a histidine BFCA for coupling to a $^{99m}Tc(CO)_3^+$ core, accomplished by using the $Re(CO)_3^+$ core as the protecting group.[64-66]

The bonding, structure, and stoichiometry of the reaction of the $Re(CO)_3^+$ core with histidine was further probed by Herrick and coworkers, using the modified histidines His-OMe, Ac-His-OH and His-His-OH.[69] While the reaction of stoichiometric equivalents of the $Re(CO)_3^+$ core and His-OMe yielded the tridentate structure similar to the one seen above in Scheme 1.3, reactions using Ac-His-OH and His-His-OH yielded the two new complexes seen below in Scheme 1.4.[69] The Ac-His-OH showed a tridentate bonding to the $Re(CO)_3^+$ core via the imidazole N_δ atom, the carboxylate oxygen and a deprotonated amide nitrogen. The His-His-OH ligand reacted with two stoichiometric equivalents of the $Re(CO)_3^+$ core to yield the zwitterion structure shown below in which one core is bound via the deprotonated carboxyamido nitrogen, with a N_α,N_δ,O binding motif while the other core is bound via carbonyl oxygen atom of the bridging deprotonated peptide bond, with a N_α^-,N_δ,O^- binding motif.[69] The tight binding of the His-His-OH with the $Re(CO)_3^+$ cores was demonstrated by incubating the complex with an excess of N-methylimidizole in $[D_6]$dmso. No change in the NMR spectra was observed even after two weeks. This work supports the use of His-tagged peptides as delivery systems for the $Re(CO)_3^+$ core, which will be discussed elsewhere in this manuscript.[69]

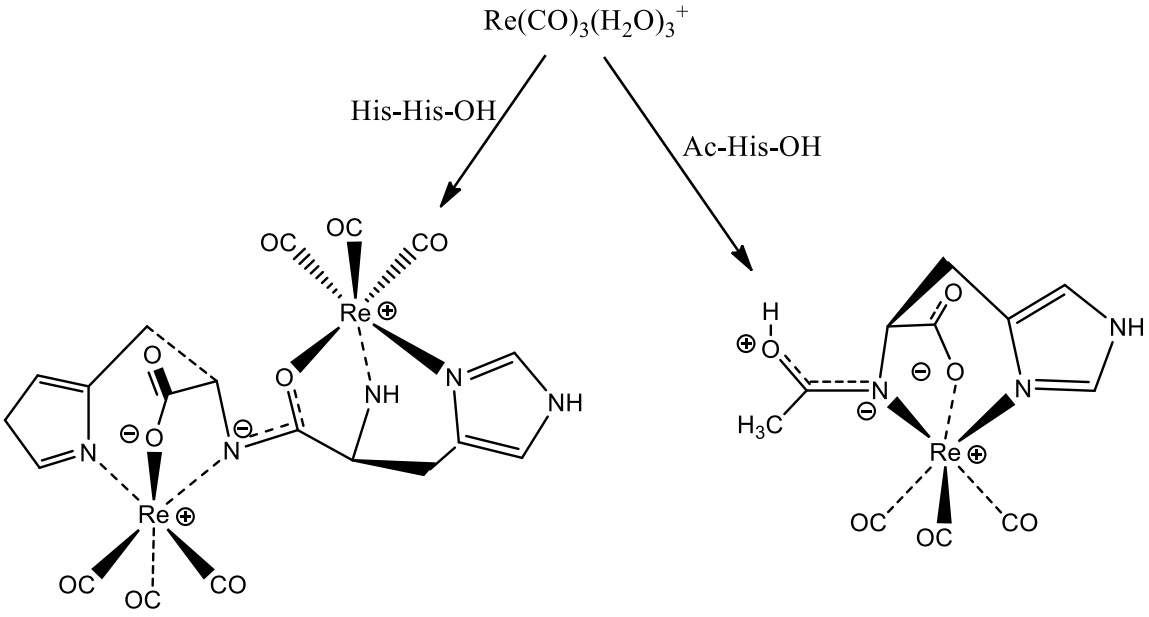

Scheme 1.4: Reaction of Ac-His-OH and His-His-OH with $Re(CO)_3(OH_2)_3^+$.[69]

There are many examples of bidentate ligands systems for the $M(CO)_3^+$ core in the literature. Some bidentate ligands are developed from tridentate ligands that have one of the binding sites derivatized for binding to a targeting moiety.[66] Examples of naturally occurring of bidentate chelators would be N-terminal methionine or histidine.[66] Since bidentate chelators replace only two of the three labile waters of the $[M(CO)_3(OH_2)_3]^+$ complex, the additional water is often replaced by a halide in solution for charge balance.[43, 65, 66] A notable class of bidentate chelators of the form $M(CO)_3$(bidentate chelator)X are the dioximes, which coordinate through two imine nitrogens.[70] While typically not as stable under physiological conditions as their tridentate counterparts, certain bidentate ligands can be labeled with the $M(CO)_3^+$ core at concentrations approaching 10^{-5} M.[43, 66] The halide can be exchanged with biomolecules which is a detriment in radiopharmaceutical administration, as binding to plasma proteins could slow elimination of the complex *in vivo*.[10, 22] Examples of bidentate chelators appear in Figure 1.15 below.

Oxime ligands

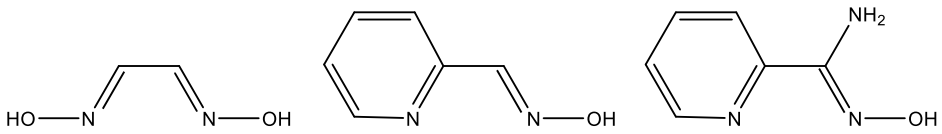

Examples of highly efficient bidentate chelators

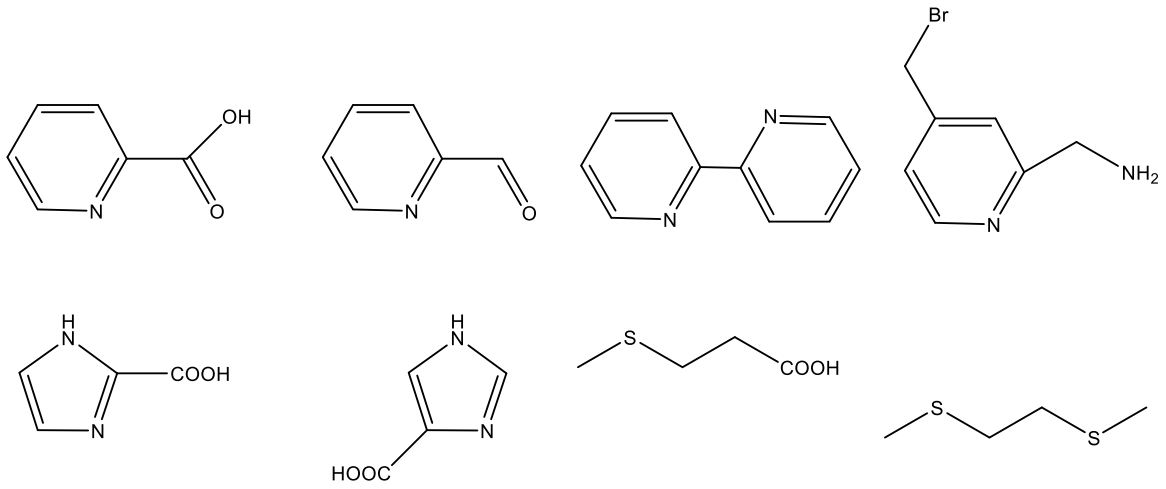

Figure 1.15: Examples of bidentate chelators for the $M(CO)_3^+$ core.

Monodentate ligands incorporating one of the functional groups mentioned previously (including amines, imidazoles, pyridines, pyrazoles, amides, thioethers, thiols, phosphines, carboxylic acid) are also suitable for binding to the $M(CO)_3^+$ core in ligand to metal ratios of 1:1, 2:1 and 3:1, although the latter requires long reaction times.[17, 64, 66] Coordination of the $M(CO)_3^+$ core with solely monodentate ligands is not generally considered a viable route to radiopharmaceutical development, as cross-linking to two different biomolecules is often observed.[66] However, monodentate ligands have other uses in the field of nuclear medicine, namely the direct labeling of biomolecules, as will be discussed in the next section. Monodentate ligands are also used in conjunction with

bidentate ligands in the TFCA approach for radiopharmaceutical development, as mentioned previously.

One of the advantages of the TFCA approach, also called the 2+1 approach, to chelate system design, is that it allows integration of two targeting moieties without the synthetic challenge of incorporating both on the same bi-functional chelating agent.[43, 46] Scheme 1.5 below shows an example of a nuclear targeting radiopharmaceutical designed using the TFCA approach.[46] In this example, the fluorescent nuclear dye acridine orange undergoes alkalation with N-(4-bromo-butyl)formamide and then dehydration to produce an isocyanide derivative. In a separate synthesis, bombesin, a receptor targetic peptide, was produced and attached to 2,4-pyridinedicarboxylic acid via solid phase synthesis. This product was reacted with $[M(CO)_3(OH_2)_3]^+$ and then with the isocyanide derivative of acridine orange to produce the radiopharmaceutical.[46] The fluorescent acridine orange moiety allowed researchers to track this molecule in real time via fluorescent microscopy. This complex did indeed accumulate without toxicity in the cytoplasm of cells. However, this study and similar attempts by other groups have yet to overcome the barrier of cytoplasmic cleavage of the cell targeting moiety, without which the nuclear targeting moiety cannot deliver the isotope to the nuclear DNA, in order for the complex to be considered a viable radiopharmaceutical.[46, 71]

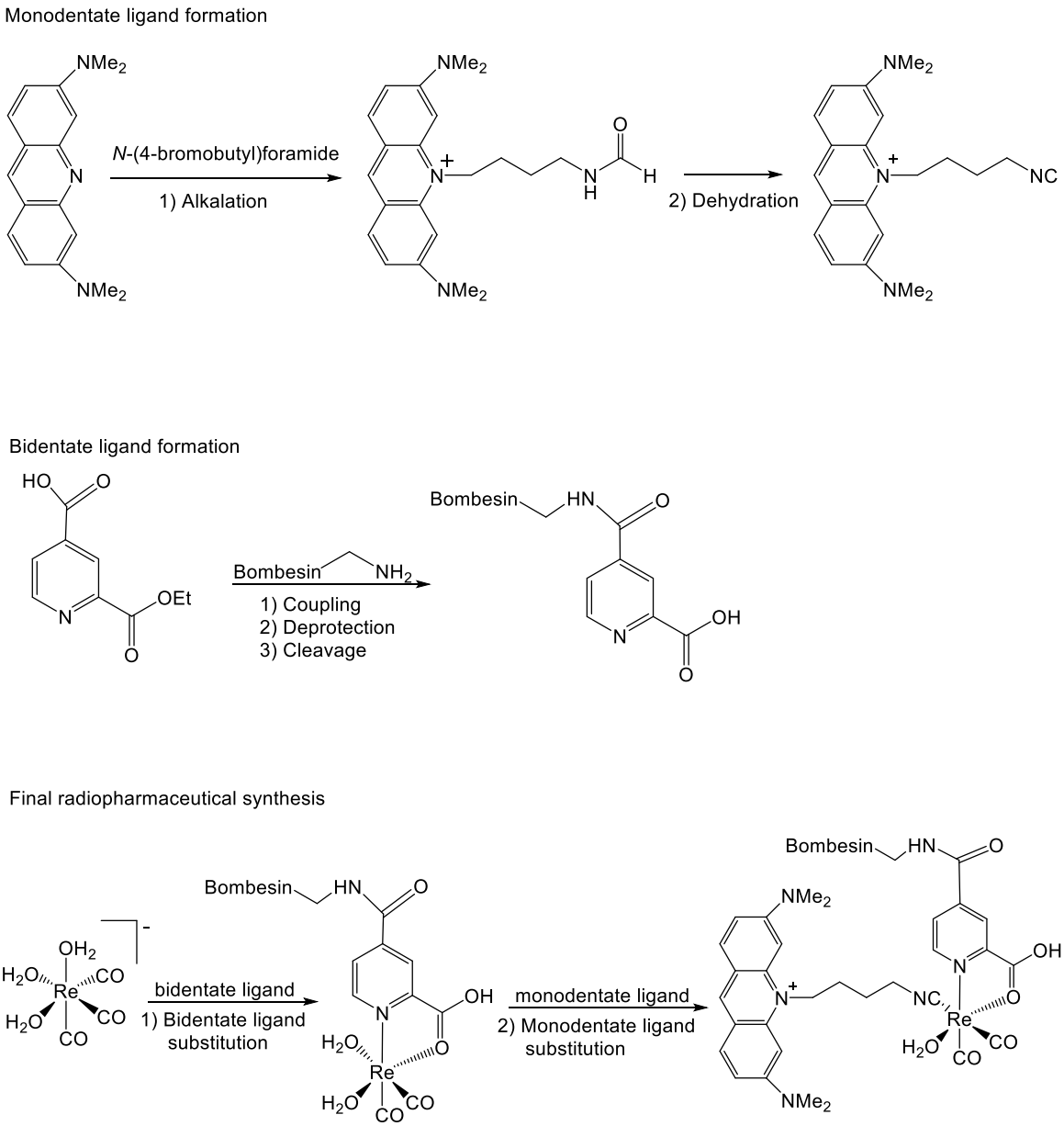

Scheme 1.5: An example of the 2+1, or TFCA approach to radiopharmaceutical development. A nuclear targeting moiety, acridine orange is the monodentate ligand and a cell targeting moiety, bombesin is attached to the complex via a bidentate ligand .[43, 46]

1.7 Interaction of $M(CO)_3^+$ (M= Tc. Re) complexes with biomolecules

The binding of the $M(CO)_3^+$ core (M= Tc, Re) with a variety of biomolecules has been studied in the literature and conjugates of $M(CO)_3^+$ cores with groups from small molecules like sugars and steroids[66,23,72] to large biomolecules such as proteins[9,55,73-78] and monoclonal antibodies[79] have been reported. The resulting compounds are designed to serve a variety of purposes, such as fluorescent probes, electron transfer models, and radiopharmaceuticals. This portion of this introduction is devoted to a review of the interaction of the $M(CO)_3^+$ core with biomolecules relevant to this work.

The Interaction of the $M(CO)_3^+$ Core with Amino Acids

In addition to acting as models for the complexation modes of $M(CO)_3^+$ to peptides and proteins, the interaction of the $M(CO)_3^+$ core with amino acids can be a direct route for radiopharmaceutical development. Single amino acids can act as neurotransmitters (such as GABA, glycine, and glutamate)[72] as well as being the ubiquitous building blocks for everything from peptides and hormones to enzymes and monoclonal antibodies. Thus the binding mode of the $M(CO)_3^+$ core to a single amino acid has implications in many biological processes.[72] Direct binding of the $M(CO)_3^+$ core to an amino acid is a desirable target for radiopharmaceutical development, as the resulting complex is not as likely to stimulate an immune response as compared to an artificial chelate system.[23] The binding modes of several amino acids are shown in the previous figures, however there are some examples that directly correlate to radiopharmaceutical development and thus merit additional discussion.

As previously discussed, stable complexes of bidentate and tridentate chelation of amino acids to the $M(CO)_3^+$ center generally requires that the amino acid contain a heteroatom for binding in its side chain. Cysteine is one such amino acid, containing thiol, amino, and carboxyl groups for complexation to the metal. Park and co-workers found that L-cysteine binds to the $^{99m}Tc(CO)_3^+$ core in a tridentate fashion as shown in the straightforward synthesis described by Scheme 1.6 below.[80] This resulting complex was found to have similar renal imaging characteristics in rabbits compared to ^{99m}TcMAG, mentioned previously and included in Figure 1.9.[80] Although the $[^{99m}Tc(CO)_3(cysteine)]^-$ complex only proved to be stable for 3 hours, the synthesis of the complex was accomplished in less than 30 minutes, at tracer level concentrations, and it rapidly localized in the kidneys of the rabbit model.[80] The complex was eliminated by the kidneys via the same route as ^{99m}TcMAG and the favorable target to background ratio of the cysteine complex led the authors to suggest that it could be used as a renal function diagnostic agent.[80]

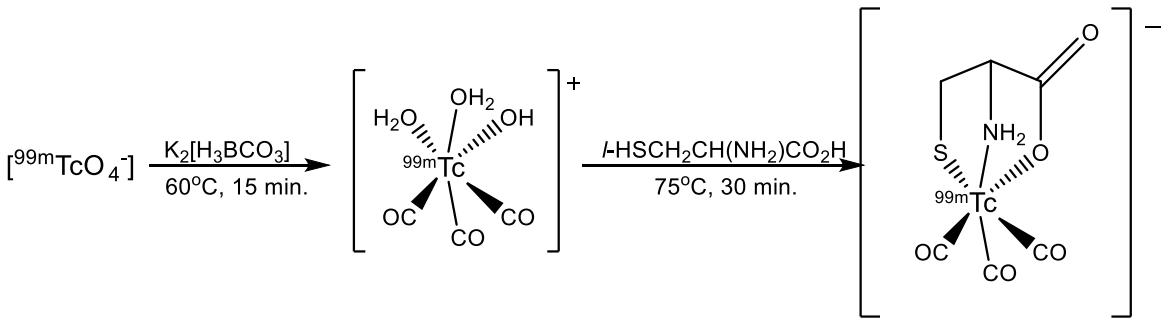

Scheme 1.6: Synthesis of ^{99m}Tc(I) tricarbonyl cysteine.[80]

Complexes of $M(CO)_3^+$ histidine have much longer stabilities than their cysteine counterparts and are perhaps the most studied amino acid ligands for the $M(CO)_3^+$ core. In addition to the tridentate and bidentate binding of histidine mentioned previously, the

monodentate binding of histidine to the $M(CO)_3^+$ core has also been studied. Protein side chains rich in histidine, such as His-tags, could singly replace each of the water ligands in $[M(CO)_3(OH_2)_3]^+$ preventing the crosslinking that can occur with monodentate ligands. The feasibility of using His-tags as a delivery system for the $M(CO)_3^+$ core was demonstrated by Herrick and co-workers using His-His-OH, as described previously.[65] In this instance each histidine residue bound one $Re(CO)_3^+$ core, which the authors note would be unlikely at tracer level concentrations of $Re(CO)_3^+$, as would be the case in clinical applications.[65] However, Waibel and coworkers showed that an antibody fragment synthesized with a His_5 tag and incubated with aqueous $[Tc(OH_2)_3(CO)_3]^+$ largely retained the $Tc(CO)_3^+$ core when incubated in human serum and solutions of excess histidine.[81] The $Tc(CO)_3^+$ core bound to the His_5 tag was active and stable in the murine animal model as well. The coordination sphere of the $Tc(CO)_3^+$ core bound to a His_5 tag is not precisely mapped and the authors hypothezise that it is likely a mixture of coordination modes, such as the two shown in Figure 1.16 below, in which neighboring histidines each bind to the $Tc(CO)_3^+$ core via their N_δ imidazole atoms. The labeled antibody showed no observable trans-chelation and retained its binding activity.[66, 81, 82]

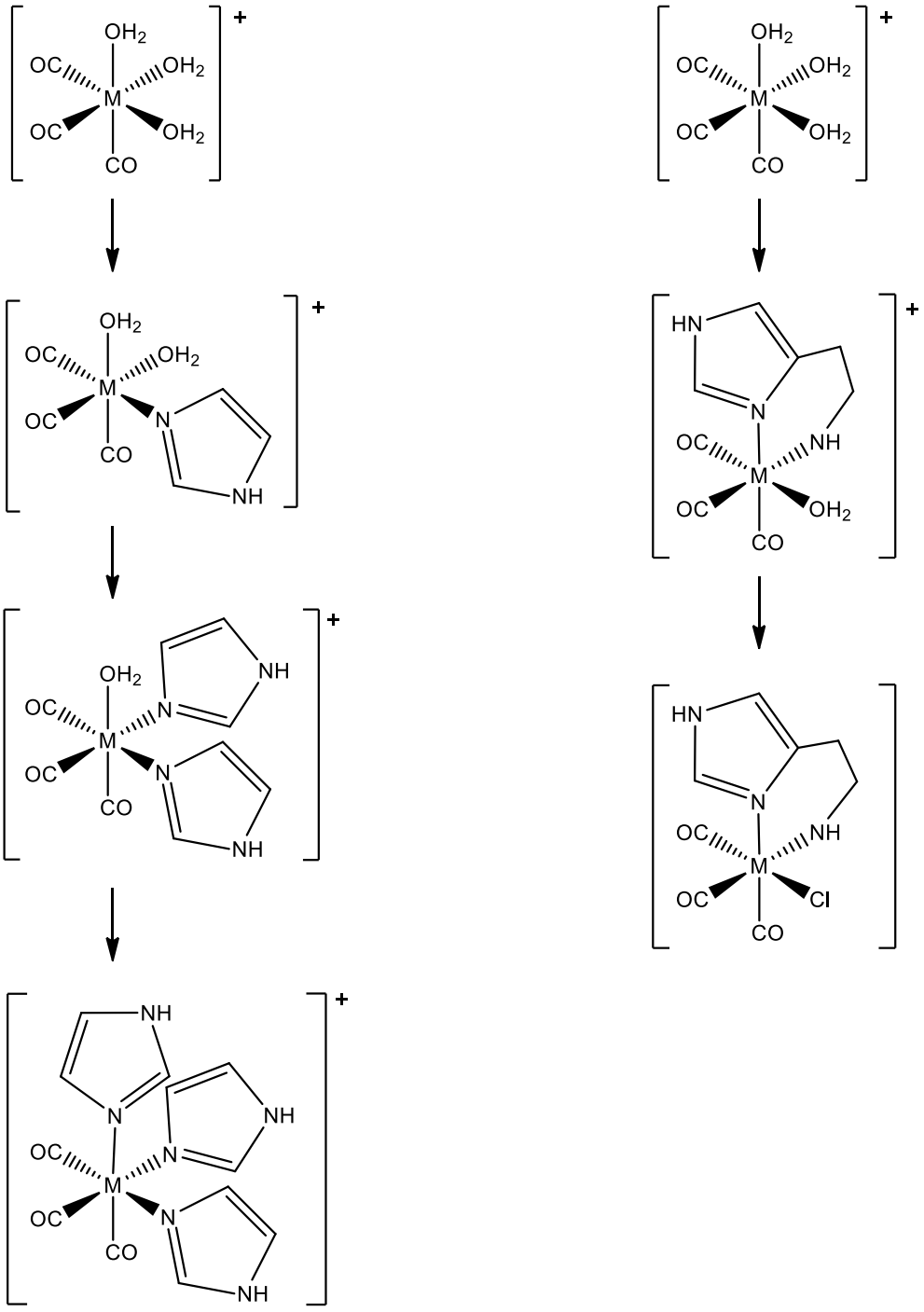

Figure 1.16: Proposed complex formation of the $M(CO)_3^+$ core with imidizole ligands analogous to the ones in a His tagged protein (a) and a bidentate coordination of $Re(CO)_3Cl$ with histamine, a model for an N-terminal histidine residue (b).[82]

The metal complexes of lysine and tyrosine with $^{99m}Tc(CO)_3^+$ have been synthesized and studied similarly to their cysteine and histidine counterparts.[83, 84] One study found that some amino acid complexation could be achieved simply by heating eluted pertechnetate with tyrosine and lysine, in the presence of stannous chloride, although with very low yields (22% and 15%, respectively).[84] Reducing the pertechnetate and production of the $[^{99m}Tc(OH_2)_3(CO)_3]^+$ precursor allowed complexation of these amino acids to increase to 95.5% and 89.5%, respectively, forming complexes with possible structures shown in Figure 1.17 below.[83, 84] As bidentate chelators, these complexes are less stable *in vitro* and *in vivo* as compared to their cysteine and histidine counterparts. *In vitro* protein binding studies showed significant binding to human serum albumin with up to 67% of the tyrosine complex bound in 20 minutes.[84] This value is much larger than the protein binding value for pertechnetate and only somewhat smaller than the protein binding value for the $[^{99m}Tc(OH_2)_3(CO)_3]^+$ precursor. The authors attribute the high protein binding values to the exchange of the remaining water on the amino acid complexes with binding sites on the protein.[84] Not surprisingly, the amino acid complexes also showed poor stability *in vivo*, characterized by accumulation in the blood, liver, kidneys and intestines of a rat animal model.[84] While the $[^{99m}Tc(CO)_3(OH_2)(Tyr)]$ and $[^{99m}Tc(CO)_3(OH_2)(Lys)]$ molecules were not fully characterized and do not fit the parameters normally desired for radiopharmaceutical synthesis,[23] modified versions of these amino acids are used in several approaches to radiopharmaceutical development, including the SAAC approach mentioned previously and other methods discussed elsewhere in this work.

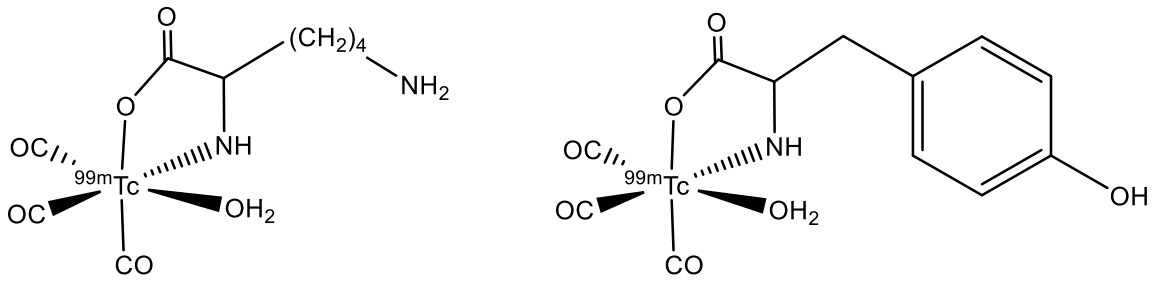

Figure 1.17: [^{99m}Tc(CO)$_3$(OH$_2$)(Tyr)] and [^{99m}Tc(CO)$_3$(OH$_2$)(Lys)].[84]

While histidine, cysteine, and other heteroatom containing amino acids are by far the most studied examples of amino acids bound to the M(CO)$_3^+$ core seen in the literature, additional examples of monodentate binding of amine nitrogens or carboxylate oxygens exist, as can be seen in the Re(CO)$_3$(Ala)$_2$Br complex shown in Scheme 1.5 below.[85] The interaction of a hard base ligand, such as the amine nitrogen of alanine, with the soft, Lewis acid metal center is considered a weak interaction and therefore not a viable ligation strategy for pharmaceutical development.[65]

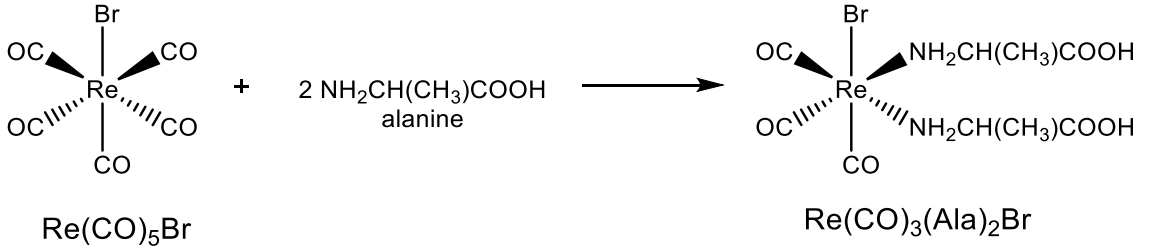

Scheme 1.7: Formation of Re(CO)$_3$(Ala)$_2$Br.[85]

Successful ligation of amino acids to the M(CO)$_3^+$ center more often relies on functionalization some part of the amino acid. The functionalization of lysine, discussed

previously, and shown in Figure 1.13, is the key to the SAAC approach to radiopharmaceutical development. Tyrosine has been functionalized at the phenolic oxygen to produce a tridentate ligand for $Tc(CO)_3^+$ and $Re(CO)_3^+$, and the resulting complexes can be seen in Figure 1.18.[86] These complexes are similar to a ^{18}F radiopharmaceutical and the authors state that the analogous $M(CO)_3^+$ pharmaceutical could prove useful for tumor imaging/therapy.[86] There are several examples in the literature of amino acids functionalized at the amino group for binding to the $M(CO)_3^+$ core. Glycine and derivatives of glycine have been functionalized at the amino group to produce a bidentate diphosphine chelating system as can be seen in Figure 1.18 below.[87] The resulting complexes are cytotoxic as will be discussed in the next section. Herrick and co-workers have functionalized the amino group of a variety of ester protected amino acids by reaction with pyridine-2-carboxyaldhyde to produce the strong binding diimine bidentate chelating amino acid derivatives. These derivatives then react with $Re(CO)_5Cl$ to form complexes of the type shown below in Figure 1.18.[88] The $Re(CO)_3^+$ complexed with the pyca functionalized H-β-alanine-OEt fluoresces at room temperature, a property the authors state could be exploited as a microscopy probe.[65, 88]

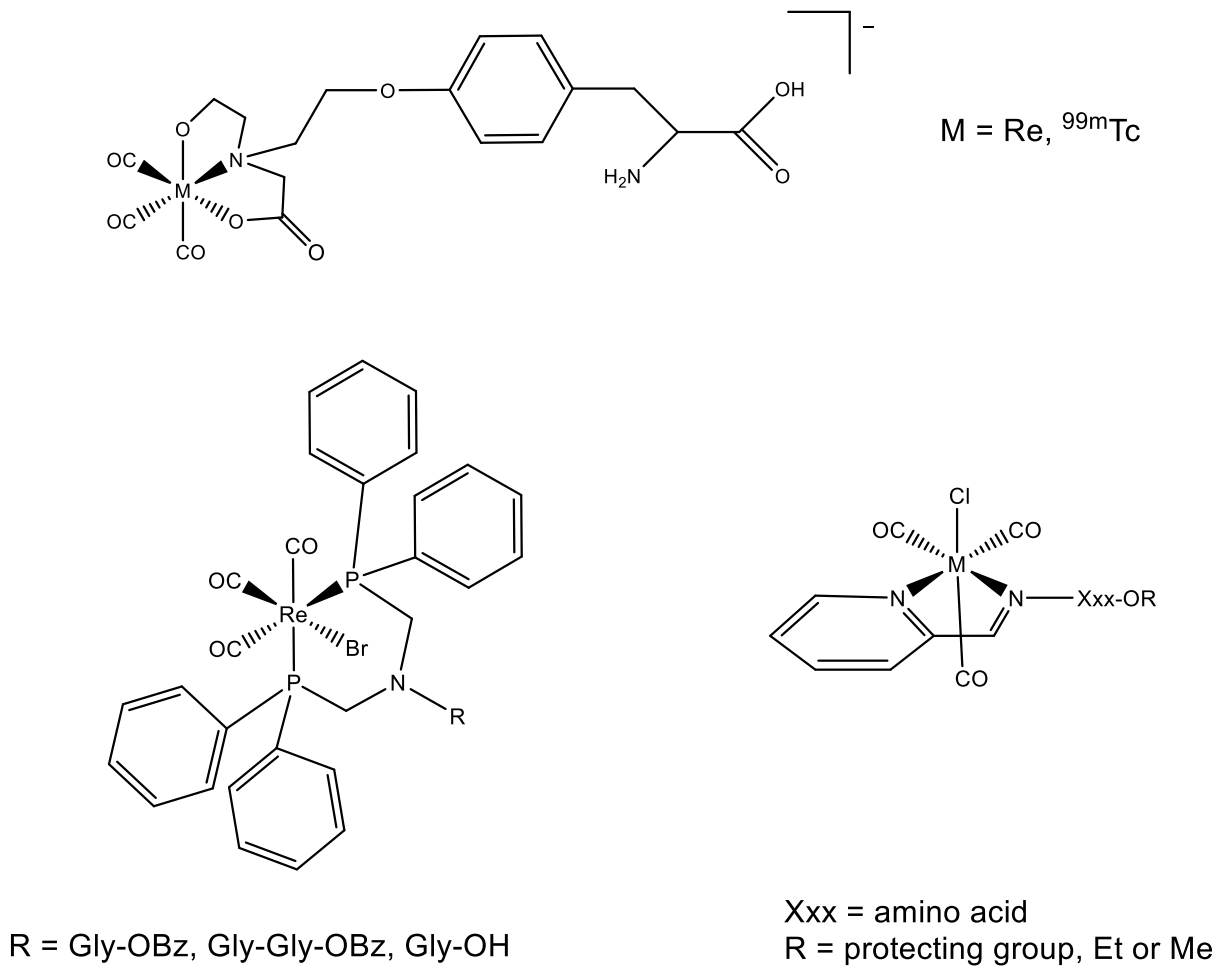

Figure 1.18: Examples of functionalized amino acids for chelation to the $M(CO)_3^+$ (M= Re, Tc) core[65, 86-88]

The Interaction of the $M(CO)_3^+$ Core with Nucleic Acids

Zobi and co-workers have investigated the binding of the $M(CO)_3^+$ core with DNA to determine if this binding could be an additional source of cytotoxicity which could be exploited in a therapeutic radiopharmaceutical application.[89-91] The authors likened this metal-induced cytotoxicity to the cytotoxicity of *cis*-diamminedichloroplatinum(II), or cisplatin, and other platinum (II) derivatives.[92] In light of this comparison, the cytotoxity

of platinum derivitives of the type *cis*-PtA_2X_2, where A_2 are two amines or a bidentate amine ligand and X is an anionic leaving group, merits a brief discussion here. While many of the cisplatin-type drugs are eliminated from the body after interaction with plasma proteins, the molecules that arrive at a cell membrane can diffuse across in their neutral state, such as *cis*-$[Pt(NH_3)_2Cl_2]$. Once inside a cell, the chlorides are replaced in the cytoplasm, which contains a much lower concentration of chloride compared to serum, by aqua and hydroxyl ligands. The now positively charged complex arrives at the nucleus due to the electrostatic interaction with the negatively charged chromatin. The toxicity of cisplatin type chemotherapeutics arises from the exchange of the aqua ligands with the N7 of purine nucleotides and the subsequent formation of 1,2-interstrand adducts of the N7 atoms on adjacent purine residues.[92] Additionally, for these platinum drugs to demonstrate anticancer activity, the amine ligand has to have more than one proton available to stabilize the DNA distortion with hydrogen bonding.[89] Cisplatin-type anticancer drugs can bind the two guanine nucleotides in either a head to head (HH) or head to tail conformation (HT).[89, 92] The HH conformer seems to be the indicator of anticancer activity. Lippard hypothesized that the HH conformer is recognized by a damage recognition protein, whose subsequent binding prevents DNA repair.[93] Marzilli, in a supporting hypothesis, stated that the HT conformer causes weaker binding of the same damage recognition protein, making the HT conformation easier to repair than the HH conformation.[94]

This mode of toxicity is similar to the one hypothesized for $Re(CO)_3^+$ complexes such as bis(diphenylphosphinomethyl)amine tricarbonylrhenium(I) shown in Figure 1.18.[87] These complexes proved to be very stable in aqueous solution and were toxic to several fast-dividing, cancer cell lines while relatively non-toxic in a non-cancerous cell

line control. These rhenium complexes were found to interfere with nucleic acid metabolism at multiple enzyme sites in L1210 lymphoid leukemia cell and caused DNA strand sission in a 60 minute incubation. The authors hypothesize two causes for this toxicity. The toxicity could be attributed to bromide substitution and subsequent coordination of the metal complex with N7 of the purine DNA bases, as is the case with cisplatin type compounds. However, since the stability of the [$Re(CO)_3$(diphosphine)] complex showed marked stability in aqueous solution, this complex would only have one bromide ligand available for substitution. The fate of the complex could also be coordination to an amino acid side chain on a protein, which would then promote cell death through some other pathway.[87]

Alberto and co-workers further probed the binding of $M(CO)_3^+$ complexes with the derivatives of the purine base guanine, such as 9-methyl guanine (9-MeG), and were able to produce X-ray structures of the $M(CO)_3^+$ cores coordinated to the guanine derivatives via their N7 atoms as shown below in Figure 1.19.[89, 91] The two bases can bind in the head to tail or the head to head conformations responsible for toxicity in the analogous binding modes of cis-Pt (II) complexes, mentioned previously.[89] Each conformation is stabilized by a single hydrogen bond, such as is seen in the analogous structures of *cis*-$[Pt(NH_3)_2(9\text{-}EtG)_2]^{2+}$.[95] The rate of guanine binding for the $Re(CO)_3^+$ complex was also similar to the binding rate of guanine to an active form of cisplatin, $[Pt(NH_3)_2(OH_2)_2]^{2+}$.[89, 91] Not only does this suggest a similar mode of toxicity for certain rhenium compounds and cisplatin, but also that certain rhenium compounds could have both chemotherapeutic and therapeutic radiopharmaceutical applications.[87, 89, 91]

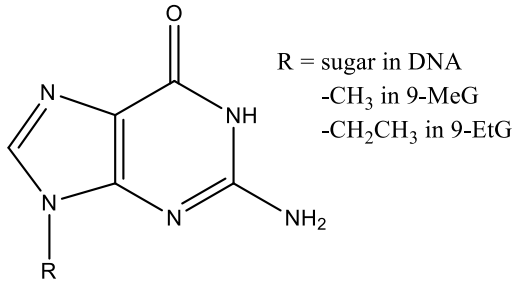

Guanine

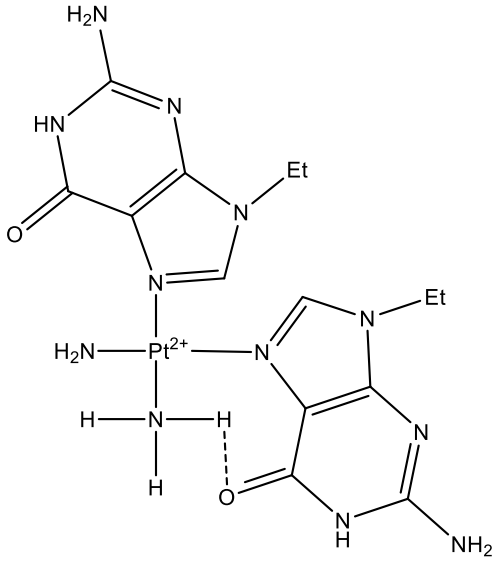

H-H cis$[Pt(NH_3)_2(9\text{-}EtG)_2]^{2+}$

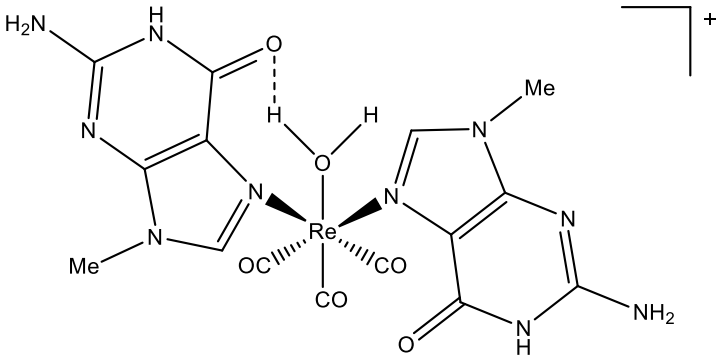

H-T $[Re(CO)_3(OH_2)(9\text{-}MeG)_2]^{+}$

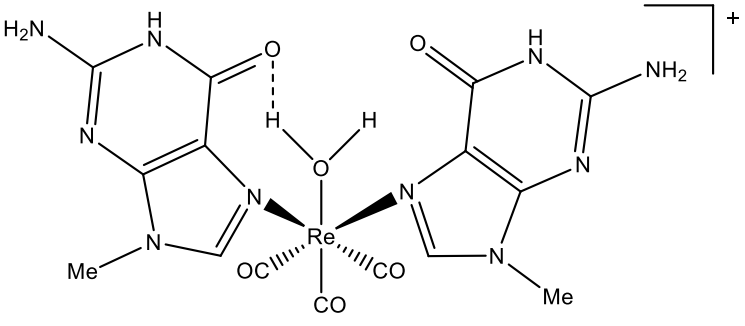

H-H $[Re(CO)_3(OH_2)(9\text{-}MeG)_2]^{+}$

Figure 1.19: HH and HT conformations of guanine derivatives bound to $Re(CO)_3^{+}$ along with HT *cis*-$[Pt(NH_3)_2(9\text{-}EtG)_2]^{2+}$.[89]

The Interaction of the $M(CO)_3^+$ Core with Peptides

The attachment of the $M(CO)_3^+$ core to peptides is a desirable route to radiopharmaceutical development for several reasons. Peptides are involved in more biological processes than any other class of molecule and can function as neurotransmitters, neuromodulators, cytokines, hormones and growth/growth inhibition factors.[72] Biologically relevant peptides are smaller and more easily prepared than proteins or monoclonal antibodies, and many have higher receptor affinity.[72] High target tissue signal to background ratios can be achieved with peptide based radiopharmaceuticals because of their fast clearance from the blood.[72, 96] Peptides tend to have low toxicity because of their relationship to naturally occurring compounds and are easily eliminated from the body.[72, 96, 97] While native peptides are rapidly metabolized by peptidases in the blood, the smaller size of these species allows for modification by solid phase synthesis to produce peptide, and binding sequence only, analogs that can better withstand enzymatic breakdown.[72, 96, 97] Labeling of peptides can often occur during synthesis of the peptide with solid phase synthesis methods.[72] Many peptides are large enough that the addition of the metal or metal chelate does not significantly affect their distribution.[98] In addition, while other ^{99m}Tc cores can be large, hydrophilic, and react with the cysteine disulfide bonds present in many peptides, the $M(CO)_3^+$ core is small, lipophilic, and largely unreactive with cysteine (relative to other amino acids).[65] Thus, the attachment of $^{99m}Tc(CO)_3^+$ and $^{186/188}Re(CO)_3^+$ with biologically active peptides is a convenient route to diagnostic and therapeutic radiopharmaceutical development, respectively.

There are several examples in the literature of peptide based radiopharmaceuticals that incorporate the $M(CO)_3^+$ core. One of the most studied peptides used in radiopharmaceutical development is somatostatin, which is a 14 amino acid cyclic neuropeptide with a host of regulatory functions, including the inhibition of human growth hormone, insulin, glucagon, thyrotropin, and other hormones.[72, 98] In addition, somatostatin receptors are overexpressed on a variety of tumors, including cancers of the gastroenteropancreatic system, brain, breast, kidney, lymphatic system and certain lung tumors.[98] Imaging the somatostatin receptor with a somatostatin analog was first accomplished in 1976 and was a research target of increasing interest when somatostatin was later found to inhibit tumor growth.[72] The fast degradation of somatostatin *in vivo* limited its effective use as an imaging (or treatment) tool until a variety of degradation resistant analogs were developed, starting in the late 1980's.[72, 98]

Octreotide is an 8 amino acid, degradation resistant analog of somatostatin that retains somatostatin's ability to inhibit tumor growth. These peptides can be seen below in Figure 1.20. Labeling octreotide with ^{111}In allowed imaging of tumor therapy and led to the development of ^{111}In-diethylenetriaminepentaacetic acid (DTPA)-octreotide (OctreoScan®), mentioned previously, and shown in Figure 1.1.[23] ^{111}In-(DTPA)-octreotide was the first peptide-based imaging agent approved by the FDA, in 1994.[98, 99] Despite the success of ^{111}In-DTPA-octreotide, the lower cost and greater accessibility of ^{99m}Tc has motivated the search for ^{99m}Tc labeled somatostatin analogs, which led to the development and subsequent approval of ^{99m}Tc-depreotide, sold under the brand name NeoTect®.[100] Rhenium analogs of ^{99m}Tc-depreotide, like [^{188}ReO]P2045 shown below, and other

somatostatin analogs are also currently being studied for treatment of cancers that overexpress somatostatin receptors.[101, 102]

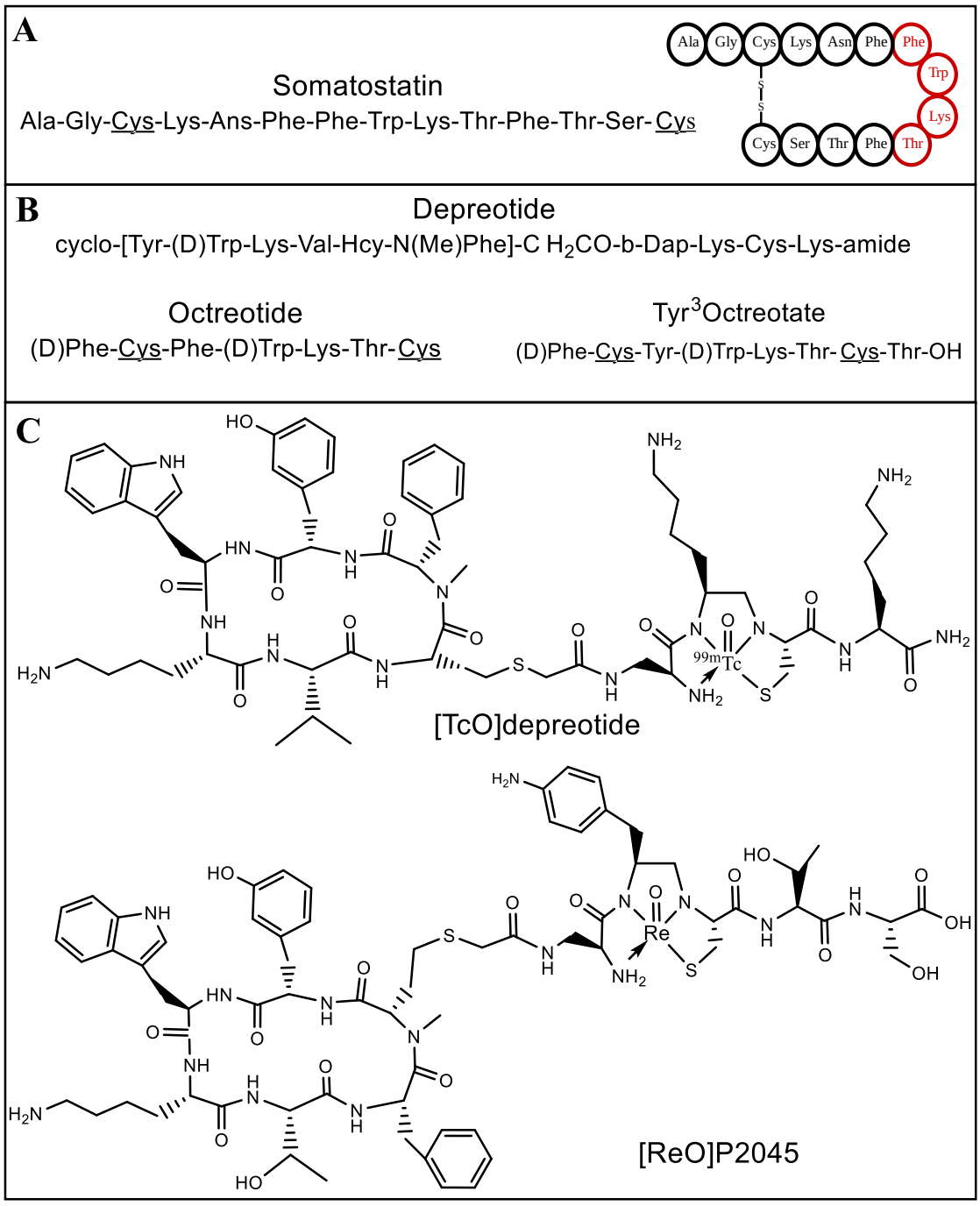

Figure 1.20: The amino acid sequence of somatostatin and structural diagram of somatostatin, showing the di-cysteine bond and the receptor binding motif, highlighted in red (A). Somatostatin analogs (B). ^{99m}Tc-depreotide and ^{188}ReO]P2056 (C).[10, 101-103]

The $^{99m}Tc(CO)_3^+$ core is ideal for labeling somatostatin analogs, since it does not interact with cysteine disulfide bonds, which are an integral part of the somatostatin peptides.[10] Depreotide, discussed previously, circumvents the tendency of Tc(V) and Re(V) to break cysteine disulfide bonds by replacing those residues with a cyclic peptide artificially bound to a linear peptide that chelates the metal.[103] However, this lowers the binding affinity of depreotide for the somatostatin receptors, narrowing the imaging efficacy of ^{99m}Tc-depreotide to only certain tumors, such as small cell lung cancers.[101, 102] A modified version of octreotide, called octreotate and shown in Figure 1.20 B, in which the 3rd amino acid is exchanged with tyrosine, has also shown to be resistant to enzymatic breakdown. This somatostatin analog has been labeled with $[^{99m}Tc(CO)_3]^+$ via bidentate chelators such as histidine and tridentate chelators such as N_α-Ac-His. These functionalized octreotate analogs can be seen in Figure 1.21 below.[10] Specifically, the tridentate coordination complex, $[^{99m}Tc(CO)_3$-N_α-Ac-His-^{0}Tyr^{3}octreotate$]^0$ showed excellent *in vivo* imaging pancreatic tumors in a rat model.[10]

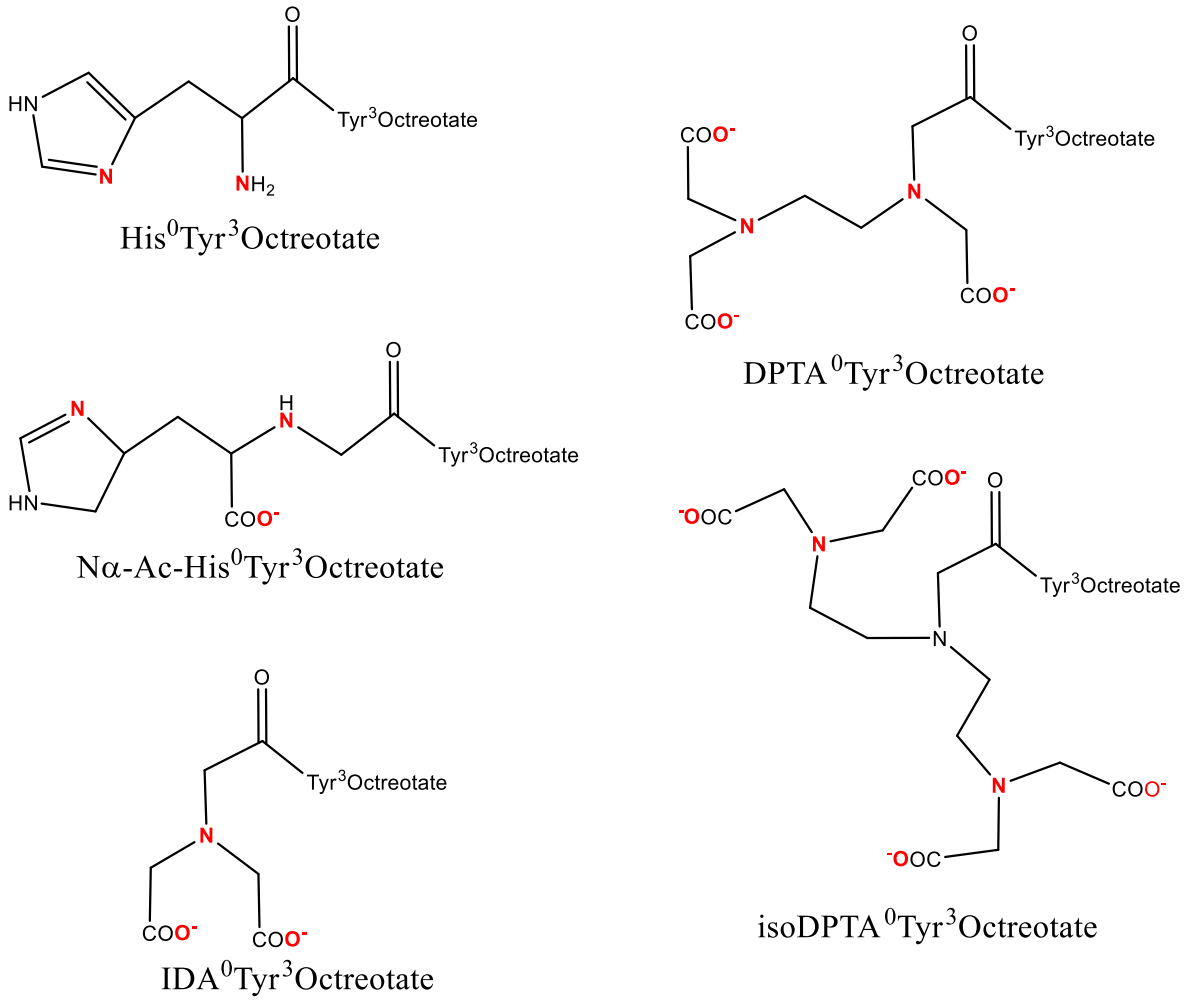

Figure 1.21: Octreotate analogs functionalized for ^{99m}Tc-complexation (red indicates proposed metal binding sites).[10]

Another widely studied peptide that has been a target for $M(CO)_3^+$ labeling is neurotensin. Neurotensin (pGlu-Leu-Tyr-Glu-Asn-Lys-Pro-Arg-Arg-Pro-Tyr-Ile-Leu, underlined portion denotes receptor binding motif) is a neuropeptide that acts as a neurotransmitter and a local hormone.[97] It is involved in vasodilation, hypothermia, intestinal function, and the regulation of dopamine. Neurotensin receptors are overexpressed on several different types of cancers, including pancreatic tumors, making neurotensin a viable targeting moiety for the development of $M(CO)_3^+$

radiopharmaceuticals of both the diagnostic and therapeutic variety.[97, 104] The binding motif, consisting of amino acids 8 through 13, abbreviated NT(8-13), is susceptible to enzymatic degradation at three sites; Arg^{8}-Arg^{9}, Pro^{10}-Tyr^{11}, and Tyr^{11}-Ile^{12}.[97] Substitution at one or more of these sites has led to the development of numerous NT(8-13) analogs.[96, 97, 104, 105] Many of these have been functionalized with Nα-Ac-His for chelation to the $^{99m}Tc(CO)_3^+$ core, as shown in Figure 1.22 below.[96, 97, 105] The simplest of these analogs, [$^{99m}Tc(CO)_3$](Nα-Ac-His)-Ac-NT(8-13) contains a single substitution, tertiary leucine (Tle) for isoleucine. However the tumor uptake of this complex is quite low; 0.33% injected dose per gram of tumor tissue (% iD/g) with a standard deviation of 0.10%.[98] The complex with the highest amount of tumor uptake is $^{99m}Tc(CO)_3$NT-XI, at 9.1% iD/g.[98] This complex has undergone human testing and did image pancreatic tumors that expressed the neurotensin receptor, albeit with high kidney and intestinal uptake of the tracer.[106] The complex$^{99m}Tc(CO)_3$NT-XII also has encouraging tumor uptake in animal models; up to 6.26% iD/g.[105]

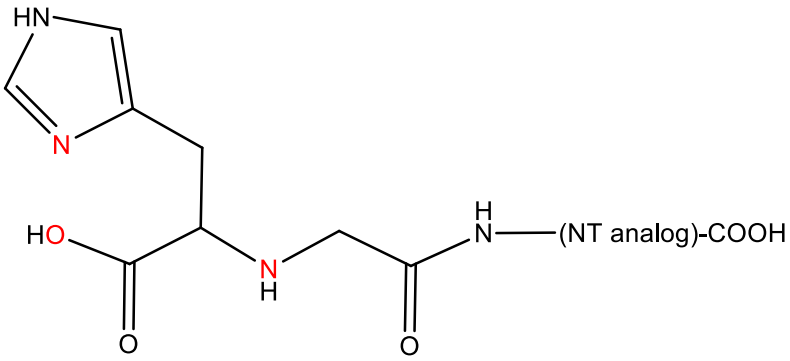

NT Analogue	Sequence
NT(8-13)	Arg-Arg-Pro-Tyr-Ile-Leu
NT-XI	(Nα-His)Ac-Lys-Ψ(CH_2NH)-Arg-Pro-Tyr-Tle-Leu
NT-XII	(Nα-His)Ac-Arg-(N-CH_3)-Arg-Pro-Tyr-Tle-Leu
NT-XIII	(Nα-His)Ac-β^3Arg-Arg-Pro-Tyr-Tle-Leu
NT-XVIII	(Nα-His)Ac-Lys(3,4,5-trihydroxy-1-cyclohexene-1-carboxylic acid)-Arg-(N-CH_3)-Arg-Pro-Tyr-Tle-Leu

Figure 1.22: Neurotensin analogs functionalized with (Nα-Ac-His)-Ac for binding to the $M(CO)_2^+$ core.[96, 97, 105]

Bombesin is a 14 amino acid peptide with a high affinity for the gastrin-releasing peptide receptor (GRPR) which is over-expressed on small cell lung cancers, cancers of the breast, prostate, pancreas, colon, and stomach, and glioblastoma tumors.[107] Labeled bombesin analogs are especially studied in relation to prostate cancer, as current detection methods rely on the ^{111}In tagged antibody ^{111}In-capromab (ProstaScint®) which only detects these cancers with up to 75% accuracy.[107] Many bombesin analogs have been developed to resist enzymatic breakdown in the body and functionalized for labeling with the $M(CO)_3^+$ core. One such sequence, representing the bombesin sequence from amino acids 7 through 14, BBN(7-14) was first labeled with the 99m$Tc(CO)_3^+$ core by Schubiger and co-workers via the Nα-Ac-His linking moiety dicussed previously and shown below in

Figure 1.23.[108] Despite being relatively susceptible to proteolytic cleavage, a tumor to blood ratio of 2.7 could be visualized in the mouse model for the [^{99m}Tc(CO)$_3$]Nα-Ac-His-Ac-BBN(7-14) complex.[108]

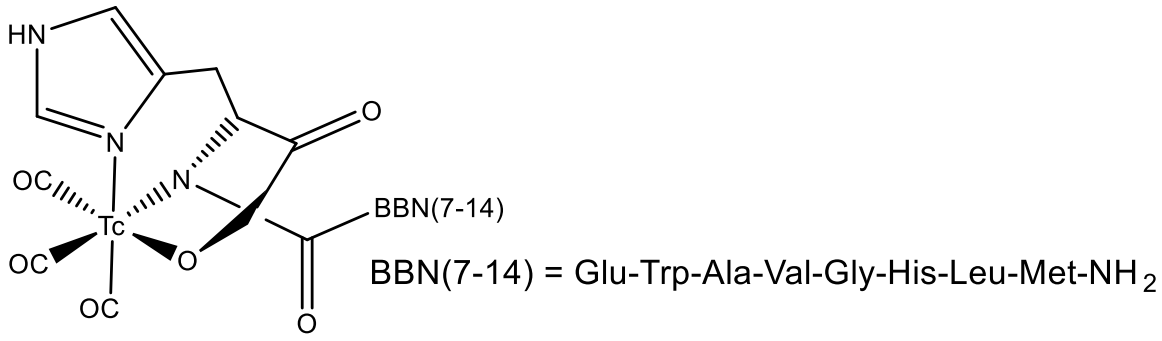

Figure 1.23: [^{99m}Tc(CO)$_3$]Nα-Ac-His-Ac-BBN(7-14) and BBN(7-14).[108]

Because the Nα-Ac-His linking moiety was the source of the *in vivo* instability of this complex, a variety of other linkers have been used to chelate Tc(CO)$_3^+$ to BBN(7-14) in the search for an ideal radiopharmaceutical. Some of these are shown in Figure 1.24. PADA-AVA (2-picolylamine-N,N-diacetic acid and an aminovaleric acid spacer),[109] DTMA (2-(N,N'-bis(tertbutoxycarbonyl)diethylenetri-amine acetic acid),[110] Dpr (diaminopropionic),[111] and pryazolyl linkers,[112] have been used to make M(CO)$_3$-BBN(7-14) conjugates that are more resistant to enzymatic degredation. The [^{99m}Tc(CO)$_3$]PADA-AVA-BBN(7-14) complex had a high affinity for the bombesin receptor in the tumor and pancreas of a mouse model bearing prostate tumors.[109] The [^{99m}Tc(CO)$_3$]L-Dpr-Ser-Ser-Ser-BBN(7-14) (L=H_2O or P(CH_2OH)$_3$) complex has reasonably high tumor uptake and superior in vitro stability compared to Tc(V) complexes also being studied to image prostate cancer.[111] The tumor retention of this complex in the mouse model was also the highest of the complexes shown here, which led the authors to synthesize the ^{188}Re analog.

Long term retention of this complex in prostate tumor cells *in vitro* and in the mouse model suggests its use as a therapeutic radiopharmaceutical.[111] While the [^{99m}Tc(CO)$_3$]DTMA-βAla-BBN(7-14) showed similar uptake characteristics to the complexes formed with PADA-AVA and Nα-Ac-His-Ac linkers, tumor uptake for this molecule in the mouse model was very low, which the authors attribute to carbon- nitrogen bond cleavage on the pendant arm of this purely aliphatic linker or distribution properties arising from the lipophilic nature of the core and high liver absorption.[110] The pyrazolyl linker used in [^{99m}Tc(CO)$_3$]pyrazolyl-βAla-BBN(7-14) showed a similar drop in uptake from tissue culture to the animal model, although the authors comment that results of studies using animal models for BBN(7-14) receptor binding do not always correlate well to human biodistribution of these complexes.[112] In summation, the stability and ability to bind to the bombesin receptor shown by all four of these complexes are promising results in an arena where no ideal diagnostic or therapeutic radiopharmaceuticals exist.[108-112]

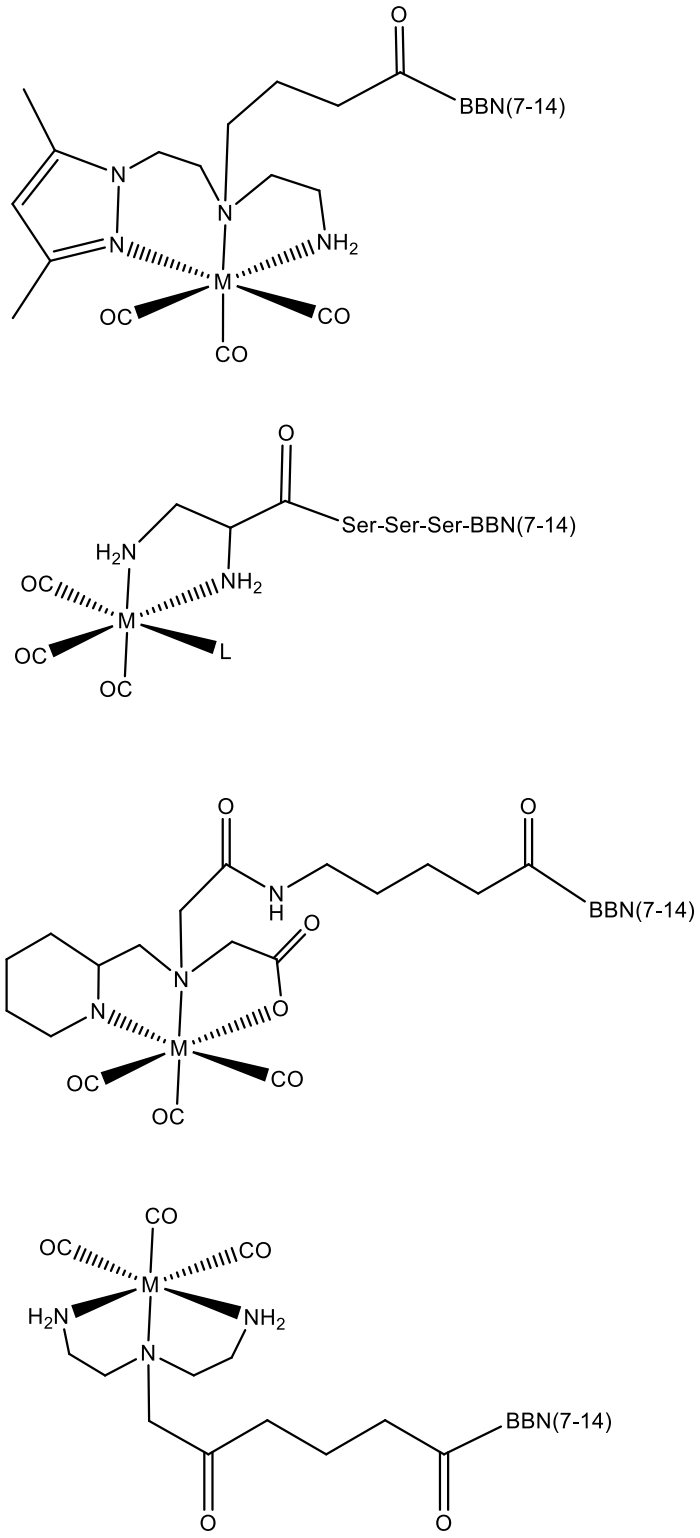

Figure 1.24: Four bombesin receptor targeting potential radiopharmaceuticals incorporating the $M(CO)_3^+$ core (M= ^{99m}Tc, ^{188}Re).[108-112]

The Interaction of the $M(CO)_3^+$ Core with Proteins

Attachment of the $M(CO)_3^+$ (M= ^{99m}Tc or $^{186/188}$Re) core to proteins is an attractive synthetic goal due to the wide variety of possible applications for these conjugates, including the use of the $Re(CO)_3^+$ core as a heavy atom phasing agent,[113] protein-$[Re(CO)_3(diimine)]^+$ conjugates to study electron transfer,[77, 114] and both $[^{99m}Tc(CO)_3]^+$ and $[^{186/188}Re(CO)_3]^+$ protein complexes as targets in diagnostic and therapeutic radiopharmaceutical development, respectively[10, 65, 73, 79, 82, 115-118]. Additionally, the conjugates formed when proteins are incubated with the $[M(CO)_3(OH_2)_3]^+$ precursor offer insight into the biological processing of this metal core. The methods of attaching $M(CO)_3^+$ cores to proteins vary and include all of the previously described methods of attaching these cores to amino acids and peptides, including direct labeling via amino acid side chains, and linking via BFCAs or functionalized amino acids.

The preferential binding of the $M(CO)_3^+$ cores to histidine residues, as mentioned previously, suggests that $Re(CO)_3^+$ could also be used as a phasing agent to aid in the structural elucidation of proteins. The $Re(CO)_3^+$ core fits all the requirements of an ideal phasing agent.[113] It is a heavy atom, like the more commonly used iron and lead phasing agents, but is relatively non-toxic. The $Re(CO)_3^+$ core is water soluble and is stable in biological media, as mentioned above. Additionally, the binding of the $Re(CO)_3^+$ core does not alter the overall structure or activity of proteins, as will be shown in the examples below.

The study of electron transfer, using $Re(CO)_3^+$-protein conjugates has been pioneered by Gray and co-workers using copper and zinc azurin proteins with histidines

expressed at varying positions for metallation with the $Re(CO)_3^+$ core. These proteins were all metallated through the histidine imidazole nitrogen with $[Re(CO)_3(L)]^+$ (L= 1,10-phenathroline (phen), 4,7-Me_2phen, and other phen based ligands) by allowing the protein and *fac*-$[Re(CO)_3(L)(H_2O)]^+$ to incubate for 3 weeks. The resulting proteins were able to be crystalized and structurally characterized via X-ray diffraction. The numerous positioned histidines, and thus the $Re(CO)_3^+$ units, are designed to study the effect of the route of the electron transfer, from the copper to the rhenium, among other properties of electron transfer. Tyrosine and tryptophan residues were also engineered at specific locations in the azurin proteins studied since they can potentially participate in electron transfer.[74, 77, 78, 114, 119, 120]

The direct labeling approach has been used to label single-chain antibody fragments (scFvs) with the $M(CO)_3^+$ core. Availability from combinatorial libraries and high tumor to background ratios are a couple of the reasons that labeled scFvs are attractive starting points for radiopharmaceutical development. These proteins are especially suitable for labeling with the $M(CO)_3^+$ core, since the higher oxidation state ^{99m}Tc normally used to label these proteins can result in unspecific coordination to cysteine residues resulting interference with disulfide bridges. This interference can cause misfolding and loss of biological activity in the scFvs. These scFvs can be conveniently labeled with the $M(CO)_3^+$ core via the His tags, mentioned previously, and shown in Figure 1.16. Incubation of the scFvs with $[^{99m}Tc(CO)_3(OH_2)_3]^+$ at 37 ˚C for 15 minutes results in greater than 90% yield of the radiolabeled scFvs which is especially significant compared to the yield of just 16% and 25% for scFvs with no His tag or only endogenous histidines, respectively.

Labeling scFvs and larger antibodies with $^{188}Re(CO)_3^+$, via His-tags or endogenous histidines can be a convenient route to therapeutic radiopharmaceutical development. Antibiodies are good candidates for labeling with an isotope that emits therapeutic radiation because they exhibit slower elimination from the body compared to smaller proteins and peptides, which is a necessary feature allowing the cytotoxic radiation to accumulate at the disease site.[10] One such antibody is the anti-MUC1 antibody. The production of MUC1 mucin is increased in bladder cancer.[116] Murray and co-workers compared the labeling efficacy of $^{188}Re(CO)_3^+$ for anti-MUC1 antibodies and the traditional 2-mercaptoethanol reduced and labeled $^{188}Re(V)$.[116] *In vitro* results showed 80% retention of the $^{188}Re(CO)_3^+$ labeled anti-MUC1 antibody at 48 hours compared to 20% retention of the $^{188}Re(V)$ labeled species, suggesting that the $^{188}Re(CO)_3^+$ labeled anti-MUC1 antibody could be used as a possible therapeutic radiopharmaceutical.[10, 116]

Stable protein-$[^{99m}Tc(CO)_3]^+$ conjugates can be accomplished with as few as three histidine residues in a row, as shown by Tait and co-workers in their work with the protein Annexin V.[118] Annexin V has a high affinity for phosphotidyl serine, which is expressed on the exterior of the cell membrane in the early stages of apoptosis.[79, 118] Thus, this protein can be used to detect apoptosis and is used in the clinic to measure cell death during chemotherapy. Direct labeling of annexin V, which contains 3 endogenous histidine residues, with $[^{99m}Tc(CO)_3]^+$ gives a radiolabeled product yield of only 40%. Addition of a His_3 or His_6 tag to the N-terminus of these proteins did not alter their bioactivity and allowed site-specific coordination of the $[^{99m}Tc(CO)_3]^+$ core.[118] Alternatively, treatment of annexin V with commercially available 2-iminothiolane, which reacts with the free amino group in the lysine amino acid side chain, results in the formation of a mercaptobutyrimidyl

group, which is then available for complexation to the $[^{99m}Tc(CO)_3]^+$ core.[79] Biechlin and co-workers found that, while only 1 of 22 lysine residues in annexin V were available for functionalization, radiolabeled product yields using this method increased to 55% without the use of His-tags. This approach is shown below in Figure 1.25.[79]

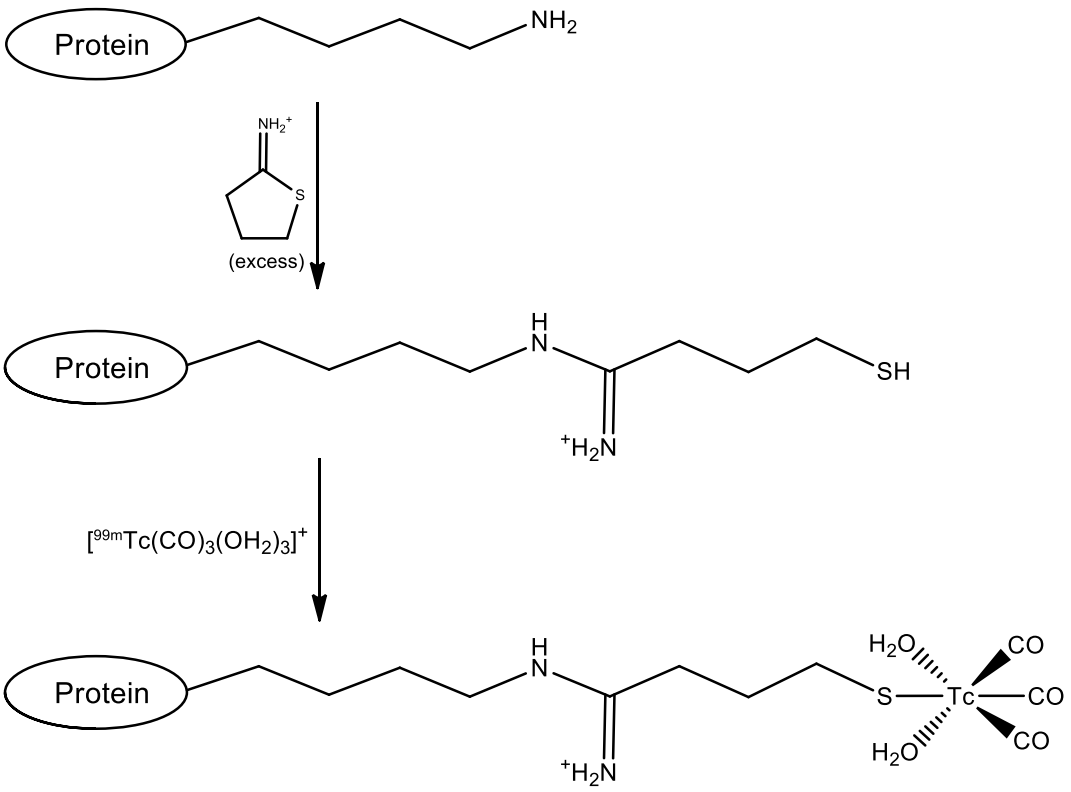

Figure 1.25: Functionalization of lysine side chain of annexin V for labeling with the $[^{99m}Tc(CO)_3]^+$ core.[79]

A direct labeling approach was exploited to label surfactant protein B, also without the use of a His-tag. Surfactant protein B has been used in the clinic to treat patients with acute respiratory distress syndrome with mixed results. In order to study the spreading properties of this protein and thus its ability to reach and treat all areas of the lung, the authors of this study labeled this protein with $[^{99m}Tc(CO)_3]^+$. This extremely hydrophobic

protein is particularly suited to the lipophilic nature of the $[^{99m}Tc(CO)_3]^+$ core. The mixture of surfactant protein B and $[^{99m}Tc(CO)_3(OH_2)_3]^+$ did indeed produce a single, labeled product with a 50% yield. More importantly, introduction of the metal core had no effect on the dimeric structure or the properties of the protein. While the authors didn't structurally characterize the interaction, they speculate that the $[^{99m}Tc(CO)_3(OH_2)_3]^+$ compound could have bound to the imidazole nitrogen in the side chain of the single histidine residue present in this protein, which would account for the presence of a single labeled product. The labeled surfactant protein B could be used to study administration techiques for the introduction of this protein into the lungs.[73]

1.8 Summary

Since the introduction of ^{99m}Tc Sestamibi in the 1980's by Davidson and coworkers,[121] radiopharmaceuticals incorporating ^{99m}Tc have been a mainstay of nuclear medicine. Yet, the desire to diagnose disease states earlier, with greater accuracy, drives many groups to continue investigation into new, targeted radiopharmaceuticals. With the development of the $^{99m}Tc(CO)_3^+$ and $^{188/186}Re(CO)_3^+$ cores, a new branch of radiopharmaceutical research is possible. ^{99m}Tc and $^{188/186}Re$ pharmaceuticals featuring these cores take advantage of the many favorable characteristics of the parent $[M(CO)_3(OH_2)_3]^+$ (M= Tc, Re) complex mentioned previously; such as its aqueous preparation, tightly binding d^6 coordination environment, and small size.[65] Despite the many advances made in this field, mentioned in this introduction and present in the literature, to date, no radiopharmaceuticals featuring this complex have made it to clinical

use. While some of the delay can be attributed to the difficulties of drug development, kit production, and registration procedures,[66] the lag in the development of pharmaceuticals featuring the $M(CO)_3^+$ core can also be attributed to the need to better understand the basic bioorganometallic chemistry of the $M(CO)_3^+$ cores. The following chapters explore some basic properties of $[Re(CO)_3(OH_2)_3]^+$; the tightly binding 1,1,1-trisaminomethylethane ligand and the toxicity of the $[Re(CO)_3(TAME)]X$ (X= Cl^-, Br^-, NO_3^-, PF_6^-, ClO_4^-) complexes in cell culture, the interaction of $[Re(CO)_3(OH_2)_3]^+$ with the protein lysozyme, and preliminary investigations of this core with other ligand systems and biomolecules of interest.

CHAPTER II

THE TOXICITY OF TRIPODAL TRICARBONYL RHENIUM COMPLEXES AS RADIOPHARMACEUTICAL MODELS

2.1 Introduction

Non-invasive imaging techniques play an increasing role in the diagnosis of disease states, and this has spurred the continuing development of new imaging agents. Radiological techniques, such as SPECT- and PET-based methods, require the use of radionuclide-based drugs, and the most common nuclide currently used in the clinic is the ^{99m}Tc isotope.[18, 22, 23, 27] Since the development of Cardiolite® (Sestamibi), new generations of ^{99m}Tc drugs have appeared in the clinic, and current research is focusing on developing the chemistry of the $Tc(CO)_3^+$ unit as the nuclide containing moiety.[38, 122-124] Imaging agents containing this fragment can be readily generated in aqueous solution from the $[Tc(H_2O)_3(CO)_3]^+$ ion, which can be synthesized in one step from TcO_4^- solutions by use the IsoLink® kit developed by Mallinkrodt. However, in spite of the potential importance of this species, much of the fundamental chemistry and biological processing of $[Tc(H_2O)_3(CO)_3]^+$ and $Tc(CO)_3^+$-based compounds has yet to be elucidated.

One advantage for the development of $Tc(CO)_3^+$ based drugs is that the chemistry of this moiety can be readily modeled by using the analogous, non-radioactive $Re(CO)_3^+$ fragment.[24] Although the chemistry of the two elements do differ slightly, the chemistries

of both metals in the +1 oxidation state are similar, and this is particularly true for the $M(CO)_3^+$ moieties.[125] Both ions form facial octahedral geometries upon complexation, and the resultant complexes are typically quite inert to substitution. The fundamental chemistry of the $Re(CO)_3^+$ fragment has recently been investigated and complexes that exhibit remarkable stabilities in aqueous solution, even in the presence of competing biological ligands, such as histidine and cysteine have been developed.[62, 126, 127] Ziegler *et al*. has reported on the structures and stabilities of several tripodal complexes of $Re(CO)_3^+$, and have found that a complex incorporating the 1,1,1-trisaminomethylethane (TAME) ligand, $[Re(TAME)(CO)_3]^+$ (Figure 2.1) showed no degradation under biologically relevant challenge conditions.[67]

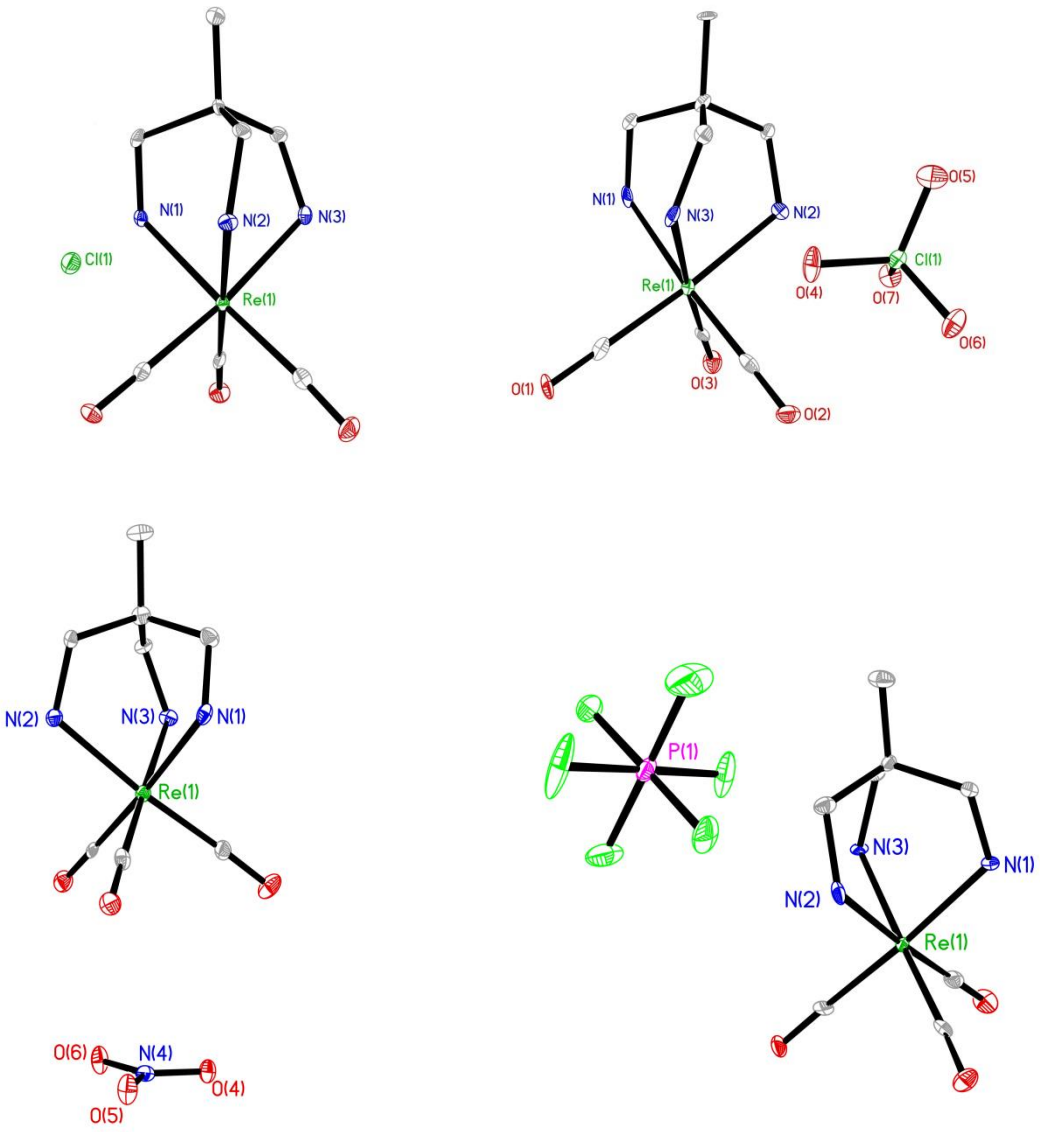

Figure 2.1: The structures of the $[Re(CO)_3(TAME)]X$ salts where X = Cl^- (**2**, top left), ClO_4^- (**3**, top right), NO_3^- (**4**, bottom left) and PF_6^- (**5**, bottom right) with 35% thermal ellipsoids. Hydrogen atoms and the solvate waters in **2** have been omitted for clarity.

The chemical inertness of the $[Re(TAME)(CO)_3]^+$ ion indicates that this complex should exhibit little or no toxicity. Since the complex is inert to substitution and unreactive to either histidine or cysteine, we wanted to continue to examine the effect of this complex on living cells. In general, the toxicity of radionuclide-containing compounds is not as

important as in other imaging agents.[10] Typically, the doses of the drug are so low that only the radioactivity is of concern, and clearly the diagnostic benefit of the imaging technique outweighs the radiological risk. However, any demonstrable lack of toxicity due to inertness does bode well for rapid and complete clearance from the patient, which is a requirement for any radionuclide-based imaging agent.[128]

This chapter reports the synthesis, characterization, and *in vivo* cellular studies of a series of tri-carbonyl 1,1,1-trisaminomethylethane (TAME) rhenium(I) salts. The salts incorporate both halide (chloride and bromide) and non-coordinating anions (nitrate, hexafluorophosphate, and perchlorate). Our characterization of these salts indicate that the identity of the anions does not affect the structures of the rhenium complex cations. In two separate cell line studies, no appreciable toxicity was observed, with the exception of the bromide salt. The bromide salt did increase mortality in the vascular smooth muscle cells, but we propose that this toxicity resulted from the halide anion rather than the complex itself.

2.2 Experimental

General Materials/Methods: All reagents and solvents were purchased from Sigma, Aldrich, Acros Organics or Strem and used without further purification. Compound **1** was prepared as previously described,[67] and as shown in Scheme 2.1, below. Sterile cell culture materials (i.e. plates, pipettes, media) was obtained from VWR and used without further sterilization. High resolution mass spectrometry experiments were performed at the Mass Spectrometry and Proteomics Facility of Ohio State University on a Micromass

ESI-Tof™ II (Micromass, Wythenshawe, UK) mass spectrometer equipped with an orthogonal electrospray source (Z-spray) operated in positive ion mode. Sodium iodide was used for mass calibration for a calibration range of m/z 100-2000. Samples were prepared in a solution containing acidified methanol and infused into the electrospray source at a rate of 5-10 μl min^{-1}. Optimal ESI conditions were: capillary voltage 3000 V, source temperature 110°C and a cone voltage of 55 V. The ESI gas was nitrogen. Data was acquired in continuum mode until acceptable averaged data was obtained. Elemental analysis was conducted at the University of Illinois, School of Chemical Sciences Microanalysis Laboratory. Cells were obtained from ATCC. All media and staining assays were obtained from Invitrogen. Additional vessels and reagents were obtained from VWR. Cell viability was visualized using fluorescent microscopy (Axiovert 200, Carl Zeiss) and imaged with a CCD camera (AxioCam HRm, Carl Zeiss).

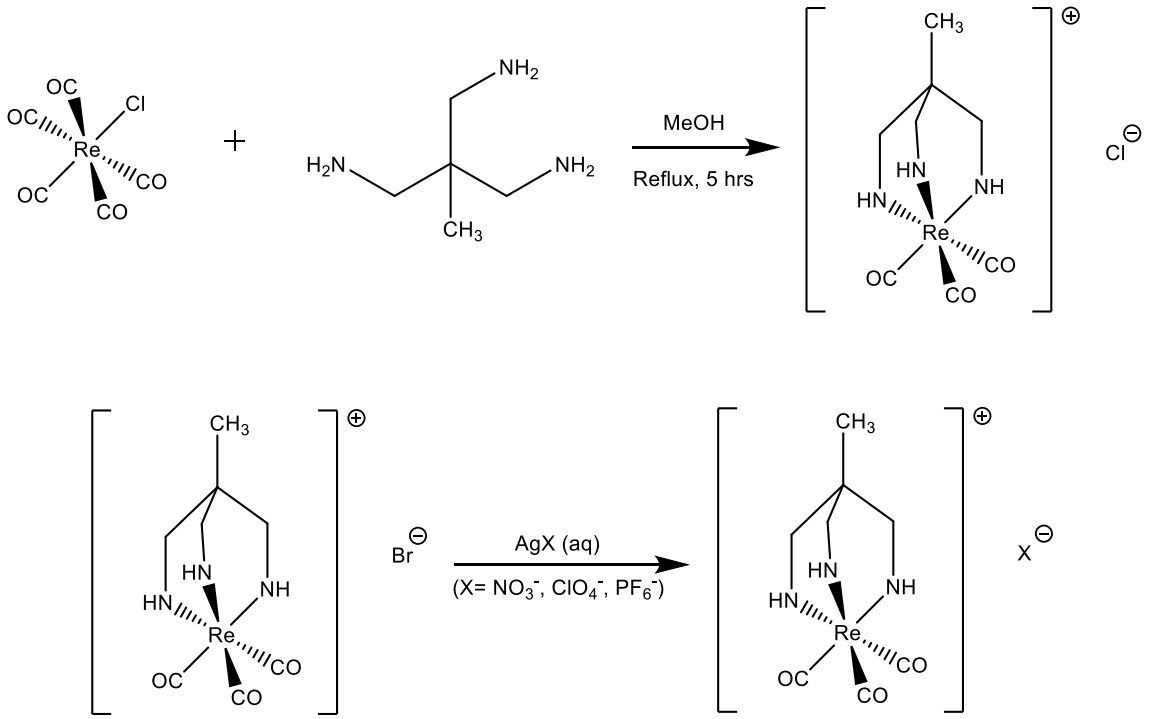

Scheme 2.1: Synthesis and Metathesis of $[Re(CO)_3(TAME)]X$

Single crystal X-ray diffraction data was collected at 100 K (Bruker KRYO-FLEX) on a Bruker SMART APEX CCD-based X-ray diffractometer system equipped with a Mo-target X-ray tube (λ = 0.71073 Å) operated at 2000 watts power. The detector was placed at a distance of 5.009 cm from the crystal. Integration and refinement of crystal data was done using Bruker SAINT software package and Bruker SHELXTL (version 6.1) software package, respectively.[129] Absorption correction was completed using the SADABS program. Crystals were placed in Paratone oil upon removal from the mother liquior and mounted on a plastic loop in the oil. Data collection and refinement parameters for crystals of **2** through **5** are shown in tables 2.1, 2.2, 2.3, and 2.4, respectively (crystal data for **1** was previously published.[67])

Table 2.1: Crystal data and structure refinement for **2**.

Identification code	**2**
Empirical formula	$ReC_8H_{19}N_3O_5Cl$
Formula weight	458.91
Temperature	100(2) K
Wavelength	0.71073 Å
Crystal system	Monoclinic
Space group	P2(1)/n
Unit cell dimensions, Å	a = 6.8635 (18)
	b = 12.951 (3)
	c = 15.970 (4)
β, deg	93.803 (4)
Volume, $Å^3$	1416.5 (6)
Z	4
Density (calculated)	2.152 Mg/m^3
Absorption coefficient	8.783 mm^{-1}
F(000)	880
Reflections collected	11,742
Independent reflections	3210
Goodness-of-fit on F^2	1.074
Final R indices [I>2sigma(I)]	R1 = 0.0300, wR2 = 0.0658
R indices (all data)	R1 =0.0366, wR2 = 0.0677

Table 2.2: Crystal data and structure refinement for **3**.

Identification code	**3**
Empirical formula	$ReC_8H_{15}N_3O_7Cl$
Formula weight	486.83
Temperature	100(2) K
Wavelength	0.71073 Å
Crystal system	Monoclinic
Space group	Cc
Unit cell dimensions, Å	a = 13.579 (4)
	b = 8.441 (3)
	c = 11.878 (4)
β, deg	98.193 (4)
Volume, $Å^3$	1347.5 (6)
Z	4
Density (calculated)	2.370 Mg/m^3
Absorption coefficient	9.250 mm^{-1}
F(000)	904
Reflections collected	5493
Independent reflections	2819
Goodness-of-fit on F^2	0.869
Final R indices [I>2sigma(I)]	R1 = 0.0245, wR2 = 0.0490
R indices (all data)	R1 =0.0271, wR2 = 0.0571

Table 2.3: Crystal data and structure refinement for **4**.

Identification code	**4**
Empirical formula	$ReC_8H_{15}N_4O_6$
Formula weight	449.44
Temperature	100(2) K
Wavelength	0.71073 Å
Crystal system	Monoclinic
Space group	Cc
Unit cell dimensions, Å	a = 7.778 (4)
	b = 13.745 (6)
	c = 12.281 (5)
β, deg	92.507 (7)
Volume, $Å^3$	131107 (10)
Z	4
Density (calculated)	2.276 Mg/m^3
Absorption coefficient	9.293 mm^{-1}
F(000)	856
Reflections collected	5340
Independent reflections	2709
Goodness-of-fit on F^2	1.016
Final R indices [I>2sigma(I)]	R1 = 0.0305, wR2 = 0.0649
R indices (all data)	R1 =0.0329, wR2 = 0.0656

Table 2.4: Crystal data and structure refinement for **5**.

Identification code	**5**
Empirical formula	$ReC_8H_{15}N_3O_3PF_6$
Formula weight	532.40
Temperature	100(2) K
Wavelength	0.71073 Å
Crystal system	Monoclinic
Space group	Cc
Unit cell dimensions, Å	a = 14.396 (7)
	b = 8.675 (4)
	c = 11.829 (6)
β, deg	97.877 (8)
Volume, $Å^3$	1463.2 (12)
Z	4
Density (calculated)	2.417 Mg/m^3
Absorption coefficient	8.495 mm^{-1}
F(000)	1008
Reflections collected	5799
Independent reflections	3060
Goodness-of-fit on F^2	0.889
Final R indices [I>2sigma(I)]	R1 = 0.0328, wR2 = 0.0605
R indices (all data)	R1 =0.0384, wR2 = 0.0620

Synthesis of $[Re(CO)_3(TAME)]Cl$ (2): 100 mg of $Re(CO)_5Cl$ (2.46 mmol) was refluxed in approximately 30 mL of methanol until dissolved and then a 1.1 molar equivalent of the TAME ligand (33 mg) was added. The mixture was allowed to reflux for 5 hours, and then the solvent was allowed to evaporate overnight. The resulting white crystals were then recrystallized from water. Yield: 86.9 mg (74% yield) High res. ESI MS (positive ion): 388.0674 M/z (M+) CHN Analysis Calc. for $ReC_8H_{19}N_3O_5Cl$: C, 21.23%; H, 3.58%; N, 8.85%. Found: C, 21.69%; H, 4.32%; N, 9.49%. IR (CO stretch, cm^{-1}): 2023, 1884.

Synthesis of $[Re(CO)_3(TAME)]X$, X= ClO_4^-, NO_3^- and PF_6^- (3, 4, 5): 50 mg of **1** (1.06 mmol) was added to 25 mL of water and heated with stirring until completely dissolved. A molar equivalent of a solution of AgX (X = ClO_4^-, NO_3^- and PF_6^-) in 10 mL water was then added and the resultant mixture was stirred for at least 3 hours in the dark to ensure the reaction went to completion. The resulting AgBr precipitate was removed by filtration with a 0.2 μm syringe filter. The solvent water was then allowed to evaporate resulting in large white crystals.

3: Yield: 59.6mg (57.2% yield) ESI MS (positive ion): 388.1 M/z (M+) CHN Analysis Calc. for $ReC_8H_{15}N_3O_7Cl$: C, 19.74%; H, 3.11%; N, 8.63%. Found: C, 19.88; H, 2.87%; N, 8.29%. IR (CO stretch, cm^{-1}): 2021, 1875.

4: Yield: 63.2 mg (65.7% yield) ESI MS (positive ion): 388.7 M/z (M+) CHN Analysis Calc. for $ReC_8H_{15}N_4O_6$: C, 21.38%; H, 3.36%; N, 12.47%. Found: C, 21.41%; H, 3.03%; N, 12.51%. IR (CO stretch, cm^{-1}): 2015, 1875, 1859

5: Yield: 84.9mg (74.5% yield) ESI MS (positive ion): 388.1 M/z (M+) CHN Analysis Calc. for $ReC_8H_{15}N_3O_3PF_6$: C, 18.05%; H, 2.84%; N, 7.89%. Found: C, 18.25%; H, 2.94%; N, 7.91%. IR (CO stretch, cm^{-1}): 2025, 1870

General Biology: Spontaneously Hypertensive Rat vascular smooth muscle cultures. The vascular smooth muscle cell cultures used were isolated from thoracic aorta explants from spontaneously hypertensive rats using a modified form of the Ross procedure for explants.[130] The rats were obtained from the SHR breeding colony that has been maintained on Standard Purina Laboratory Chow and tap water, *ad lib*, in the animal facility at the University of Akron and treated according to NIH guidelines.

The vascular smooth muscle cells were subcultured and plated on 6 well plates in a 50:50 mixture of Dulbecco's modified eagle medium (DMEM) and Ham's F12 medium supplemented with 10% FBS, 10mM HEPES buffer, 7.5%(w/v) $NaHCO_3$ and 1% antibiotic/antimycotic mixture. The cells were incubated at 37°C and 5% CO_2.and were 40% confluent when the compounds were added. The cells were returned to the incubator for 24 hours before being washed with 0.4% PBS (phosphate buffer solution) and treated with 0.025% trypan blue for 3 minutes. After being washed again with PBS, the cells were manually counted, in four fields, from each quadrant of the well, under 20x magnification, ensuring that over 400 cells total were counted.

Hela Culture: HeLa-S3 cells were obtained from ATCC, grown in Ham's F12-K media supplemented with 10% FBS, 10 mM HEPES buffer, 7.5% (w/v) $NaHCO_3$ and 1% antibiotic/antimycotic mixture on 100mm plates. The cells were subcultured every 72 hours. Cells were seeded onto 24 well plates, after counting in a hemacytometer, to ensure that approximately 20,000 cells were plated per well. Cells were incubated overnight to

allow them to adhere to the plates before being treated with the complexes in media. After treatment cells were incubated for 24 hours before being stained with Invitrogen's LIVE/DEAD® Viability Assay. The cells were excited at 488 nm and fluorescence was observed at 530 and 570 nm. Photos were taken of the wells such that counts of 400 cells in each well were observed.

2.3 Results and Discussion

Synthesis and characterization: We previously reported the synthesis and *in vitro* stability of $[Re(CO)_3(TAME)]Br$ (**1)** in comparison to other tripodal complexes based on the *fac*-$Re(CO)_3^+$ core.[67] Because of the superior stability of **1** in comparison to the other compounds, we felt that it would be an excellent candidate for an imaging agent model. Since bromide has been reported to have some genotoxicity,[131] we synthesized the chloride salt (**2**). This second complex was generated by refluxing $Re(CO)_5Cl$ and the TAME ligand in methanol and then recrystallizing the product in water. Salts with the non-coordinating anions perchlorate (ClO_4^-) (**3**), nitrate (NO_3^-) (**4**), and hexafluorophosphate (PF_6^-) (**5**) salts were synthesized via anion methathesis from **1**. A molar equivalent of the corresponding silver salt was added to **1** in aqueous solution, and the resulting precipitate was filtered away and the solvent was evaporated to give solid crystals of **3**, **4**, and **5**. Each compound was fully characterized by electrospray MS, elemental analysis, IR spectroscopy and single crystal X-ray diffraction.

The structures of compounds **2-5** are shown in Figure 2.1. The structure of the bromide salt (**1**) was reported previously in a preliminary communication.[67] All five complexes have essentially isostructural cations where the Re(I) ion adopts an octahedral coordination environment. The carbonyls adopt a facial coordination mode, and the TAME

ligand binds to the metal in a facial tridentate mode similar to that seen in scorpionate ligand binding. The Re-C and C-O bond lengths for all of the complexes are identical and are in agreement with those observed in other $Re(CO)_3^+$ complexes. The Re-N bonds range between 2.0 and 2.3 Å, with an average value of ~2.22 Å. The C-Re-C angles around the metal are close to the ideal 90˚ values for an octahedral coordination geometry, but the N-Re-N angles of the TAME ligand are more acute and closer to 80˚. The ligand adopts a chiral twist in the X-ray structures, resulting in a lower symmetry (C_3) than the expected C_{3v}. However, we believe this is a product of the solid state packing and not a fundamental aspect of the molecule's structure; all of the space groups have inversion centers, indicating that both enantiomers are present in the unit cell.

The spectroscopies for all three compounds are essentially identical. The IR spectra for these complexes show two intense C-O stretching frequencies. In chloroform solution, the three complexes have identical CO stretching frequencies at 2024 and 1902 cm^{-1}, but in the solid state compounds **1-5** show some differences. The CO stretching frequencies for dried samples of compounds **1-5** are shown in Table 2.5. As in the solution IR spectrum, due to the C_3 axis, these stretches show the expected a_1 and e symmetries observed at ~2020 cm^{-1} and ~1880 cm^{-1} respectively. Additional shoulder peaks were observed in compounds **1** and **4**, which result from carbonyl interactions with the anion in the solid state and from hydrogen bonding to neighboring NH groups on adjacent rhenium complexes. A similar interaction is observed in crystals of **2**, which exhibit two solvent water molecules per asymmetric unit. Prior to drying, a peak appears at 1915 cm^{-1} resulting from hydrogen bonding interactions with these water molecules.

Table 2.5: Solid state CO stretching frequencies for compounds 1-5.

Compound	CO stretching frequency (cm^{-1})
1	2018, 1888, 1853 (sh)
2	2023, 1884
3	2021, 1875
4	2015, 1875, 1859
5	2025, 1870

Partition Coefficient Determination: The partition coefficient of **1** was determined by using the shake flask method employing water and octanol as the hydrophilic and hydrophobic phases, respectively.[132] The concentration of **1** in both phases was determined by ICP elemental analysis and the log P was found to be -1.84. This partition coefficient is as expected for an ionic species, in spite of the hydrophobic nature of the organometallic cation. This log P value is less negative than that observed for simple salts,[15] and is equivalent to those observed for some nucleotides and amino acids.[133] Due to the negative value of the log P for **1**, this species most likely would not diffuse across cell membranes and would have to enter the cell through either a channel or via receptor mediated endocytosis.[134] It is important to note that pH will most likely not affect the log P value, since the cation of **1** does not engage in acid-base chemistry over the physiological pH range.

Cellular Toxicity Studies: **HeLa-S3 toxicity studies**: In addition to being analogs for technetium chemistry, rhenium complexes incorporating radioactive isotopes of the

metal can be used to both image and treat cancer cells.[135, 136] For this reason among others, HeLa-S3 cells were chosen as a robust cell line in which to probe anion toxicity.[137] Data from the concentration studies are shown in Figure 2.2 through Figure 2.6. The cells were grown in 24-well plates and incubated for 24 hours before being treated with aqueous solutions of the complexes in cell media. After treatment, the cells were incubated for another 24 hours before being stained with a fluorescent live/dead cell assay, photographed, and counted to determine percent viability. The cells were exposed to 10^{-8} M to 10^{-3} M concentrations of **1-5**. We compared the toxicity of the rhenium complexes to that of the common OTC analgesics acetaminophen (**6**) and acetylsalicylic acid (**7**) by exposing cells to aqueous solutions of these compounds at similar concentrations. Aqueous sodium bromide (**8**) was used to probe bromide toxicity in the same manner. Additional cells were treated with water or 2 mM hydrogen peroxide to provide a positive and negative control, respectively. Each study was repeated three times on three separate days. After the live:dead cell ratio was determined, the results were averaged to determine the percent viability of the cells. Errors associated with these measurements were calculated to be less than 4%. No significant toxicity was observed even at the highest concentration of every complex. Some slight toxicity is observed in compound **2**, although even at the highest concentration of **2** cell viability remains greater than 95%. Attempts were made to increase the concentration of the complexes in solution, in order to determine an LD_{50}, but thus far these experiments have been unsuccessful due to their limited solubility in aqueous solution.

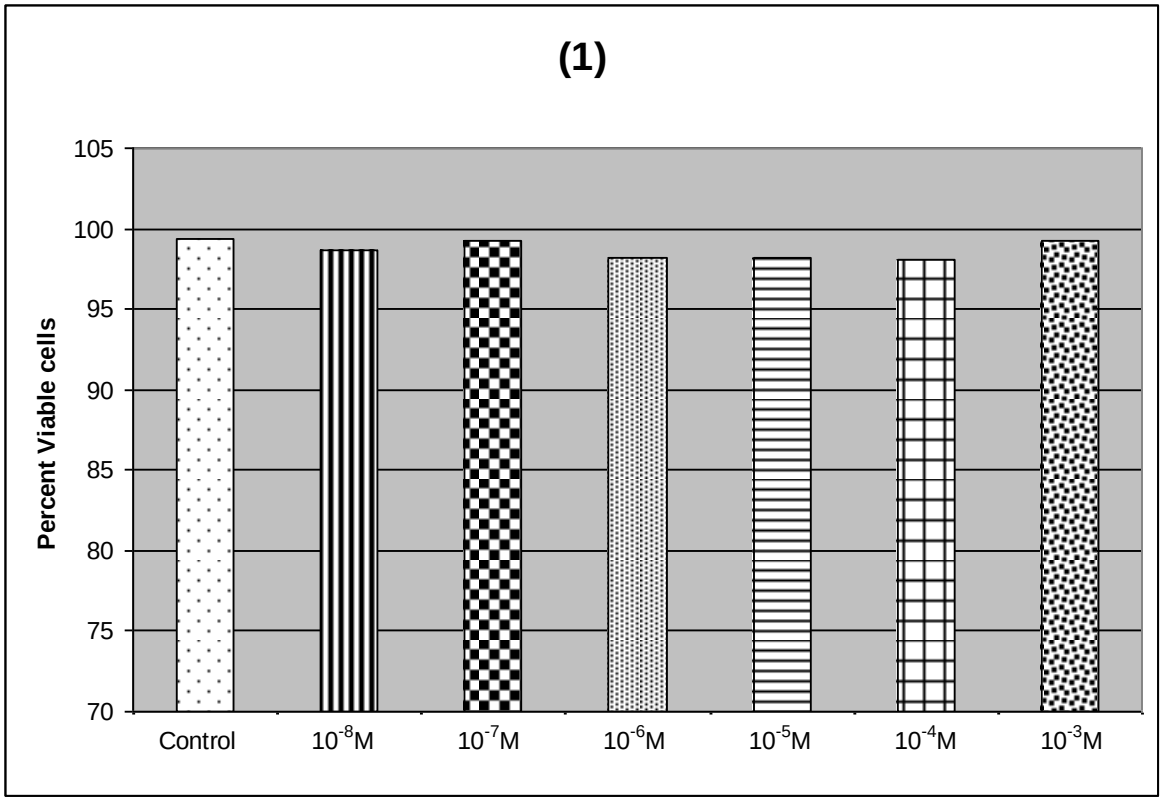

Figure 2.2: Toxicity of complex **1** in HeLa-S3 at concentrations of 10^{-8} to 10^{-3} M. Errors on these measurements are approximately ±3%.

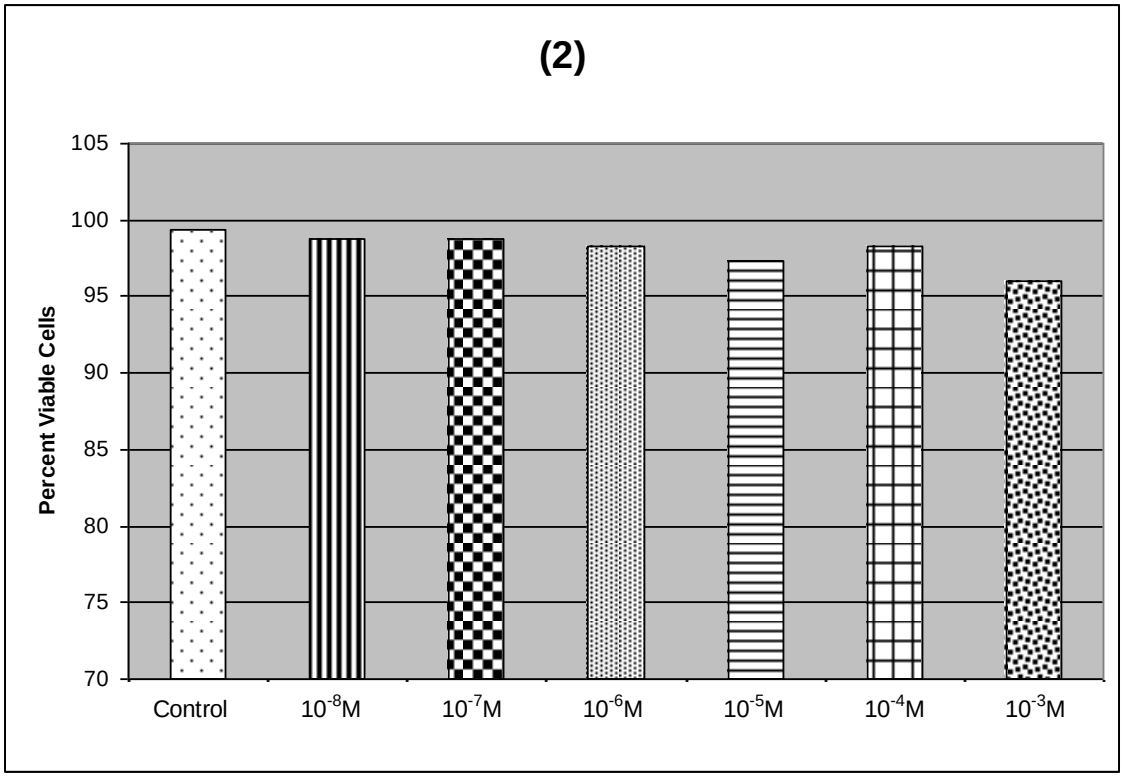

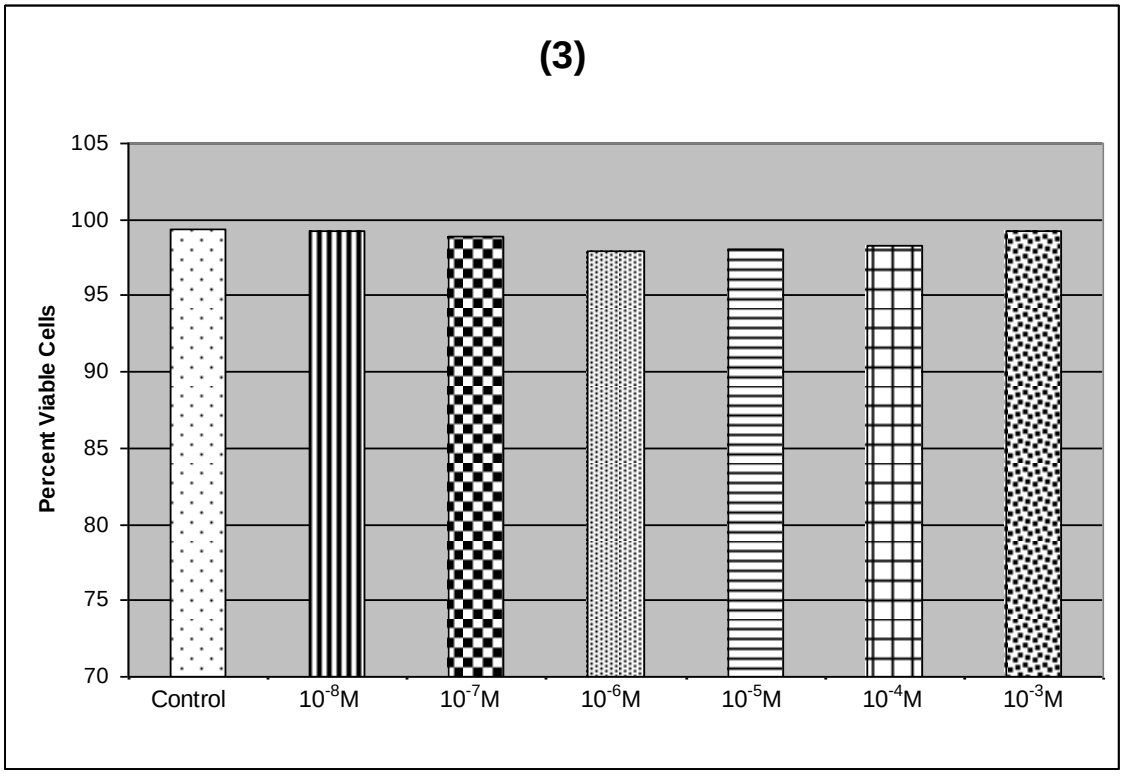

Figure 2.3: Toxicity of complexes **2-3** in HeLa-S3 at concentrations of 10^{-8} to 10^{-3} M. Errors on these measurements are approximately ±3%.

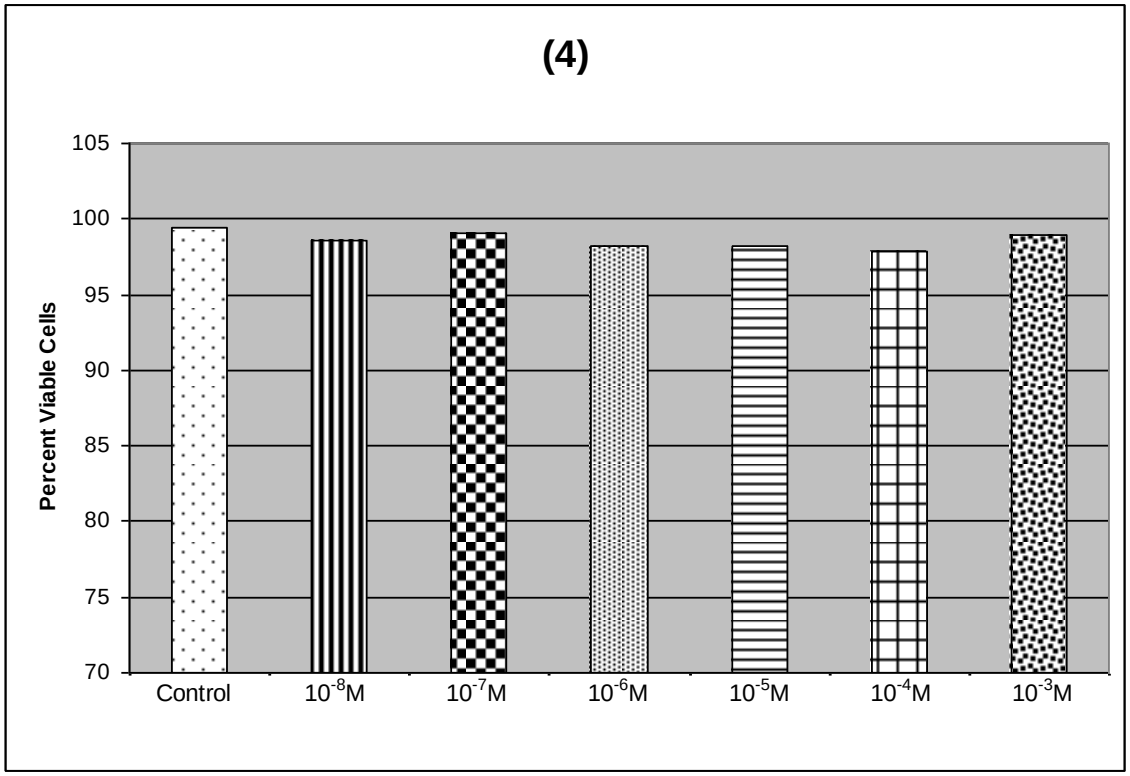

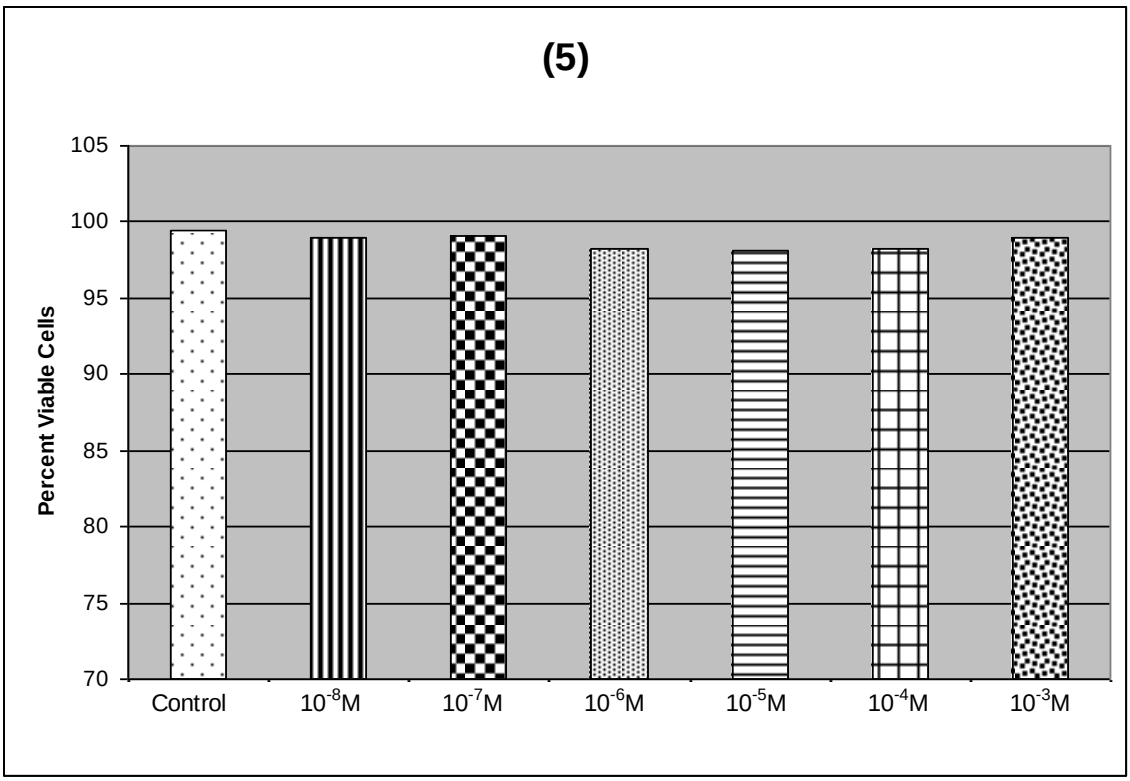

Figure 2.4: Toxicity of complexes **4-5** in HeLa-S3 at concentrations of $10^{-8?}$ to 10^{-3} M. Errors on these measurements are approximately ±3%.

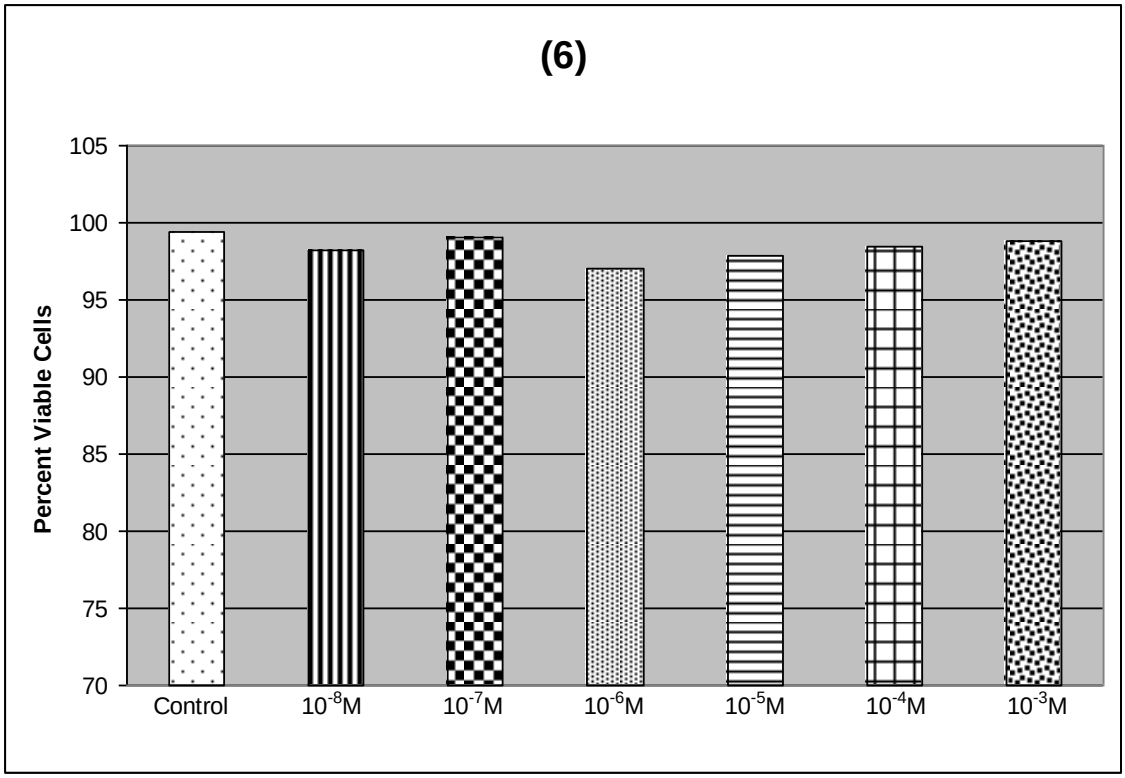

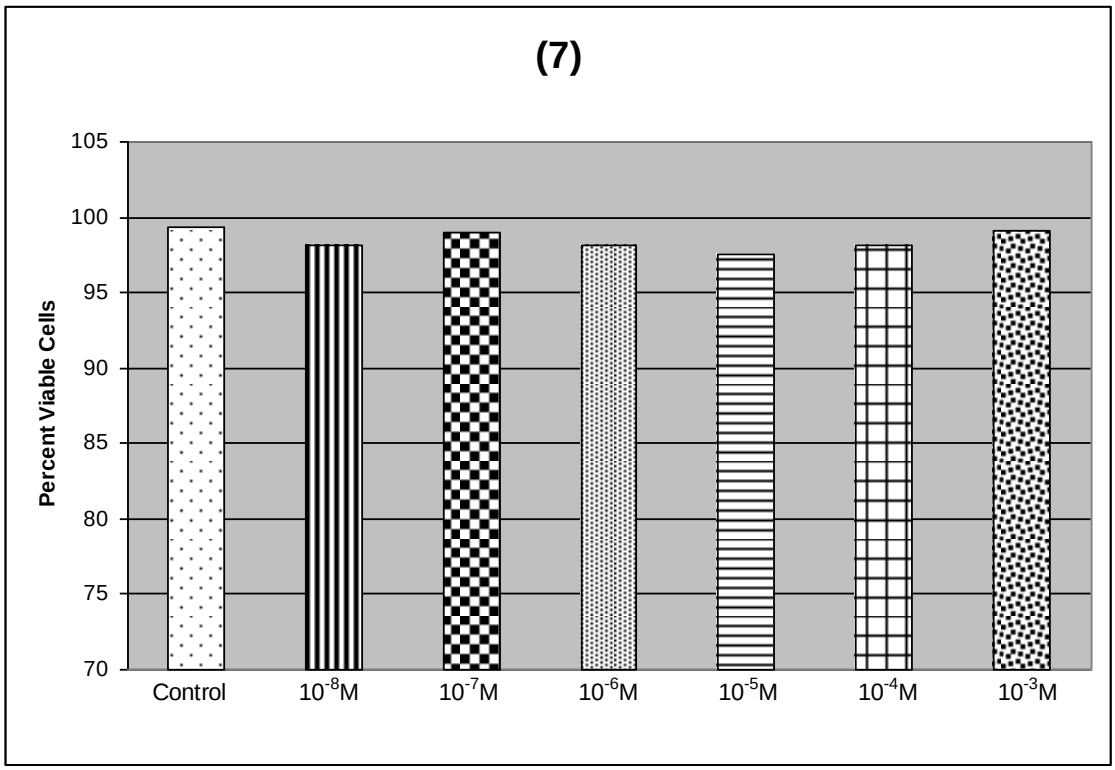

Figure 2.5: Toxicity of complexes **7-8** in HeLa-S3 at concentrations of $10^{-8?}$ to 10^{-3} M. Errors on these measurements are approximately ±3%.

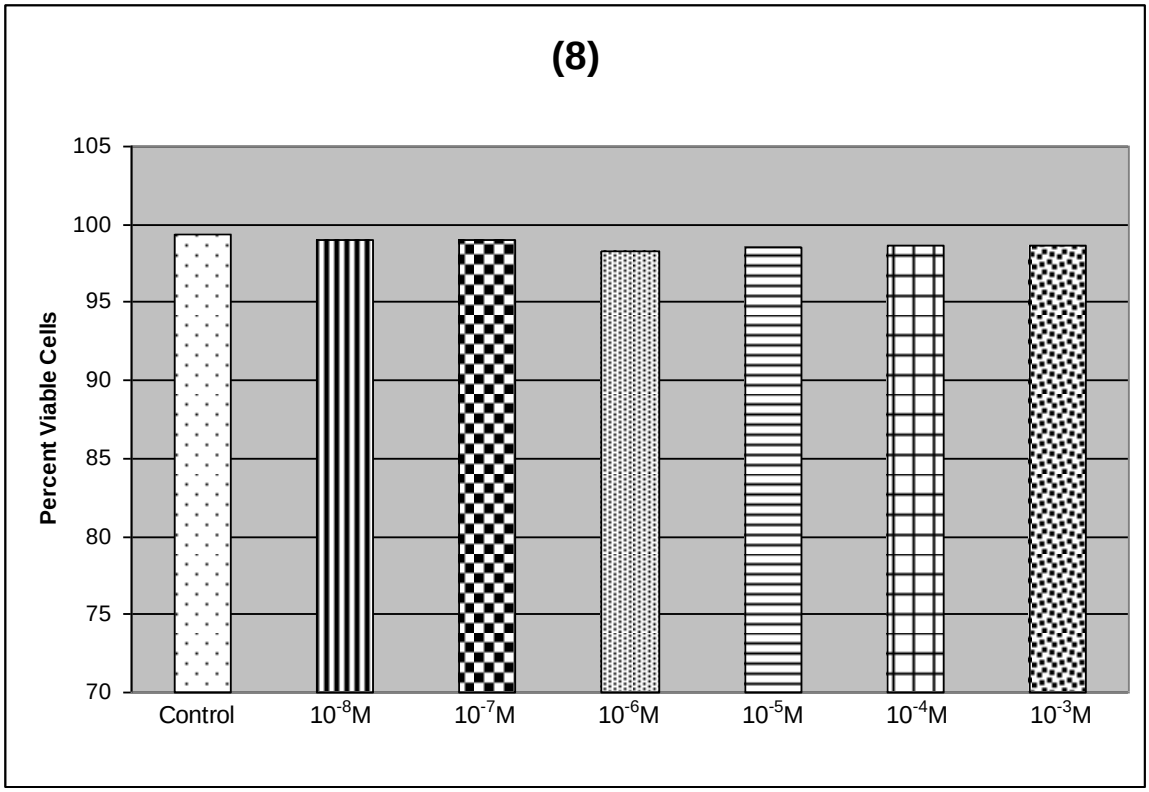

Figure 2.6: Toxicity of complex **8** in HeLa-S3 at concentrations of $10^{-8?}$ to 10^{-3} M. Errors on these measurements are approximately ±3%.

Figures 2.7 and 2.8 are micrographs of the positive and negative controls of the S3 HeLa cells as well as cells exposed to 10^{-3} M concentrations of compounds **1**, **6** and **7**. The positive control shows predominantly healthy squamous cells as indicated by their morphology and red fluorescence. The negative control was carried out by exposing cell to 2 mM H_2O_2 for 4 h at 37˚ C. The cells were fixed to the plate with cold methanol, and the live/dead® assay exhibits the expected green fluorescence of dead cells resulting from incorporation of SYTOX® green stain. Cells exposed to 10^{-3} M compound **1** are nearly identical in appearance to the positive control, and exhibit no obvious morphological changes. Cells exposed to 10^{-3} M acetominophen and aspirin also show predominantly

living cells, but closer inspection of morphology shows a higher concentration of rounded cells that are detached from the plate surface, indicating some stress induced by these OTC medications.

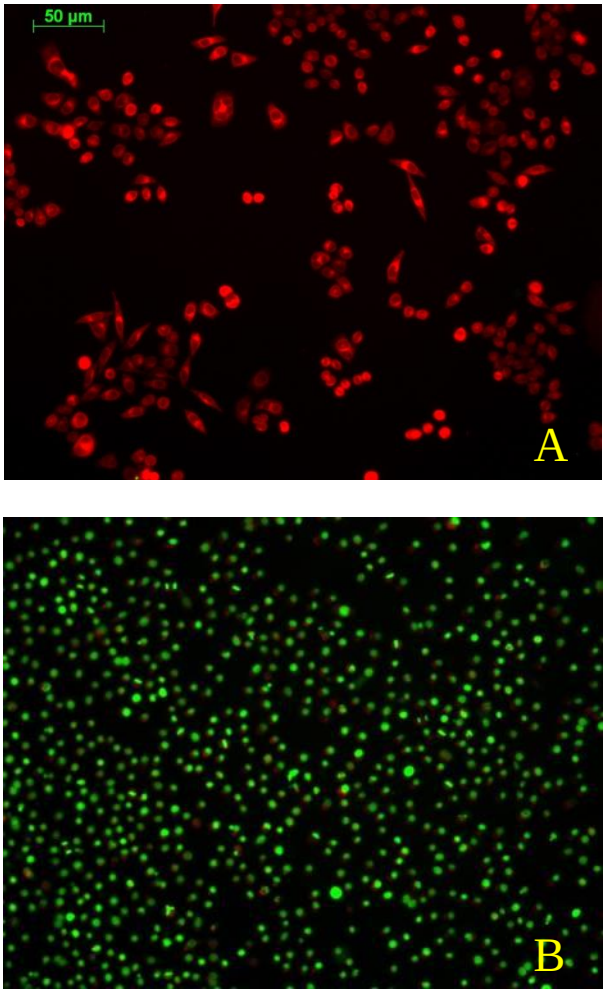

Figure 2.7: Micrographs of S3 HeLa cells: positive control (A) and negative control (2 mm M H_2O_2 for 4 h at 37 ˚C (B)

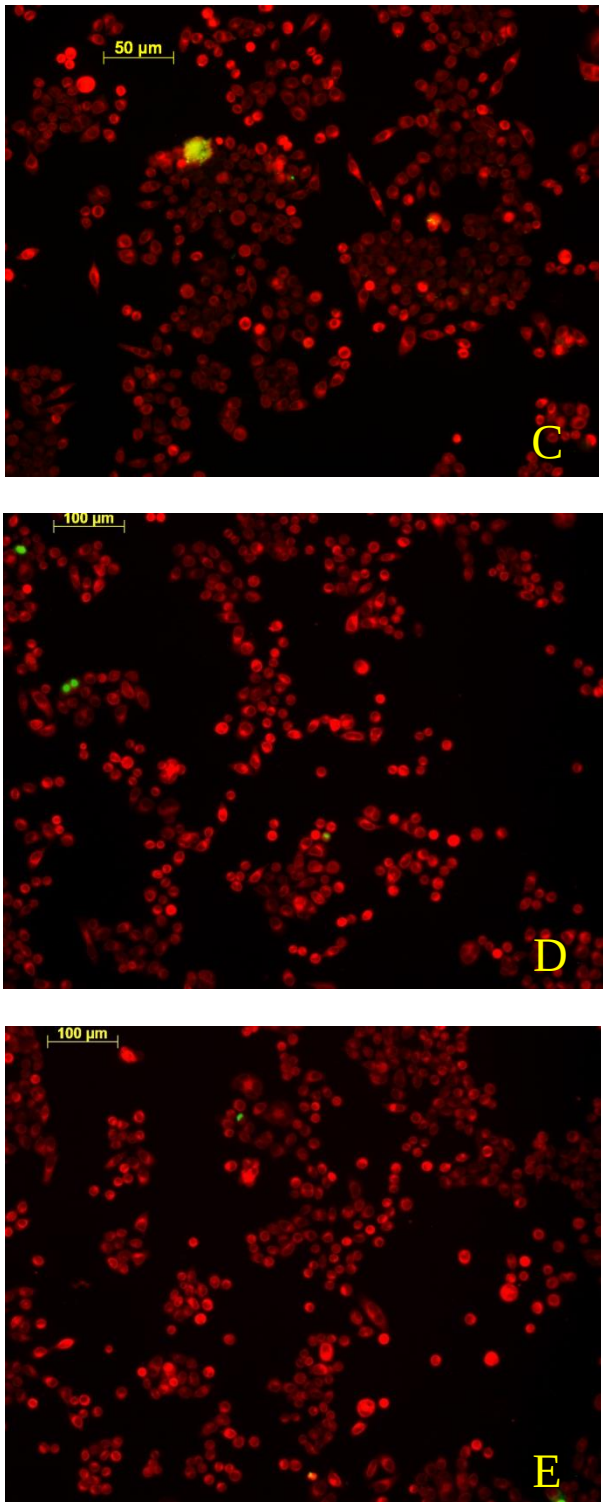

Figure 2.8: Micrographs of S3 HeLa cells: 10^{-3} M $[Re(TAME)(CO)_3]Br$ (**1,** C), 10^{-3} M acetylsalicylic acid (**6**, D), and 10^{-3} M acetominophen (**7**, E)

Rodent cell toxicity studies: Because one of the intended targets of the technetium analogs of our rhenium complexes is a perfusion imaging agent, we also conducted preliminary toxicity studies in rat vascular smooth muscle cell cultures, isolated from the thoracic aorta and donated by Dr. Milsted's research group.[138] The cells were plated and incubated for 24 hours before being treated with aqueous solutions of **1**, **4**, and **5** in cell media. The treated cells were incubated for another 24 hours before being stained with 0.025% trypan blue solution and analyzed to determine the percent of viable cells. Figures 2.9 and 2.10 show the results from this study. Significant cell death was present in the control cells since these cells were more sensitive to variations in cell concentration versus the S3 HeLa cell line. A lower percentage of viable cells was found in the cells treated with **1** at 1 $x10^{-4}$ M, which we attribute to the toxicity of the bromide ion, and not the complex itself. The number of viable cells did not vary significantly from the control cells to the treated cells at all other concentrations of **1**, **4**, and **5** tested. Compound **1** shows limited toxicity at the highest concentration as compared to the untreated control wells. Average errors for measurements made for the three compounds were ~±8% for **1**, ~±3% for **4**, and ~±4% for **6**.

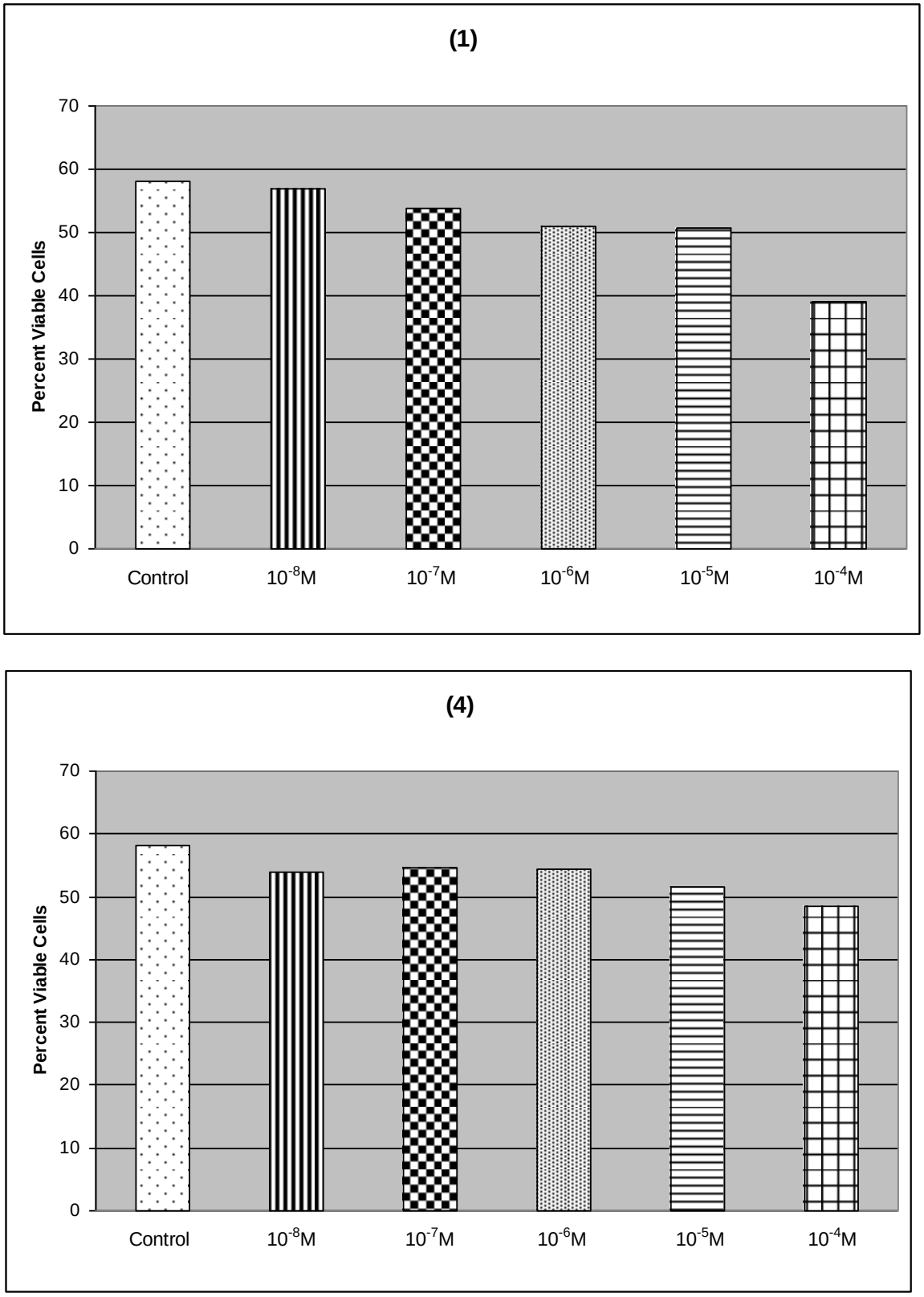

Figure 2.9: Toxicity results for rat vascular smooth muscle cells exposed to compounds **1** and **4** at concentrations of 10^{-5}M - 10^{-9}M.

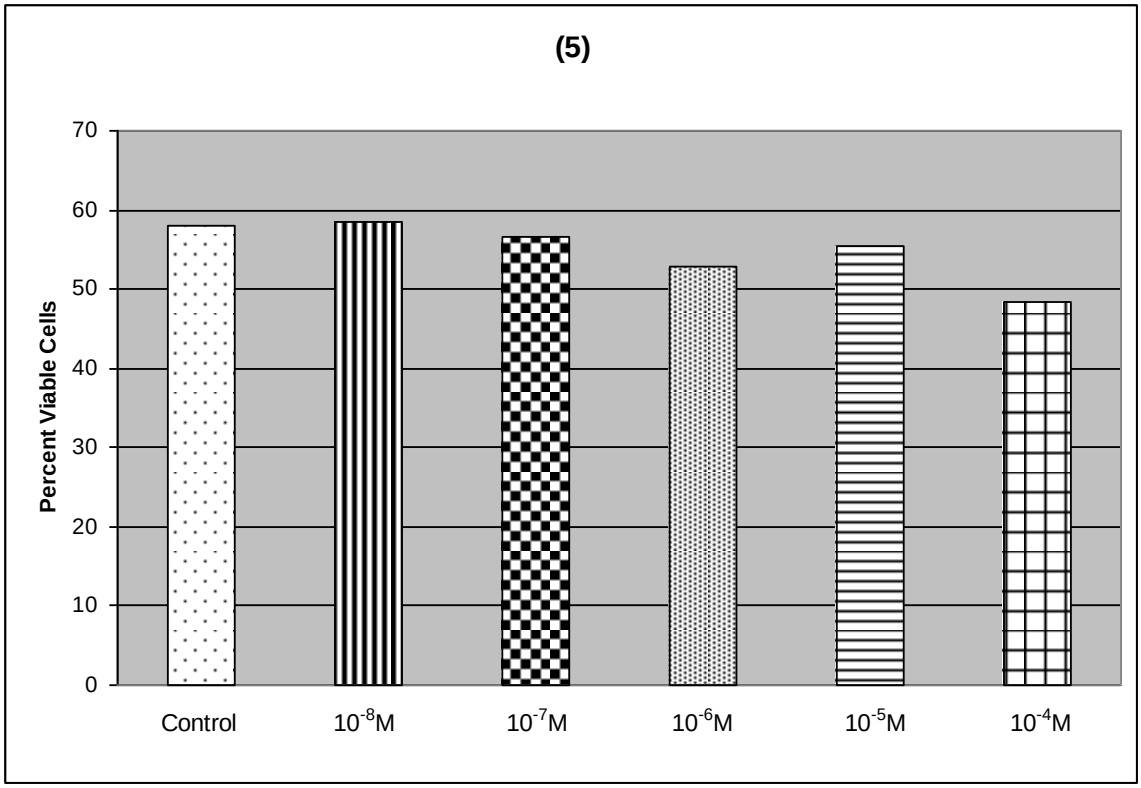

Figure 2.10: Toxicity results for rat vascular smooth muscle cells exposed to compound **5** at concentrations of 10^{-5}M - 10^{-9}M.

2.4 Conclusion

In conclusion, we have shown that complexes of the formula the $[Re(TAME)(CO)_3]X$ exhibit little or no toxicity to both an immortalized cell line (HeLa-S3) and a harvested animal cell line (vascular smooth muscle from spontaneously hypertensive rats). We believe this lack of biological activity results from the inert nature of the complex. In marked contrast, the majority of third row transition metal complexes typically exhibit moderate to high toxicity.[139-142] The cells examined in this report are able to tolerate high concentrations of $[Re(TAME)(CO)_3]X$ salts with no observable

morphological changes and at much higher doses than the OTC drugs acetaminophen and acetosalicylic acid (aspirin). We are continuing this work with investigations into other tripodal $Re(CO)_3$ complexes as well as bifunctional chelating agents incorporating the $Re(TAME)(CO)_3^+$ moiety.

CHAPTER III

SPECIFIC DERIVATIZATION OF LYSOZYME IN AQUEOUS SOLUTION WITH TRIAQUA TRICARBONYL RHENIUM (I)

3.1 Introduction

The aqueous chemistry of the organometallic cation $Re(CO)_3(H_2O)_3^+$ has received much attention over the past decade,[60, 65] due to its relevance to the design of $^{186/188}Re$ radiopharmaceuticals[10, 57] as well as its ability to act as a surrogate for the chemistry of $^{99m}Tc(CO)_3^+$.[23, 122, 143] In many cases, these investigations have focused on reactions between biomolecules and $Re(CO)_3(H_2O)_3^+$.[57] Although much work has been carried out investigating interactions between $Re(CO)_3$-based compounds and nucleic acids,[90, 144-147] amino acids and oligopeptides,[12, 38, 148, 149] little work has been carried out on reactions between rhenium prodrug or drug model complexes and proteins. Such interactions can be crucial to the biological processing of Tc/Re-based imaging agents, since proteins, rather than nucleotides or single amino acids, would be encountered in plasma. Alternatively, protein–Tc/Re adducts could be novel targets for use as imaging or therapeutic agents. In order to probe this chemistry, we began to examine the interactions between $Re(CO)_3(H_2O)_3^+$ and the readily crystallizable protein, lysozyme.

3.2 Experimental

Materials and Methods: Triple re-crystallized, lyophilized hen egg white lysozyme (HEWL) was obtained from MP Biomedicals. All reagents and solvents were purchased from Sigma, Aldrich, Acros Organics or Strem and used without further purification. Solutions of $[Re(CO)_3(H_2O)_3]Br$ were prepared as previously described[63] and evaporated to dryness to produce a solid compound previously identified as $[Re(CO)_3(H_2O)_3][Re_2(CO)_6(\mu_2\text{-}Br)_3] \cdot 6H_2O$.[62] IR spectra were recorded on a Nicolet NEXUS 870 FT-IR Esp and Perkin Elmer Spectrum One FT-IR spectrometers. Mass spectrometric analyses were carried out on a Bruker Reflex III MALDI-TOF at the Mass Spectrometry and Proteomics Facility at the Ohio State University in Columbus OH. Rhenium elemental analysis was carried out *via* ICP-OES at the University of Illinois at Urbana Champaign Microanalysis Laboratory.

Mass spectrometry experiments: Lysozyme was dissolved in nanopure water and reacted with aqueous solutions of $[Re(CO)_3(H_2O)_3]Br$ in nanopure water at molar equivalents of 0, 0.1, 0.5, 1, 2, or 3 Re : protein at a final protein concentration of 1 mg/mL. The samples were incubated at 4–10 ˚C for 24 h and then analyzed by MALDI- TOF-MS.

Protein-metal complex crystallization: 50 mg of lysozyme were dissolved in 750 μL of sterile, nanopure water. $[Re(CO)_3(H_2O)_3]Br$ was dissolved in water and added to the lysozyme solution to produce a final lysozyme : Re ratio of 1 : 5. Sterile, nanopure water was added to a final volume of 1 mL and the resulting solution was incubated at 4–10 ˚C overnight. Crystals were obtained via the hanging drop method using a reservoir solution of 0.05 M MES buffer (pH = 5.5) and 0.8 M NaCl. The drop was composed of 4 μL of the

reservoir solution and 4 μl of the incubated protein– metal solution. Large, tetragonal crystals appeared in 72 h. Crystals were cryo-preserved by soaking for a few minutes in mother liquor plus 30% glycerol and flash cooling in liquid nitrogen.

X-Ray diffraction: X-Ray diffraction data to 1.6 Å resolution were collected at 1.54 Å (Oxford Diffraction Gemini R) at 110 K using the 2 kW Enhance Ultra Cu source and was integrated and scaled using CrysalisPro[150].[150] Each crystal structure was solved by molecular replacement (Phaser[151]) using PDB 6LYZ and subjected to several cycles of restrained refinement using Refmac5[152] and rebuilding in Coot.[153] The refined molecular replacement solution contained clearly identifiable electron density for $Re(CO)_3(H_2O)_2^+$ near Nε2 of His15. A set of refinement restraints were manually created for the $Re(CO)_3$ fragment in which the carbonyl ligands were disposed in a facial arrangement with orthogonal (90˚) C–Re–C bond angles, and Re–C and C–O bond lengths of 1.8 Å and 1.2 Å, respectively. The protein and rhenium tricarbonyl fragment was further refined in Refmac5, then solvent molecules and a chloride ion were modeled to account for remaining electron density. Data collection and refinement statistics are summarized in Table 3.1.

Table 3.1 Data collection and refinement statistics (PDB 3KAM)

Data collection statistics	
Wavelength	1.54 Å
Space group	$P4_32_12$
Cell parameters	$a = b = 78.71$ Å, $c = 36.99$
Resolution	11.99-1.60 Å (1.66-1.60 Å)[a]
Unique reflections	15847 (1591)
Redundancy	22.4 (16.9)
Completeness	99.7 (100)
R_{sym}	0.091 (0.670)
$I/\sigma I$	32.6 (2.78)
Refinement statistics	
Reflections in test set	794
R_{work} (%)	18.1 (25.8)
R_{free} (%)	21.5 (31.9)
R.m.s from ideal[b]	
Bond distance (Å)	0.015
Bond angle (°)	1.55
Ramachandran plot outliers (%)[c]	0.00

[a] Parentheses indicate information for highest resolution shell. [b] Based on ideal values from Engh and Huber.[154] [c] MolProbity analysis.[155]

Lysozyme-$Re(CO)_3^+$ IR spectroscopy: HEWL crystals were grown after exposure to $[Re(CO)_3(H_2O)_3]Br$ as described above via the hanging drop method. Crystals were then harvested, washed, dissolved in methanol, and the resultant solution evaporated to produce a thin film on the diamond anvil of the FT-IR.

3.3 Results and Discussion

We reacted several stoichiometries of $Re(CO)_3(H_2O)_3^+$ with hen egg white lysozyme (MP Biomedicals, 3X crystallized) in pure H_2O at 4 °C overnight and carried out an initial evaluation using MALDI-TOF mass spectrometry to determine whether the $Re(CO)_3(H_2O)_3^+$ ion binds to lysozyme. The observed mass spectra are shown in Figure 3.1. Unmodified lysozyme shows a peak at approximately 14,300 *m/z*, in agreement with its experimentally determined molecular weight.[156] As the ratio of $Re(CO)_3(H_2O)_3^+$ ion to protein increases, a peak that corresponds to an increase in mass of approximately 270 appears and increases in intensity. This mass change corresponds to the weight of the $Re(CO)_3^+$ unit, a clear indicator that the $Re(CO)_3(H_2O)_3^+$ ion is interacting with the protein, possibly *via* coordination of one or more amino acid side chains.

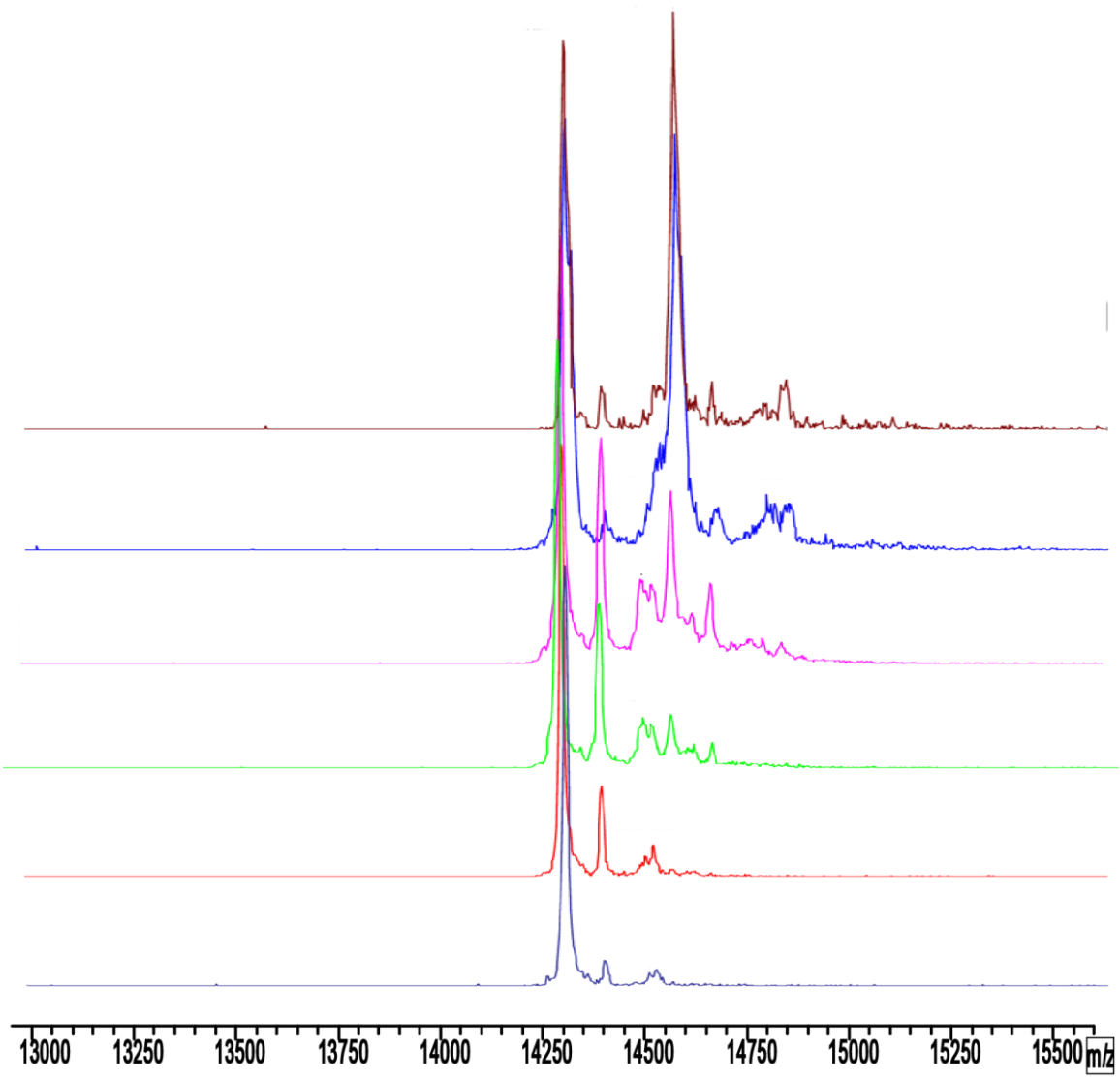

Figure 3.1: MALDI mass spectra of (a) native lysozyme, (b) 1 : 0.1, (c) 1 : 0.5, (d) 1 : 1, (e) 1 : 2 and (f) 1 : 3 native lysozyme : $Re(CO)_3(H_2O)_3^+$ reaction solution. An asterisk marks where the mass of the rhenium adduct appears.

We were able to grow crystals from HEWL solutions exposed to $Re(CO)_3(H_2O)_3^+$ at 4 ˚C overnight using the hanging drop method. The concentration of the HEWL was 50 mg mL^{-1} protein in 0.05 M MES buffer, pH 5.5, and 0.8 M NaCl. Large tetragonal crystals suitable for X-ray diffraction structure elucidation formed after 48–72 h. It is important to note that adduct formation was carried out in solution prior to crystal growth; typically,

metal ligation is achieved only by soaking crystals in reagent solutions.[157] We also observed that rhenium adducts could be produced via soaking methods; the structural parameters for these crystals were identical to those grown from solution.

The IR spectra of these rhenium-modified HEWL crystals were investigated to determine if we could observe the C–O stretching frequencies of the facial Re-tricarbonyl unit. In the 1800–2200 cm^{-1} region, unmodified lysozyme is transparent, but $Re(CO)_3^+$ compounds exhibit bands corresponding the a_1 and e modes of pseudo-C_{3v} symmetry. Rhenium modified lysozyme crystals show ν(CO) stretching bands that match these modes, as shown in Figure 3.2. These modes do not correspond to those of free $Re(CO)_3(H_2O)_3^+$ ion, which has a_1 and e bands at 2036 and 1916 cm^{-1}.[143] These rhenium-modified lysozyme crystals exhibit a splitting of the a_1 band, which we show (*vide infra*) may result from multiple rotamers of the $Re(CO)_3^+$ unit in the solid state.

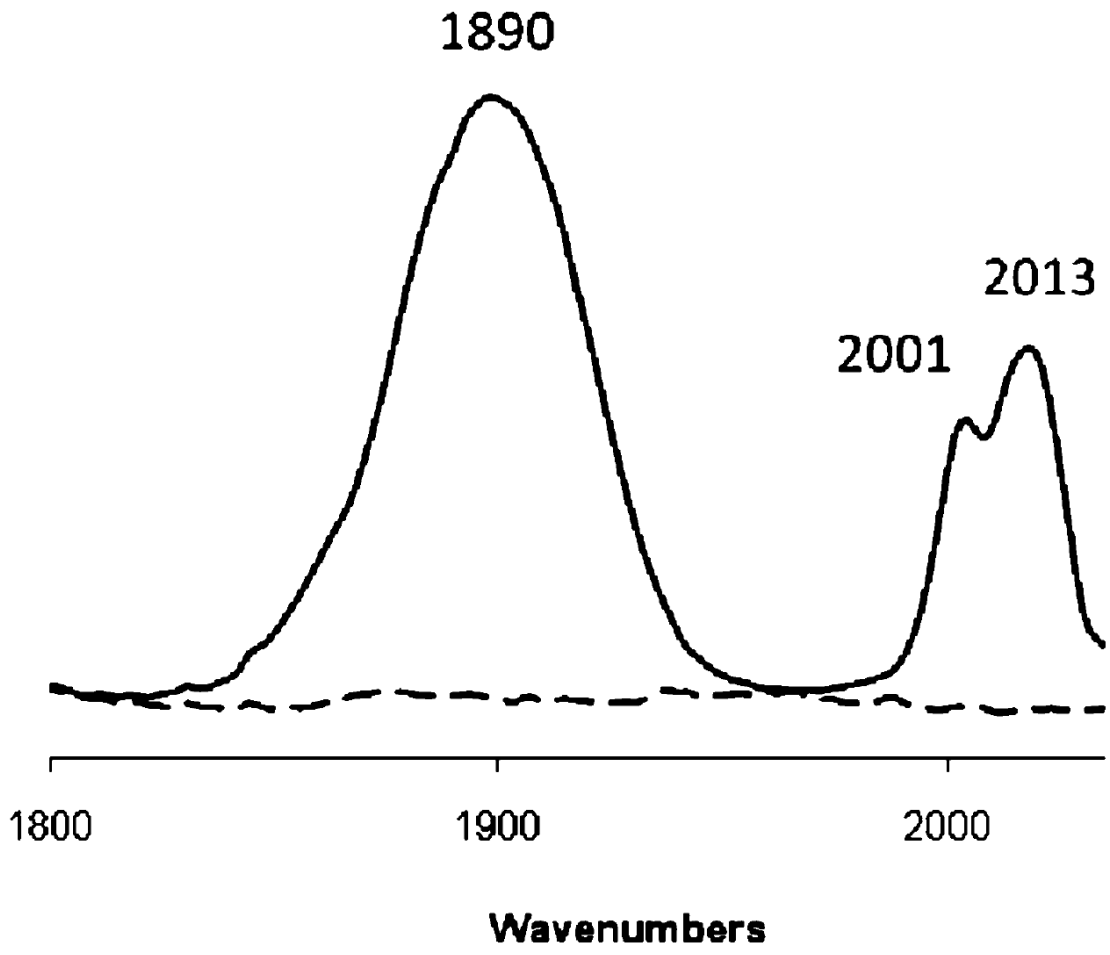

Figure 3.2: IR spectra of the carbonyl stretching region of unmodified lysozyme (dashed line) and $Re(CO)_3(H_2O)_3^+$ modified lysozyme (solid line).

We collected X-ray data on a crystal grown from the conditions described above to 1.6 Å resolution, collected at 1.54 Å (Oxford Diffraction Gemini R), and integrated and scaled using CrysalisPro (99.6% complete, R_{int} = 0.091, $I/\sigma(I)$ = 47.2, redundancy = 22.4). The structure was solved by molecular replacement (Phaser) using PDB 6LYZ and subjected to several cycles of restrained refinement using Refmac5 and rebuilding in Coot.[151-153, 158] The final structure (PDB 3KAM, R = 0.181, R_{free} = 0.215, rms bonds = 0.015 Å, rms angles = 1.6°) contained clearly identifiable electron density for $Re(CO)_3(H_2O)_2^+$

attached to Nε2 of His15, as shown in Figures 3.3 and 3.4. A ribbon diagram of the structure of the rhenium protein adduct is shown in Figure 3.3 along with a superposition of both native (PDB code 6LYZ) and rhenium-modified HEWL (Figure 3.4). The rhenium binds to the His15 imidazole side chain, and as expected, the $Re(CO)_3(H_2O)_3^+$ ion has lost a water molecule, forming an imidazole bound $Re(CO)_3(H_2O)_2^+$ fragment. Coordination of the rhenium to the His15 site does not greatly modify the structure of the protein. The RMS deviation between the α-carbons of the two protein models is 0.27 Å. As can be seen by superposition (Figure 3.4), the most obvious structural accommodations for the rhenium complex binding is a flipping of the imidazole of His15 and a slight deviation in backbone position of this residue.

Figure 3.3: Ribbon diagram of HEWL with $Re(CO)_3(H_2O)_2^+$ bound to its unique site at Nε2 of His15. Hydrogen bond between Asp87 and water W1 of $Re(CO)_3(H_2O)_2^+$ is depicted as a magenta dashed line.

Figure 3.4: A superposition of both native (PDB code 6LYZ) and rhenium-modified HEWL.

Figure 3.5 shows the F_o - F_c omit map of the lysozyme–$Re(CO)_3(H_2O)_2^+$ adduct, contoured at 2.5σ. The occupancy of the $Re(CO)_3(H_2O)_2^+$ fragment in the model is less than 1.0 and was modeled at 0.60, consistent with the MALDI-MS data that indicates partial derivatization of the protein. The refined Re–O bond distance for water W2 is somewhat long (2.6 Å compared to the expected 2.2 Å as observed for W1), suggesting that there are at least two significantly populated rotamers of the $Re(CO)_3(H_2O)_2^+$ adduct, related by a 90˚ rotation about the Re–N bond. In the final model, however, only the principal rotamer was modeled. Partial occupancy of a CO ligand at the W2 position results

in the Re–O bond having an artificially long Re–O bond distance. The observation that the electron density of the $Re(CO)_3(H_2O)_2^+$ fragment is well-ordered, rather than averaged, because of free rotation about the Re–N axis, is possibly due to the stabilizing hydrogen bond between Oδ2 of Asp87, and a water ligand (W1 in Figure 3.5) on the rhenium. The Re–N distance of 2.2 Å compares well to related small molecule structures.[127] While it is not possible to definitively rule out partial occupancy of chloride ion at position W2 of the rhenium tricarbonyl complex to explain the anomalously long Re–water bond length at this position, we believe the simplest interpretation of the data is the existence of two rotamers with water coordinated at positions W1 and W2. The Asp87–Oδ2–water distance (2.5 Å) in the X-ray structure is consistent with this interpretation. In the principal rotamer, Asp87 interacts with W1; in the minor rotamer, Asp87 interacts with W2. The Re–N distance of 2.2 Å compares well to related small molecule structures.[127]

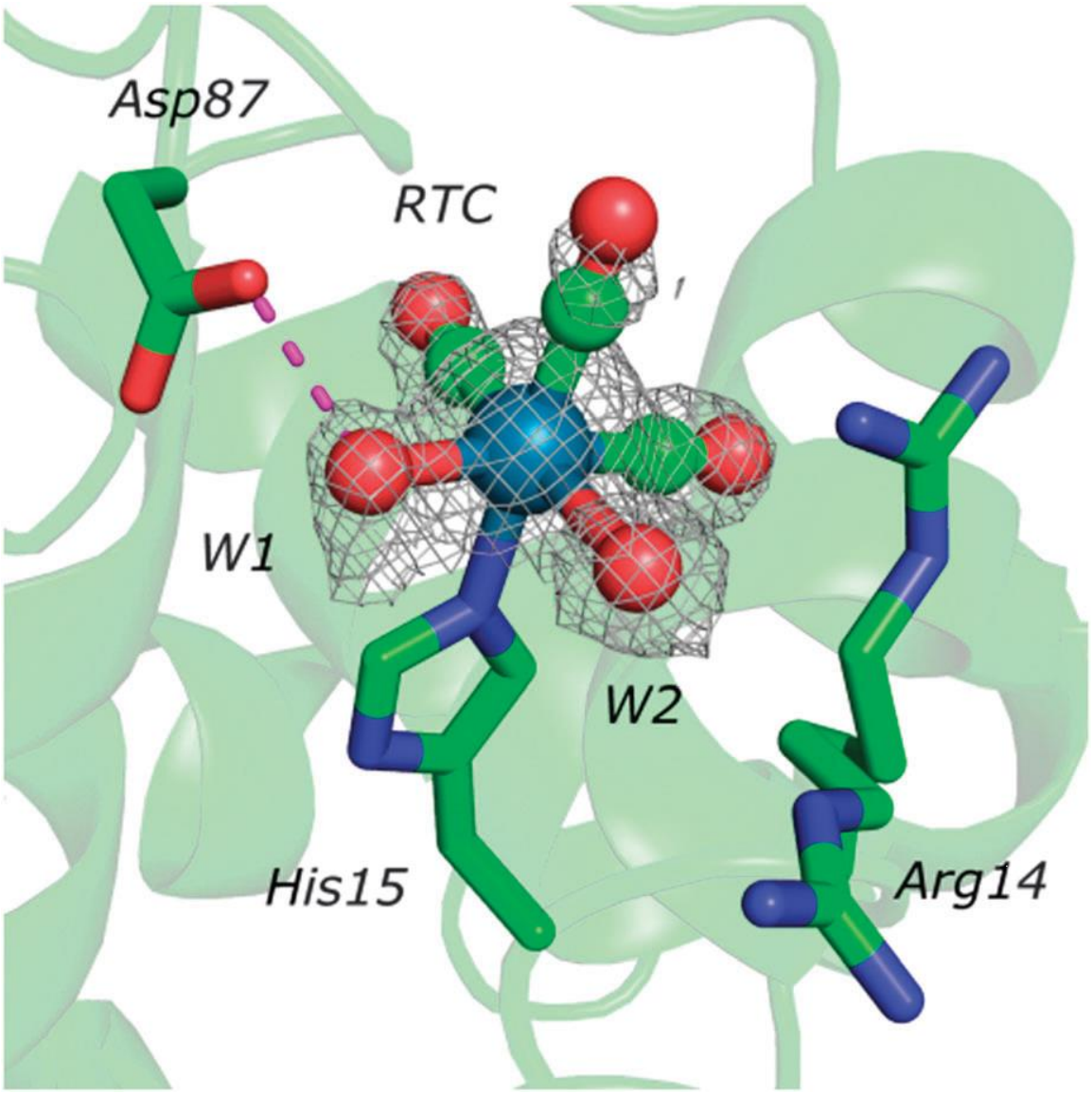

Figure 3.5: F_o - F_c omit map of the lysozyme–$Re(CO)_3(H_2O)_2^+$ adduct, contoured at 2.5σ. Arg14 has weak electron density and has alternate conformations, and does not appear to interact with $Re(CO)_3(H_2O)_2^+$.

3.4 Conclusion

To the best of our knowledge, the above described work is the first example of a crystallographically characterized $Re(CO)_3(H_2O)_2^+$–protein conjugate. There is a

significant body of work on the ligation of non-natural metal ions to the periphery of lysozyme, such as the binding of cisplatin to the His15 site.[159] More recently, organometallic complexes have been attached to this and other proteins, including Fischer-type metallocarbenes,[160] $Mn(CO)_3(H_2O)_2^+$,[161] half sandwich Ru(II) species[162] and most notably $Re(diimine)(CO)_3^+$ adducts which were used for long distance electron transfer studies and also have been crystallographically characterized.[77] In addition to the medicinal relevance of our work, the peripheral modification with $Re(CO)_3^+$ could be used to further the fundamental characterization of proteins. With regard to X-ray structural elucidation, $Re(CO)_3(H_2O)_3^+$ could be used as a heavy atom reagent to assist crystal phasing, since it meets all the essential requirements of phasing agents.[113] The cation contains a heavy atom, is water soluble, does not hydrolyze, is relatively non-toxic, has selectivity since it can readily form a covalent bond with a surface histidine but is not expected to react with other common groups such as amines and thioethers, and binds to the protein in a way that does not alter the crystal lattice of the protein. Alternatively, $Re(CO)_3(H_2O)_3^+$ could be used to generate the previously mentioned $Re(diimine)(CO)_3^+$-type adducts. The ligation of $Re(diimine)\text{-}(CO)_3X$ or $Re(diimine)(CO)_3(H_2O)^+$ to the periphery of proteins can require more than three weeks of reaction time at 37 °C.[77] In the current work, we observed that $Re(CO)_3(H_2O)_3^+$ reacts with the protein at 4 °C in as little as twelve hours. Subsequent reaction of the conjugate with a diimine would result in the desired electron transfer conjugate. We are continuing our work in the area of protein– $Re(CO)_3(H_2O)_2^+$ interactions.

CHAPTER IV

$Re(CO)_3(H_2O)_3^+$ BINDING TO LYSOZYME: STRUCTURE AND REACTIVITY

4.1 Introduction

The biological chemistry of organometallic rhenium compounds has received increasing attention over the past two decades.[24, 65] Although rhenium is not a naturally occurring biological element, two research areas have sparked interest in the medicinal chemistry of this element, and specifically the $Re(CO)_3^+$ moiety. First, rhenium is a useful cold analogue of technetium.[23, 122, 143] The isotope ^{99m}Tc is the most commonly used radionuclide in clinics, but technetium is a synthetic element with no stable isotopes. A current focus of researchers is creating new imaging agents from $^{99m}Tc(CO)_3(H_2O)_3^+$ because of the ability to convert $^{99m}TcO_4^-$ to $^{99m}Tc(CO)_3(H_2O)_3^+$, as shown in Figure 4.1, using a procedure suitable for a clinical setting.[10, 122] The chemistry of the analogous $Re(CO)_3^+$ group closely resembles that of $^{99m}Tc(CO)_3^+$, and thus its use provides a non-radioactive method for the design of new radiological imaging agent candidates. To this end, an extensive and still growing library of rhenium containing compounds has been established.[163] Second, a nuclide of rhenium is becoming an excellent candidate for the creation of therapeutic radiopharmaceuticals. A $^{188}W/^{188}Re$ generator elutes carrier-free $^{188}ReO_4^-$ suitable for use in a hospital setting, with similar ease to the molybdenum column.[164] ^{188}Re is especially attractive as a therapeutic radiopharmaceutical nuclide as it

has a relatively short half-life (18 h), a therapeutic beta emission (β^- of 2.1 MeV) and a γ emission of 155 keV that can be used to monitor the therapy with SPECT or PET. Critical to this effort, a new kit,[61, 165] similar to the kit of $^{99m}TcO_4^-$ is commercially available for the conversion of $^{188}ReO_4^-$ to $^{188}Re(CO)_3(H_2O)_3^+$, (Fig. 4.1) opening up the possibility of creating $^{188}Re(CO)_3$ derivatives in a clinical setting. The development of this kit is strong reinforcement for the ultimate goal of creating paired $^{99m}Tc/^{188}Re$ compounds that target specific tumor receptors as theranostic radiopharmaceuticals. Such compounds should be able to simultaneously image tumors with high precision and sensitivity while providing locally concentrated radiation-based therapeutic options.

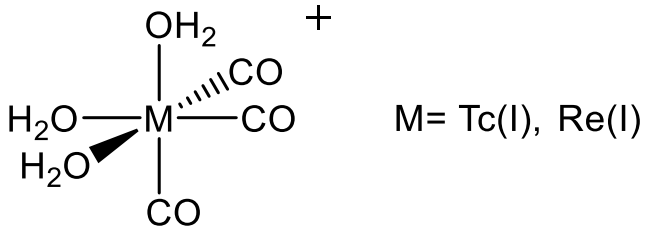

Figure 4.1: Structure of the $M(CO)_3(H_2O)_3^+$ cations.

In addition to the development of diagnostic and therapeutic compounds, complexes, complexes containing the $Re(CO)_3^+$ moiety are currently being used to measure biological electron transfer. Specifically, $Re(CO)_3(diimine)^+$ derivatives bound to a specific amino acid residue have been used as photoinduced electron transfer agents. Upon photoexcitation, the rhenium center undergoes a metal to ligand charge transfer (MLCT) transition, resulting in a transient $Re_{(II)}$ species.[166, 167] Most notably, $Re(CO)_3(diimine)^+$ fragments have been appended to the periphery of proteins via histidine groups to investigate the effects of protein structure on electron transfer kinetics.[77]

Accordingly, there has been increasing interest in the coordination chemistry of rhenium with biological molecules. In part, this chemistry has been driven as a result of the development of bifunctional chelating agent (BFCA)-based drug design strategies. Over the past few years, groups have investigated the binding of the $Re(CO)_3^+$ unit to nucleic acids and nucleotides,[90, 91, 144-146] amino acids and polypeptides.[12, 38, 148, 149] In Ziegler and Herrick's recent work, for example, $Re(CO)_3(H_2O)_3^+$ was observed to form discrete complexes with N-acetyl histidine and histidylhistidine, and the latter complex was stable in the presence of biological nucleophiles.[69] However, there has been little work on rhenium-protein complexes as models for technetium based imaging agents or rhenium-based therapeutic agents. Investigations of protein binding would provide useful information on possible biological processing of rhenium and technetium drugs, assist with the development of new protein-based drug candidates, and improve the synthesis of protein-rhenium diimine adducts for electron transfer studies.

Previously, we found that crystals of the protein hen egg white lysozyme (HEWL) grown from a solution containing $Re(CO)_3(H_2O)_3^+$ deliver a structure where the cation binds to a single amino acid side chain at the periphery of the protein via Nε2 of the His15 imidazole ring.[76] This imidazole replaces a water in the $Re(CO)_3(H_2O)_3^+$ cation, affording a mono-substituted complex. The selective binding can be readily observed by both IR spectroscopy and mass spectrometry.

In this chapter, we continue our structural study on the interaction between the $Re(CO)_3(H_2O)_3^+$ cation and HEWL. In addition to providing more detail from our previous structural characterization, we were able to generate the complexed protein by using the standard crystal soaking approach,[168] and a solution study performed by NMR

spectroscopy; in each case we observe structures identical to the structure previously reported, demonstrating that the mode of binding is independent of the mode of crystal growing and of whether the structure is packed in a crystal or dissolved in solution. In each case, the ligation of $Re(CO)_3(H_2O)_3^+$ to the periphery of the lysozyme has minimal effect on the overall structure of the protein. The NMR experiments show that the timescale for rhenium binding to the periphery of lysozyme generally agrees with the known substitution kinetics of the $Re(CO)_3(H_2O)_3^+$ ion.[169-172] Further, we comment on the bonding of the $Re(CO)_3(H_2O)_3^+$ ion and note ways it could be enhanced.

4.2 Experimental

Materials and Methods: Triple re-crystallized, lyophilized hen egg white lysozyme (HEWL) was obtained from MP Biomedicals. All reagents and solvents were purchased from Sigma, Aldrich, Acros Organics or Strem and used without further purification. Solutions of $[Re(CO)_3(H_2O)_3]Br$ were prepared as previously described[63] and evaporated to dryness to produce a solid compound previously identified as $[Re(CO)_3(H_2O)_3][Re_2(CO)_6(\mu_2\text{-}Br)_3] \cdot 6H_2O$.[62] Rhenium elemental analysis was carried out *via* ICP-OES at the University of Illinois at Urbana Champaign Microanalysis Laboratory.

Equilibrium dialysis experiments: Lysozyme was dissolved in 0.05 M sodium phosphate buffer (pH = 5.8) to make solutions with protein concentrations of 1000, 300, 100, 30, 10 and 3 μM. 3 mL of each of the preceding solutions were injected into Slide-A-Lyzers® dialysis cassettes. The protein solutions were dialyzed for 72 h against 1 μM $[Re(CO)_3(H_2O)_3]Br$ in 500 mL of 0.05 M sodium phosphate buffer (pH = 5.8). The protein

solutions and samples of the corresponding dialyte were sent for rhenium elemental analysis.

$Re(CO)_3(H_2O)_3^+$ soaking experiments: Lysozyme crystals were obtained via the hanging drop method, using a reservoir solution of 0.05 M MES buffer (pH = 5.5) and a drop composed of 4 μL lysozyme solution (50 mg ml^{-1}) and 4 μL reservoir solution. Large, tetragonal crystals appeared in 24 to 48 h. The crystals were then transferred to a 6 μL drop containing 0.10 M MES, 1.6 M NaCl, and 5 molar equivalents of $[Re(CO)_3(H_2O)_3]Br$. The drop was re-suspended over the original reservoir solution and incubated for 5 days at room temperature. Crystals were cryo-preserved by soaking for a few minutes in mother liquor plus 30% glycerol and flash cooling in liquid nitrogen.

Glyoxime soaking experiments: Lysozyme (50 mg ml^{-1}) and 3 molar equivalents of aqueous $Re(CO)_3(OH_2)_3]Br$ were allowed to incubate at 4 ˚C for 12 h. The resulting solution was crystallized via the hanging drop method. The drop was composed of 6 μl of the protein solution and 6 μL of the reservoir solution. The reservoir solution was composed of 0.05 M MES buffer (pH=5.0) with 0.8 M NaCl. Crystals appeared within 48–72 h. Large, single domain crystals were harvested with a loop and transferred to a 10 μL drop that contained 10 molar equivalents of glyoxime in 0.1 M MES buffer (pH = 5.0) with 1.6 M NaCl. The new drop was then sealed over the original well solution and allowed to react over a period of 4 days. At that point, the crystals had acquired a yellow to yellow-brown hue. They were harvested and cryoprotected in a solution of the soaking buffer to which 30% (w/v) glucose had been added.

Nuclear magnetic resonance experiments: A solution of 0.05 M sodium phosphate, pH 5.8, was made using D_2O, evaporated to dryness and then re-hydrated with D_2O to produce the buffer. This buffer was then used to make solutions of lysozyme and $[Re(CO)_3(H_2O)_3]Br$. Aliquots of these two solutions were combined to make samples containing 5 mM lysozyme with 0, 0.4, 1, or 3 molar equivalents of $[Re(CO)_3(H_2O)_3]Br$. Samples were equilibrated for several hours prior to measurement. Proton 1D spectra and 2D $^{1}H/^{13}C$ HSQC spectra[173] were collected on each of these pre-equilibrated solutions. HSQC spectra were collected with 80 complex pairs, 128 scans, a 1.2 s recycle delay, a 43 ppm carbon carrier, and sweep widths of 12,000 and 15,000 Hz (^{1}H and ^{13}C, respectively) on a 750 MHz Varian Inova spectrometer equipped with a triple resonance cold-probe. Aromatic resonances were aliased in the carbon dimension to improve resolution. For the 24 h time-course experiment, a three molar equivalent ratio of $Re(CO)_3(H_2O)_3^+$ to HEWL was employed with a sample of both species freshly dissolved in D_2O. Immediately after dissolution, a ^{1}H 1D spectrum timecourse was collected as a pseudo-2D dataset on a Varian Inova 400 MHz spectrometer with 128 scans, 8196 points, and 2 s recycle delays. Initial time points of 300, 1200, and 2100 s between experiments were used, followed by 18 spectra separated by 3600 s each. Note that for the 1D spectra significant numbers of non-exchanged indole and backbone amide protons remain in these samples even after one or two days in D_2O. Proton 1D spectra were processed and overlain in iNMR (http://www.inmr.net) while 2D datasets and 24 h pseudo-2D dataset were processed with NMRPIPE[174] and visualized with SPARKY (T. D. Goddard and D. G. Kneller, SPARKY 3, University of California, San Francisco). Chemical shift values from the 24 h time-course were fit to an exponential function and plotted using IgorPro (Wavemetric, Inc.).

4.3 Results and discussion

Since the first report of its synthesis by Alberto in 1994,[143] the $Re(CO)_3(H_2O)_3^+$ ion has been shown to form stable complexes with a variety of ligand types upon substitution of one or more of the bound water molecules. The water molecules on $Re(CO)_3(H_2O)_3^+$ are labile, and many examples of $Re(CO_3)L_3$ compounds have been isolated, including biologically relevant complexes where L includes amines, imidazoles, thiolates, thioethers, alcohols and carboxylates.[65] More recently, Ziegler and Herrick have shown that $Re(CO)_3(H_2O)_3^+$ will react with amides in peptides to form N-bound deprotonated chelates.[69] Thus, from a coordination chemistry standpoint, the $Re(CO)_3(H_2O)_3^+$ ion can potentially react with many amino acid side chains, and could even react and bind to the peptide backbone in a protein. When considering the protein lysozyme, there are a variety of potential metal binding sites at the periphery of the protein, and the external lysines have been an oft-used target.[160, 175] However, recent efforts have focused on the single peripheral imidazole ring at His15.[159] Fontecilla-Camps *et al.* observed the binding of a $Mn(CO)_3(H_2O)_2^+$ unit to the His15 site of lysozyme,[161] forming a protein adduct where the metal adopts an octahedral geometry. The coordination sphere in this protein complex consists of three facial carbonyl units, two water molecules and the imidazole ring of the histidine. Sadler et al. have reported an organometallic Ru-lysozyme complex.[162] More recently, Romao *et al.* presented a communication on the soaking of lysozyme crystals with *fac*-$Ru(CO)_3Cl(\kappa^2\text{-}H_2NCH_2COO)$.[176] The metal primarily formed an adduct at the His15 site analogous (80% occupancy) to that seen with the $Mn_{(I)}$ chemistry except with two *cis* carbonyls instead of three facial carbonyls. Additionally, ruthenium binding is also

observed at two carboxylate side chains from amino acids Asp18 and Asp52 with 50% and 40% occupancies, respectively.

The interaction of rhenium with proteins is being investigated by several groups with the goal of determining the possible fate of rhenium based radiopharmaceuticals in the bloodstream.[177] Such studies have proven valuable in determining the pharmacokinetics of platinum and ruthenium based anticancer agents.[159, 162, 178] Zobi and Spingler have published a study of the reactivity of the $[Re(CO)_3(H_2O)_2]^+$-lysozyme complex with additional ligands to further elucidate ways in which the binding of rhenium to a protein might influence the action of a rhenium based drug complex.[177] Compared to solvated fac-$[Re(CO)_3(H_2O)_3]^+$, the waters on the $[Re(CO)_3(H_2O)_2]^+$-lysozyme complex are less readily substituted, which the authors demonstrate by incubating the $[Re(CO)_3(H_2O)_2]^+$-lysozyme complex and $[Re(CO)_3(H_2O)_3]^+$ with imidazole and pyridine. The $[Re(CO)_3(H_2O)_2]^+$-lysozyme complex could be mono-substituted with the imidazole, forming fac-$[Re(CO)_3(His15)(im)H_2O)]^+$- and no pyridine substitution was observed. The reaction of the solvated $[Re(CO)_3(H_2O)_3]^+$ with imidazole gave mono-, bis-, and tris-substituted complexes and the reaction with pyridine gave the bis-substituted product. The reaction of $[Re(CO)_3(H_2O)_2]^+$-lysozyme with 2-methylaminopyridine (pn) did not yield the expected fac-$[Re(CO)_3(His15)(pn)]$, but instead gave a mixture of unmetallated lysozyme and free $[Re(CO)_3(pn)(H_2O)]^+$. Similar demetallation of the protein was observed with other primary amines such as ethylenediamine.[177]

We carried out a preliminary investigation into the binding of rhenium to lysozyme by using equilibrium dialysis. Samples of varying HEWL concentration were dialyzed against a solution of the $Re(CO)_3(H_2O)_3^+$ ion in phosphate buffer at pH 5.8. Total rhenium

concentrations inside and outside of the dialysis bag were determined by ICP-MS. These experiments with $Re(CO)_3(H_2O)_3^+$ revealed a coarsely determined K_d of about 50 μM, consistent with the NMR-observed fast exchange behavior reported below. There has been some kinetics studies on simple ligands binding to $Re(CO)_3(H_2O)_3^+$ and the system most similar to the histidine side chain is the pyrazine system studied by Alberto *et al.*[170] However, the analogous K_d for pyrazine and $Re(CO)_3(H_2O)_3^+$ (based onthe reported K_a) is in the range of $10^{-2} – 10^{-3}$. The discrepancy in K_d can be rationalized several ways. First, the pyrazine K_a was determined in a higher concentration of electrolyte (I = 1M) than was used in our protein experiments, where the concentration of phosphate was only 0.05 M. In addition, the $Re(CO)_3(H_2O)_3^+$ can readily interact with anionic residues or side chain heteroatoms on the surface of lysozyme prior to ligation, which could result in an increased affinity. Lastly, the pyrazine experiments were conducted at low pH, and we would expect the presence of deprotonated acid residues to increase the affinity of the $Re(CO)_3(H_2O)_3^+$ ion. In particular, one acidic residue, Asp87, is within 4 Å of the rhenium atom in this structure (*vide infra*).

Using NMR we have probed the nature of $Re(CO)_3(H_2O)_3^+$ interaction with HEWL. 2D $^1H–^{13}C$ HSCQ spectra were collected on 24 h equilibrated complexes with various ratios of freshly prepared $Re(CO)_3(H_2O)_3^+$ solution. For the most part, chemical shifts of the protein were unchanged from published values.[179] Only residue His15 shows appreciable chemical shift changes, as shown in Figure 4.2 (insets). Thus only one specific site in HEWL is metallated by rhenium under these conditions. Additionally, the gradual chemical shift changes observed as a function of $Re(CO)_3(H_2O)_3^+$ concentration suggest

fast chemical exchange between free metal ion and protein bound metal ion with regard to the NMR chemical shift timescale.

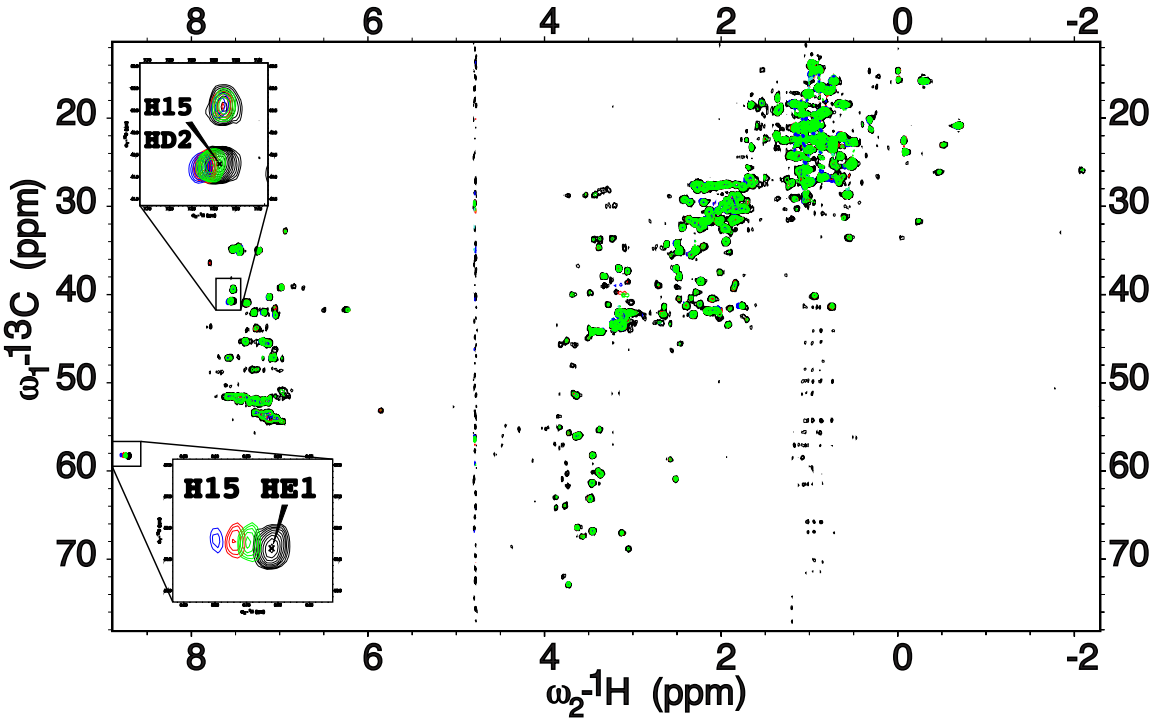

Figure 4.2: ^{13}C HSQC Spectra collected on 5 mM HEWL titrated with $Re(CO)_3(H_2O)_3^+$ at 0 : 1 (black), 0.4 : 1 (green), 1 : 1 (blue), and 3 : 1 (red) ratios.

We also collected ^1H 1D spectra on these complexes and the aromatic/ exchangeable proton region is shown in Figure 4.3. Slow and incomplete H_2O to D_2O exchange permitted observation of amide and tryptophan indole resonances that shift upon metalation. All of the peaks move with apparent fast exchange with regard to chemical shift, although the peaks shift around surprisingly slowly relative to the timing of rhenium addition. The two carbon-bound, and hence non-solvent exchangeable, proton resonances from H15 that shift and broaden upon $Re(CO)_3(H_2O)_3^+$ addition are also labeled. The

remaining resonances shift and broaden due to the combined process of slow deuterium exchange and rhenium binding. Mapping these changes onto the crystal structure of unmodified HEWL, as shown in Figure 4.4 shows that majority of the changes correlated to two places, the binding site and two tryptophan indoles nearby. These later changes are probably a result of slight changes in the H_2O to D_2O exchange properties of these residues. The sites confirmed by NMR to be high occupancy sodium and chloride, rather than low occupancy rhenium, binding sites are indicated by the small blue spheres.

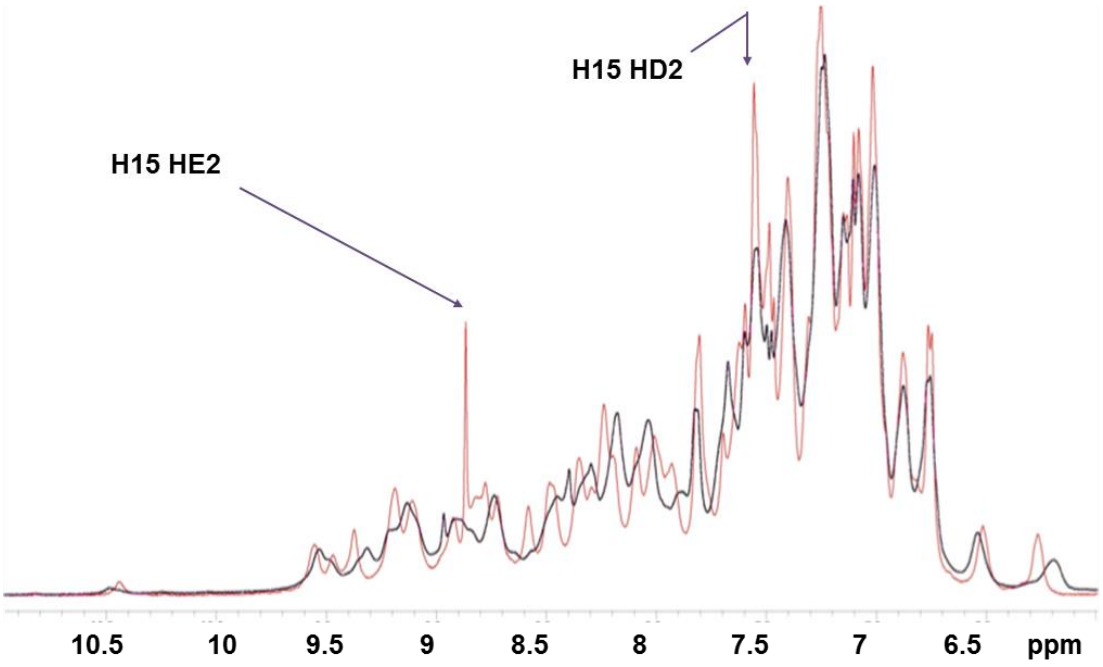

Figure 4.3: 1D spectra collected at 400 MHz on 4 mM lysozyme freshly dissolved in 100% D_2O (red), and the same sample with 2 equivalents of $Re(CO)_3(H_2O)_3^+$ after 24 h (black).

Figure 4.4: Amide chemical shift changes mapped on to the HEWL surface structure. Tentatively assigned residues that experience amide or indole chemical shift changes upon metalation are rendered purple. His15 experiences both amide and ^{13}C imidazole shift changes (the only residue with changes in the ^{13}C HSQC) and is colored cyan.

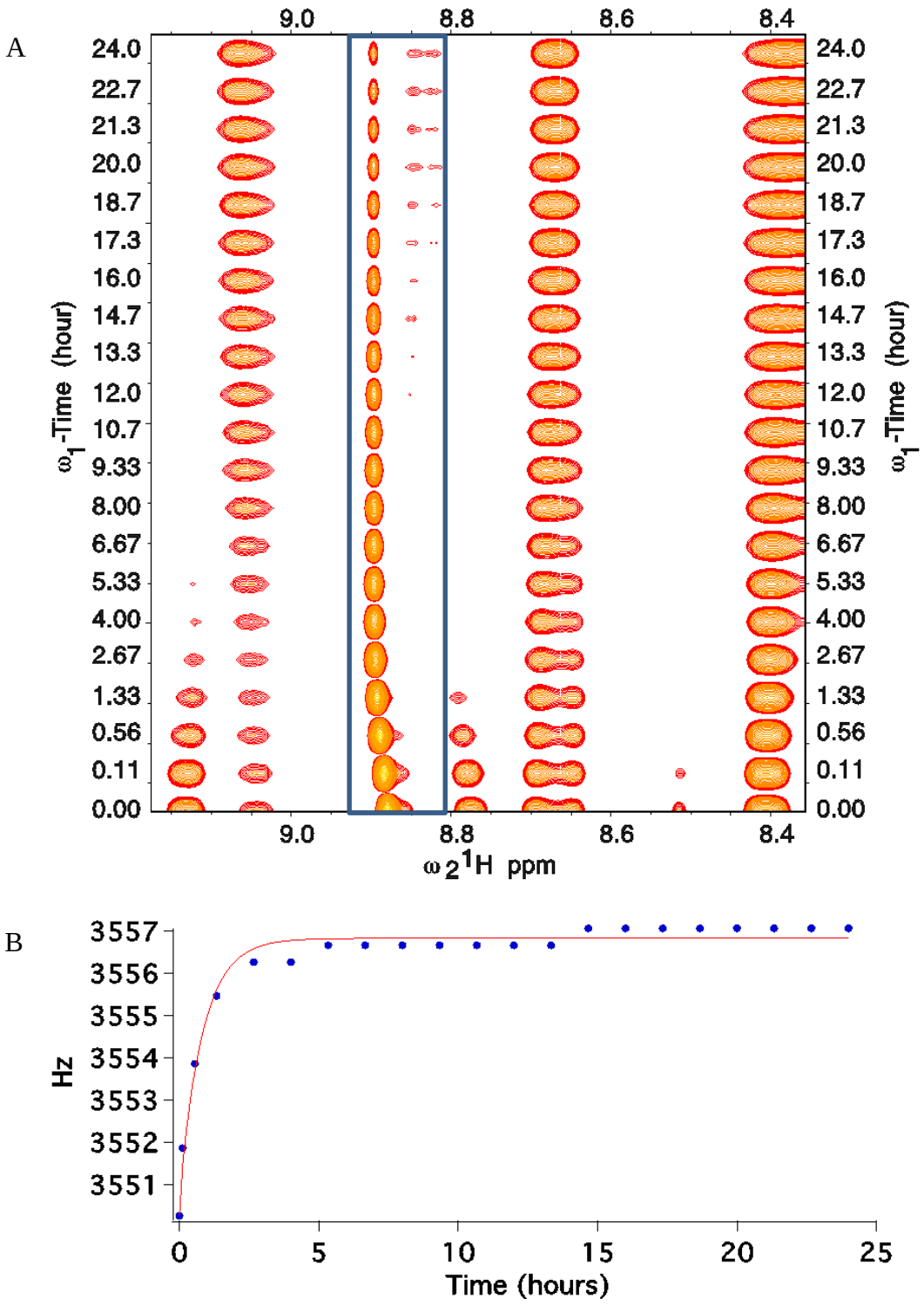

Figure 4.5: Time dependent chemical shift changes for H15 HE1 show unusually slow "fast-exchange" behavior, *i.e.* one peak shifting between starting and ending chemical shifts. (a) Interferogram of the time dependence of chemical shift changes upon metalation. (b) Nonlinear fit to $y = y_0 + A*\exp^{-Tau*x}$ of the boxed region in panel *A*. y_0 = 3556.8 ± 0.07 Hz, A = 6.15 ± 0.23, Tau^{-1} = 1.22 ± 0.13 hours.

To elaborate upon the rate of metalation, we collected a 24 h time-course, monitoring the chemical shift changes in protein resonances upon immediate introduction of an excess of $Re(CO)_3(H_2O)_3^+$ to HEWL, as shown in Figure 4.5 (above). In spite of the apparently ‘‘fast’’ chemical shift changes observed above, changes in the spectra of HEWL took at least an hour to finish. This was surprising due to the fast exchange behavior and, as will be discussed below, indicates that $Re(CO)_3(H_2O)_3^+$ metalation is not a simple on/off (i.e. bimolecular) mechanism. In addition, the water exchange rates as investigated by Merbach et al. are clearly relevant to these processes.[169]

In addition to collecting X-ray data on crystals grown from lysozyme-rhenium reaction solutions, we also investigated the soaking of lysozyme crystals with the $Re(CO)_3(H_2O)_3^+$ ion. This reaction is analogous to the soaking experiments carried out by Fontecilla-Camps and coworkers with $Mn(CO)_3(H_2O)_3^+$ ion.[161] We were able to collect data that was identical to that of the solution-based reaction crystals, with rhenium modification at His15. In addition, we also investigated soaking lysozyme–rhenium crystals with a chelating diimine, glyoxime. Glyoxime and other dioximes have been shown to avidly bind to $Re(CO)_3^+$ centers, and are structurally analogous to the diimine systems investigated by Gray *et al.*[77] However, exposure of lysozyme–rhenium crystals to glyoxime leached the rhenium metal center away from the protein, regenerating unmodified lysozyme, in a similar manner to the demetallation of the [Re(CO)3(H2O)2]+-lysozyme complex by primary amines that was observed by Zobi and Spingler and mentioned previously.[177]

4.4 Conclusions

Using both solution methods (NMR) and crystallography, we have characterized the $Re(CO)_3(H_2O)_3^+$ complex of hen egg white lysozyme and found that the surface histidine binding site is the preferred and exclusive site of ligation. The significance of the consistency of these two methods suggests that this complex is probably relevant to both *in situ* and *in vivo* preparation of rhenium–protein complexes. In particular, the use of histidine, a nearly ubiquitously surface exposed amino-acid, for metalation suggests that many targets beyond simply lysozyme are available to rhenium complexation. Thus, the general nature of this ligation may be invaluable in implementing this species to be a generic contrast agent probe.

The reversible bonding of $Re(CO)_3(H_2O)_3^+$ to His15, as indicated by the fact that soaking the metalated crystal with glyoxime completely removed the bound rhenium, suggests that vicinal surface-bound histidines might be necessary to create complexes that might withstand biological conditions. Alternatively, His-tags[69, 82] or the use of recombinant DNA techniques could produce suitable binding environments. We are currently looking for suitable candidates.

The time constant (τ) for the initial exchange of $Re(CO)_3(H_2O)_3^+$ onto HEWL is 1.2 h, *i.e.* with a rate of $\sim 2 \cdot 10^{-4}$ s^{-1} (Fig. 4.4), whereas fast exchange behavior on the chemical shift timescale (Fig. 4.1 and 4.2) is usually observed for states with lifetimes of ~100 μ*sec*. The eight orders of magnitude difference can only be explained if binding of rhenium to the protein is not simply a two-state process, but is limited due to a long-lived initially unreactive species. We hypothesize that it is the dissociative interchange from $Re(CO)_3(H_2O)_3^+$ that is the rate limiting since previous work suggested that this process

has a similar magnitude rate ($7.6 \cdot 10^{-4}$ M^{-1} s^{-1}) for the dimethyl sulfide monitored formation of $Re(CO)_3(H_2O)_2(DMS)^+$ from the triaqua compound.[180] This is significant because it suggests that protein metalation is highly dependent upon the residence time of coordinated waters. Modulation of the residence time of a single water may be achievable by substitution of the other two waters with different ligands such as 2,2'-bipyridine or similar diimines.[181] This should suppress dissociation of the remaining water and prolong its residence time. Modulation of the residence time of the remaining water, and hence speed of protein metalation, may be important for engineering rhenium to be a viable imaging probe or antineoplastic agent.

CHAPTER V

ADDITIONAL INVESTIGATIONS OF THE BIOLOGICAL INTERACTIONS OF TRIAQUA TRICARBONYL RHENIUM (I)

5.1: Introduction

While the body of this work focuses on the basic chemistry of the $M(CO)_3^+$ core (M= Tc, Re), its potential as a SPECT or PET imaging moiety, the synthesis and toxicity of tripodal $Re(CO)_3^+$ complexes, and the interaction of the $Re(CO)_3^+$ moiety with lysozyme, $Re(CO)_3^+$ cores have a wide range of potential applications. In this chapter, we will describe a two part study of the organometallic chemistry of the $Re(CO)_3^+$ core. We will explore the use of $Re(CO)_3^+$ compounds as X-ray contrast agents and explore the relationship of $Re(CO)_3^+$ with the protein, insulin. Due to the diverse nature of these experiments, a brief introduction of each topic is below.

Rhenium as a contrast agent: Introduction

While it is one of the oldest and most widely available diagnostic techniques, optimizing X-ray procedures for soft tissue is an active area of research.[182] Soft tissue X-ray procedures require the use of a higher atomic number contrast agent to attenuate the administered radiation so that tissues of similar density and composition can be distinguished on a radiograph.[183] Contrast enhancement can be primarily attributed to the photoelectron effect of higher atomic number elements. The most commonly used contrast

agents incorporate iodine or barium for this purpose. Barium, in the form of barium sulfate suspensions, is used solely for imaging of the gastrointestinal tract.[184] Sodium iodide was the first iodine contrast agent to be administered intravenously in 1923.[185] Most iodine contrast agents used in modern medicine are based on the covalently bound 1,3,5-triiodobenzene contrast agent,[182] as covalently bound iodine was found to be associated with fewer side effects.[186, 187] The iodixanol discussed below is a molecule of this type. However, all iodine contrast agents are associated with risks including cardiovascular events, nephropathy, and anaphalaxis.[187, 188]

Barium is by no means the only metal atom suitable for X-ray attenuation. There are many considerations involved in contrast atom choice. Clinical X-rays are usually produced from a tungsten X-ray tube, which generates photons with energies ranging from 20-150 keV. An ideal contrast agent must be able to absorb photons in this range. Photons are more likely to be absorbed when the binding energy of the innermost shell, or K shell, electrons is just below the energy of the photons. The binding energy of the K shell electrons is characteristic of the atom and is also referred to as the K edge energy. There is a large increase in K edge correlated with increased atomic number, as shown in Table 5.1 below.[184] Bearing in mind that the K edge of iodine is 33.2 keV, and barium is 37.4 keV, these atoms actually attenuate a much smaller percentage of the photons produced than some of the heavier metal atoms considered. Other considerations, such as patient safety and low cost, have led to the prevalence of these contrast agents in clinical use.[189]

Table 5.1: The K shell binding energies (K edge) of some representative heavy metals.[190]

Element	Atomic Number	K edge energy (in keV)
I	53	33.2
Ba	56	37.4
Gd	64	50.2
Yb	70	61.3
W	74	69.5
Re	75	71.7
Au	79	80.7

Because of the less than ideal efficiency of iodine and barium as X-ray attenuators, heavy atoms have been, and continue to be, studied for use as contrast agents. The efficacy of such heavy metal complexes was discovered serendipitously, when a patient treated with the MRI contrast agent gadopentetate dimegulumine (Magnevist™, structure shown in Figure 5.1, below) underwent a subsequent CT scan that showed the unexpected contrast enhancement. This complex is now routinely used as a contrast agent in patients with renal insufficiency or iodine allergies that would preclude the use of iodinated contrast agents.[184, 191] There are several other examples of gadolinium based MRI contrast agents that have demonstrated efficacy as X-ray contrast agents, such as gadodiamide (Omniscan™)[192] and gadoteridol (ProHance™).[184]

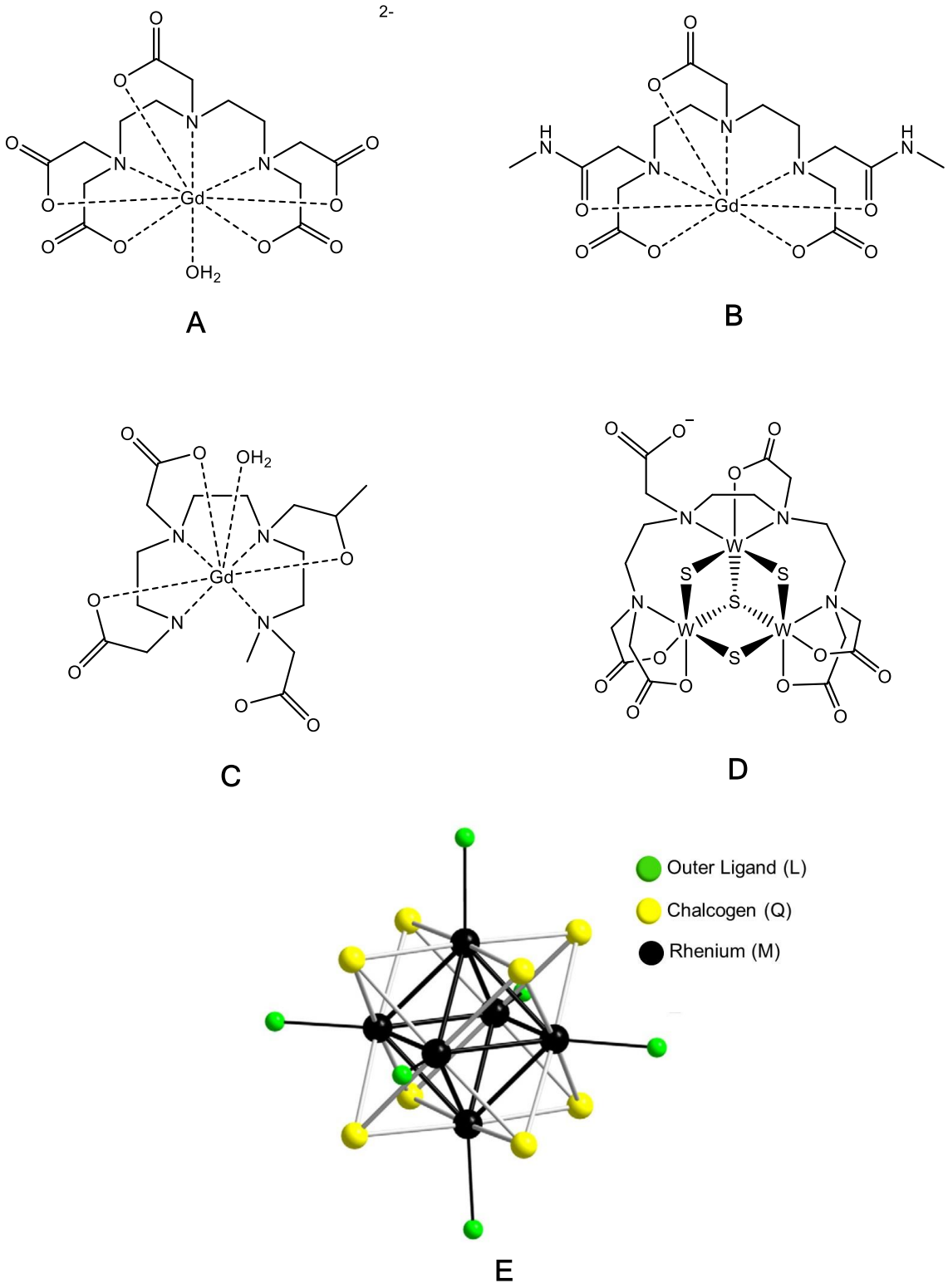

Figure 5.1: Structures of representative metal contrast compounds: (a) Magnavist,[193] (b) Omniscan,[193] (c) ProHance,[193] (d) W cluster complex,[194] (e) Re cluster complex with the general formula $[\{M_6Q_8L_6]^{n-}$.[182]

Metals have also found use as X-ray contrast agents as so-called "cluster complexes;" compounds that contain two or more metal atoms. Tungsten, bismuth,[184] molybdenum, and rhenium examples[182] of these cluster complexes that have been investigated as X-ray contrast agents are also pictured in Figure 5.1 above. The water solubility of these compounds often limits their exploration and the biological processing of the metals and complexes has to be better understood in order for these complexes to be utilized clinically. Many of the rhenium compounds that we have studied have proven to be robust in biological challenge experiments and with an atomic number of 75, robust rhenium complexes could serve as X-ray contrast agents. Targeted rhenium complexes could potentially assist in the diagnosis of smaller tumors or more complex disease processes, since they would be able to accumulate at the disease site. Additionally, the same rhenium complex could be used as an X-ray contrast agent and as a chemotherapeutic with the use of cold rhenium isotopes for the former and the beta emitting ^{188}Re for the latter. Investigations of the X-ray attenuation of the "parent" molecule of $[Re(CO)_3(H_2O)_3]Br$ could also shed fundamental insight on the biologic processing of this metal. Herein, we present introductory investigations into the use of $[Re(CO)_3(H_2O)_3]Br$ as a potential X-ray contrast agent.

Insulin binding to the $Re(CO)_3^+$ core. Introduction:

While the $Re(CO)_3^+$ modified lysozyme, discussed in the previous chapters, can offer insights into the interaction of this core with proteins and possible biological processing mechanisms, metalating the protein insulin with $Re(CO)_3^+$ would be a direct route to a viable radiopharmaceutical. [13, 55, 56] Insulin is a polypeptide hormone that has a

regulatory role in glucose uptake and metabolite storage, including lipids and proteins.[195] Abnormalities in insulin regulation are associated with diabetes, hypertension, and cancer.[196, 197] Thus, diagnostic radiopharmaceuticals based on insulin offer clinicians a non-invasive means of studying insulin disregulation in a variety of disease states. Molecular imaging agents derived from human insulin, incorporating nuclides such as ^{123}I, ^{124}I, ^{125}I, ^{18}F, and ^{67}Ga have been reported.[50-54] Valiant and coworkers have produced an insulin-$^{99m}Tc(CO)_3^+$ conjugate via the BFCA approach.[13] The binding of the cold rhenium analog of this conjugate to the insulin receptor was near that of native insulin, which further highlights the potential of $Re(CO)_3^+$ insulin conjugates as radiopharmaceutical targets.[13] In this chapter our attempt to produce and structurally elucidate an insulin-$Re(CO)_3^+$ conjugate through the direct labeling approach is described, along with its crystallization and MALDI-TOF-MS characterization.

5.2: Experimental

All reagents and solvents were purchased from Sigma, Aldrich, Acros Organics or Strem and used without further purification. Porcine insulin were obtained from MP Biomedicals. Solutions of $[Re(CO)_3(H_2O)_3]Br$ were prepared as previously described[63] and evaporated to dryness to produce a solid compound previously identified as $[Re(CO)_3(H_2O)_3][Re_2(CO)_6(\mu_2\text{-}Br)_3] \cdot 6H_2O$.[62] IR spectra were recorded on a Nicolet NEXUS 870 FT-IR Esp and Perkin Elmer Spectrum One FT-IR spectrometers. Mass spectrometric analyses were carried out on a Bruker Reflex III MALDI-TOF at the Mass Spectrometry and Proteomics Facility at the Ohio State University in Columbus OH.

5.2.1: Rhenium as an X-ray contrast agent: Experimental

Solid $[Re(CO)_3(H_2O)_3]Br$ was prepared as previously described.[63] 20% w/v ballistics-style gelatin was prepared according to literature conditions using Knox™ gelatin.[198] Concentrated solutions of NaI and $[Re(CO)_3(H_2O)_3]Br$ in water were made and added to 500 μl aliquots of room temperature water in a microcentrifuge tube. 500 μl of the 20% w/v cooled gelatin was added to each tube and the tubes were inverted several times to mix the sample without introducing air bubbles into the gelatin. Final concentration of the gelatin in each sample was 10% w/v and the final concentrations of iodine and rhenium in the samples were 0.016 M, 0.032 M, 0.076 M, 0.13 M, and 0.26 M. 500 μl of distilled water was also added to an aliquot of the 20% w/v gelatin to serve as a control. The mixed samples were transferred to wells of a 24 well tissue culture plate, as shown in Figure 5.2 below and allowed to solidify at 4-10 ˚C overnight. An X-ray radiograph of the resulting plate was obtained the following day.

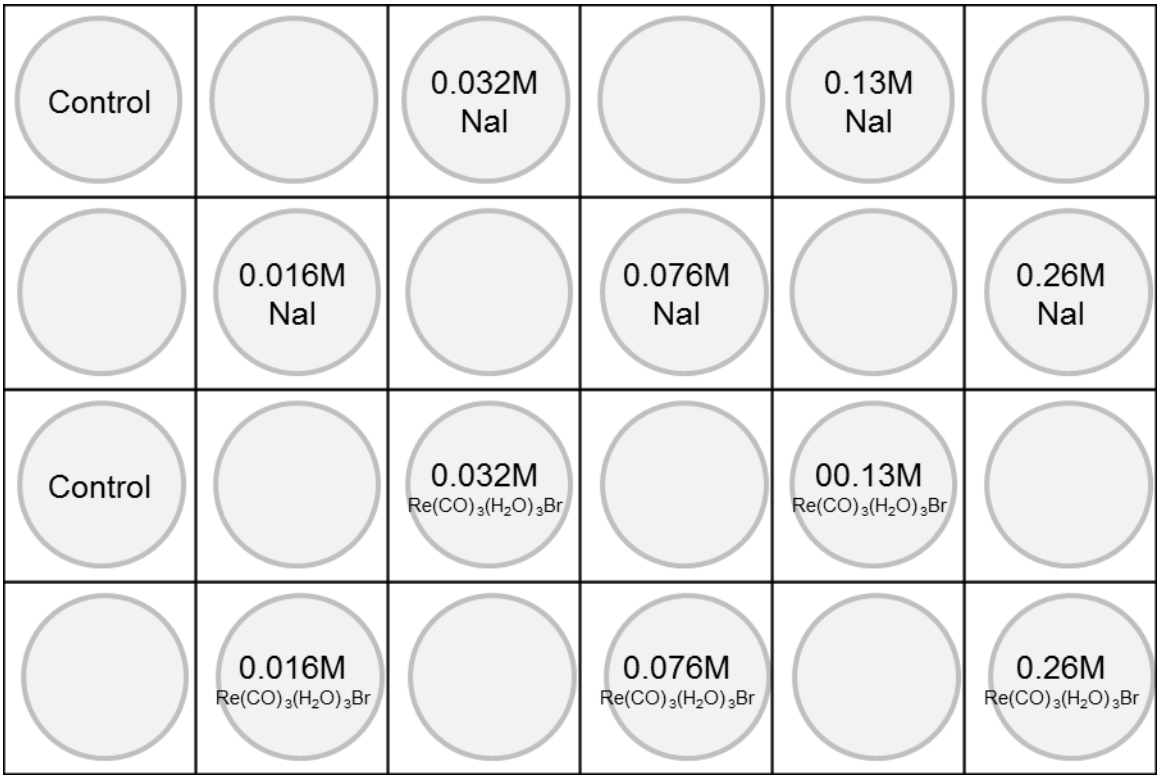

Figure 5.2: Cell culture plate containing various concentrations of NaI and $[Re(CO)_3(H_2O)_3]Br$ in the indicated positions.

5.2.2 Insulin binding to the $Re(CO)_3^+$ core. Experimental:

10 mg of porcine insulin was added to 750 µl of nanopure water, dissolved by adding 20 µL aliquots of 0.5 M NaH_2CO_3 until no more solid insulin could be seen, then diluted with nanopure water to a final insulin concentration of 10 mg mL^{-1}. Crystals were obtained via the hanging drop method using a reservoir solution of 0.05 M MES buffer (pH = 5.5) and 0.8 M NaCl. The drop was composed of 4 µL of the reservoir solution and 4 µL of the protein solution. Small to medium sized insulin crystals appeared in 72 hours. The insulin crystals were collected with a wire loop and transferred to a 8 µL drop containing 3 molar equivalents of $[Re(CO)_3(H_2O)_3]Br$, which was then resealed over the original well for 72 hours. For mass spectrometry experiments, 10 mg of insulin was added to 500 µL

of nanopure water. 10 μL aliquots of $NaHCO_3$ were then added to dissolve the protein. Next, nanopure water was added to produce a final protein concentration of 10 mg mL^{-1}. Aliquots of this protein solution were added to aliquots of $[Re(CO)_3(H_2O)_3]Br$ solution to produce samples with insulin : rhenium concentrations of 1:0, 1:0.1, 1:0.5, 1:1, 1:2, and 1:3. The solutions were incubated for 12 hours at 4 ˚C then analyzed by MALDI- TOF-MS.

5.3.1 Rhenium as a contrast agent: Results and discussion

To further explore the use of rhenium as a X-ray contrast agent, we compared the parent compound $[Re(CO)_3(H_2O)_3]Br$ to the contrast provided by ionic iodine. Iodixanol, sold under the brand name Visipaque™, is an intravenous iodine contrast agent widely used for Contrast Enhanced Computed Tomography (CECT) of head or body.[199] The structure of iodixanol can be seen below in Figure 5.3, along with $[Re(CO)_3(H_2O)_3]Br$ The molecular weight of iodixanol is 1550.20 g/mol and it is composed of 49.1% iodine by weight, which is similar to the 46.1% rhenium by mass of the $[Re(CO)_3(H_2O)_3]Br$. The lowest effective and maximum recommended doses of iodixanol correspond to an iodine molarity of 0.032 M and 0.076 M respectively.[199] Solutions of sodium iodide and $[Re(CO)_3(H_2O)_3]Br$ corresponding to a range of molarities above and below this range were prepared in ballistics gelatin to simulate the density of human tissue.

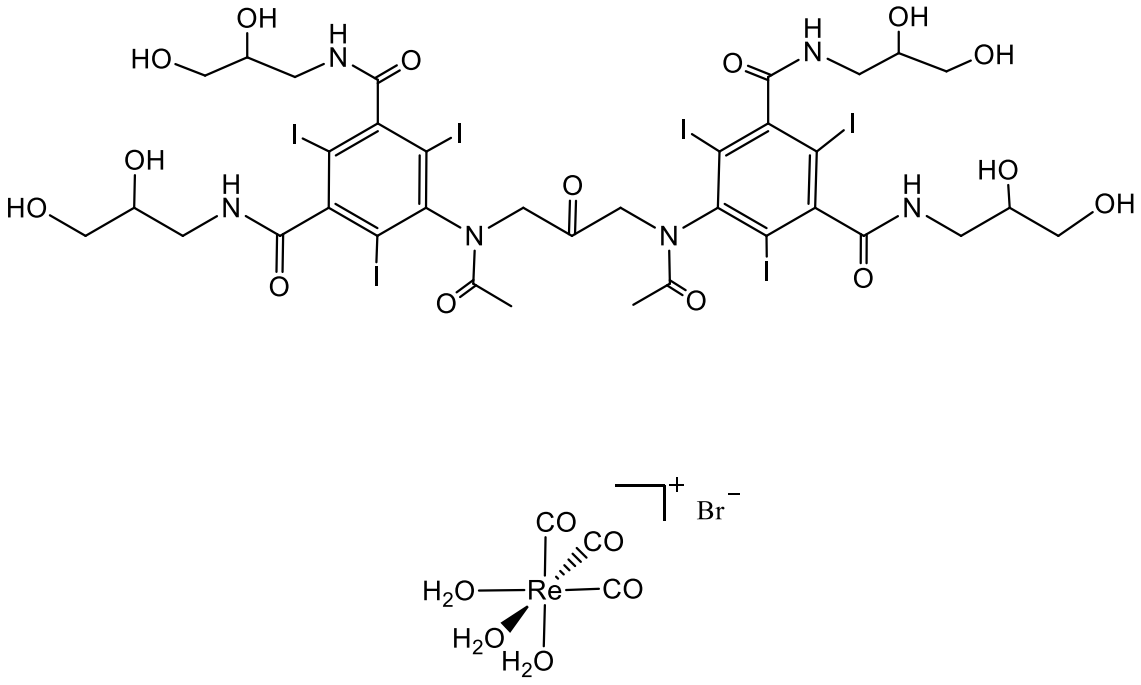

Figure 5.3: Iodixanol (Visipaque™)[199] and $[Re(CO)_3(H_2O)_3]Br$.[62]

As can be seen below in Figure 5.4, the rhenium complex did indeed provide X-ray contrast similar to that of sodium iodide. While the gelatin also attenuated the X-rays to some extent, visual inspection shows that the gelatin samples containing the sodium iodide and $[Re(CO)_3(H_2O)_3]Br$ had much greater attenuation. Further studies would be needed to determine the effects of the bromide ion on the attenuation of the $[Re(CO)_3(H_2O)_3]Br$ complex.

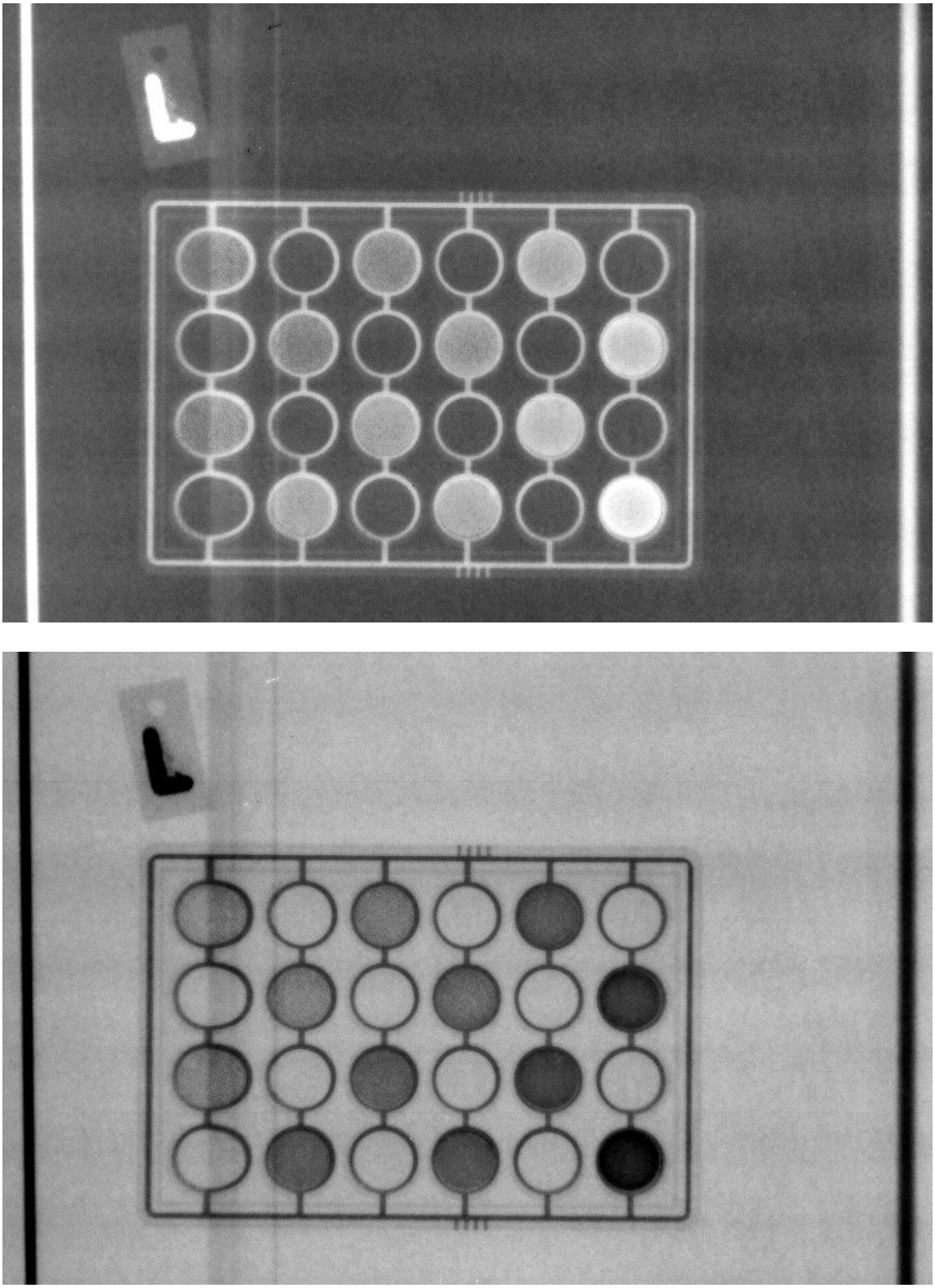

Figure 5.4: Positive (top) and negative (bottom) radiographs of ballistics gelatin samples containing various amounts of NaI and $[Re(CO)_3(H_2O)_3]Br$.

5.3.2 Insulin binding to the $Re(CO)_3^+$ core. Results and Discussion

The labeling of insulin with $Re(CO)_3^+$ would be a direct approach to radiopharmaceutical development, while also lending insight into the biological processing of the $Re(CO)_3^+$ core and the protein-metal interaction.[13] The need to monitor insulin disregulation is applicable to several disease states.[196, 197] There were several challenges to overcome in our production and characterization of a $Re(CO)_3^+$ - insulin conjugate. First, standard protocols for insulin crystallization call for the use of ammonium hydroxide to fully dissolve the insulin and phosphate buffers for crystallization.[157] Ammonium in particular is an excellent ligand for $Re(CO)_3^+$ so we replaced these two entities with $NaHCO_3$ and the non-coordinating MES buffer, to increase the chances of the $Re(CO)_3^+$ core binding to an amino acid site on the periphery of the protein, such as histidine. We were able to grow small cubic insulin crystals under these conditions that were visually similar to insulin crystals seen in the literature.[157] These crystals were cryoprotected as described previously and we were able to collect X-ray data on these $Re(CO)_3^+$-insulin crystals, although a structure solution has not yet been found.

We exposed insulin solutions (1 mg mL^{-1} protein) in pure water to several stoichiometries of the $Re(CO)_3(H_2O)_3^+$ ion, and the observed mass spectra are shown in Figure 5.5-5.7 below. Unmodified insulin shows a peak at approximately 5806 m/z, in agreement with its experimentally determined molecular weight.[157] As the ratio of $Re(CO)_3(H_2O)_3^+$ ion to protein increases, a peak that corresponds to an increase in mass of approximately 270 appears. This mass change corresponds to the weight of the $Re(CO)_3^+$ unit, a clear indicator that the $Re(CO)_3(H_2O)_3^+$ ion is interacting with the protein, possibly via coordination of one or more amino acid side chains.

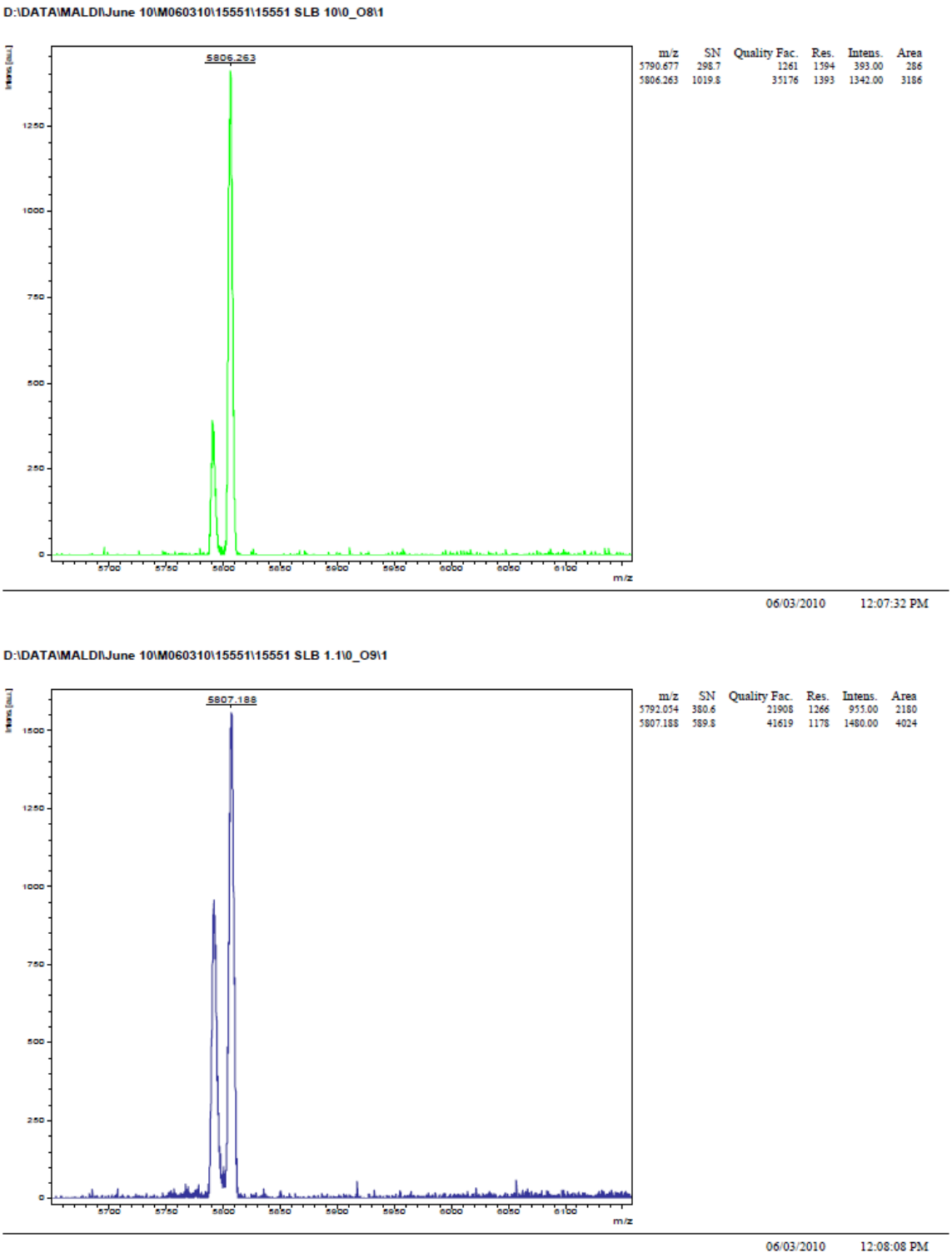

Figure 5.5: MALDI-TOF MS of 1:0 (top) and 1:0.1 (bottom) molar equivalents of insulin:$Re(CO)_3^+$.

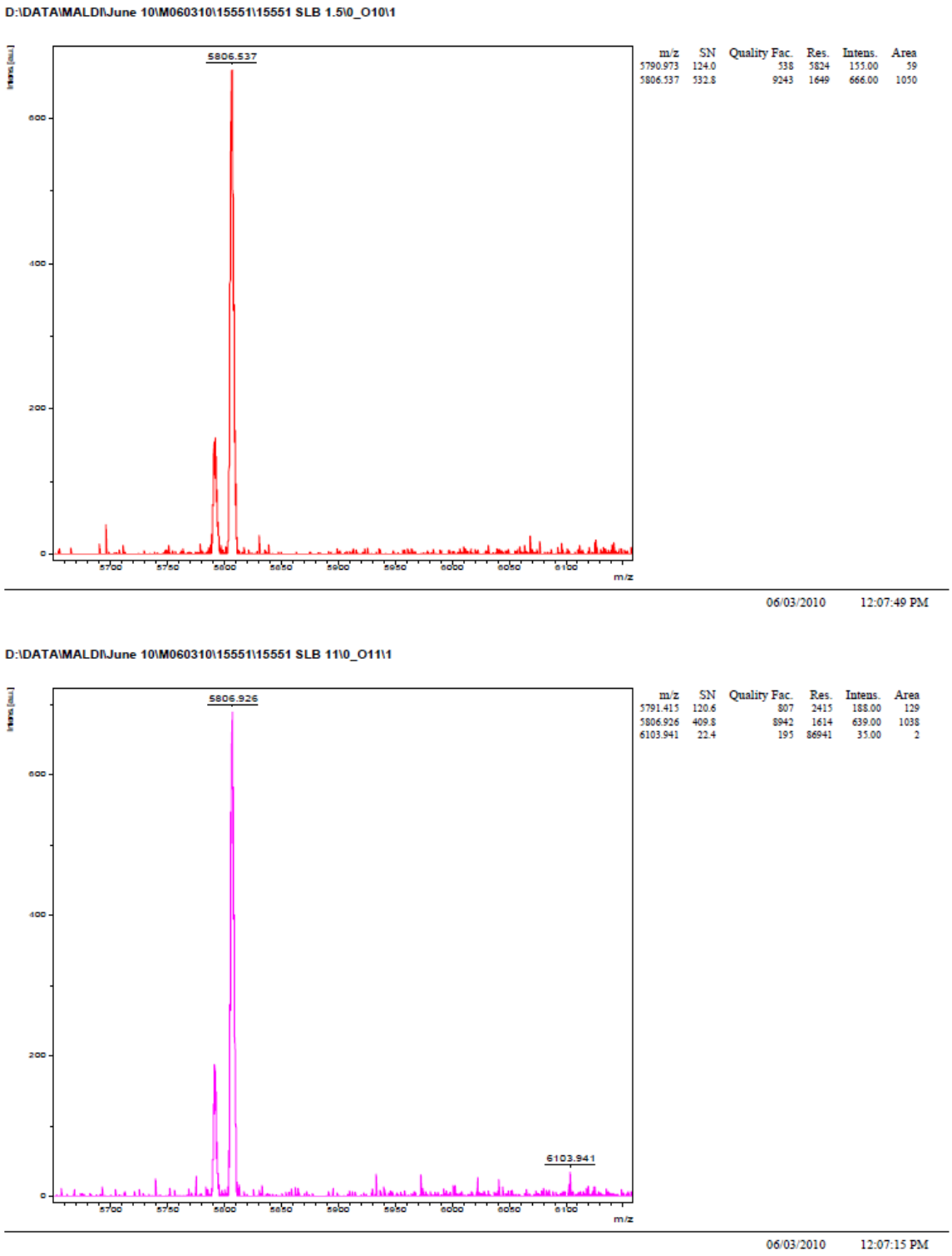

Figure 5.6: MALDI-TOF MS of 1:0.5 (top) and 1:1 (bottom) molar equivalents of insulin:$Re(CO)_3^+$.

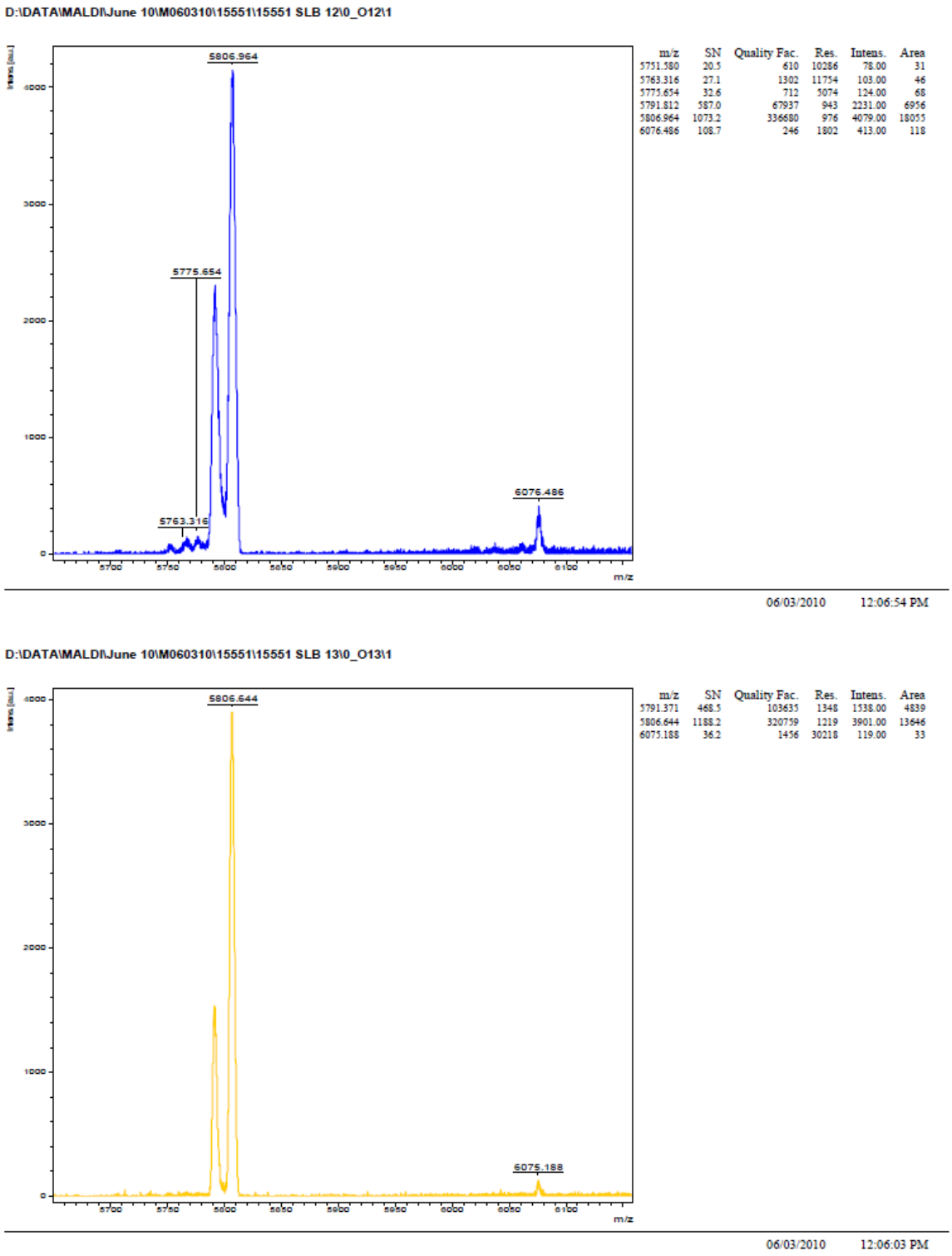

m/z	SN	Quality Fac.	Res.	Intens.	Area
5751.580	20.5	610	10286	78.00	31
5763.316	27.1	1302	11754	103.00	46
5775.654	32.6	712	5074	124.00	68
5791.812	587.0	67937	943	2231.00	6956
5806.964	1073.2	336680	976	4079.00	18055
6076.486	108.7	246	1802	413.00	118

m/z	SN	Quality Fac.	Res.	Intens.	Area
5791.371	468.5	103635	1348	1538.00	4839
5806.644	1188.2	320759	1219	3901.00	13646
6075.188	36.2	1456	30218	119.00	33

Figure 5.7: Mass spectra of 1:2 and 1:3 molar equivalents of insulin to $Re(CO)_3^+$.

5.4 Conclusions:

While the $Tc(CO)_3^+$ and $Re(CO)_3^+$ cores have been around for some time, many aspects of the fundamental chemistry of these cores has yet to be explored. In this chapter, we have explored the use of $[Re(CO)_3(H_2O)_3]Br$ as a possible X-ray contrast agent, and while further studies are needed to determine the extent of the X-ray attenuation provided by rhenium, the use of $Re(CO)_3^+$ cores as contrast agents could make ^{188}Re radiopharamaceutical treatment available to facilities that do not have access to the more expensive SPECT and PET instrumentation.

The insulin-$Re(CO)_3^+$ conjugate was visible in the MALDI-TOF mass spectra but a suitable structural solution was not obtained through X-ray diffraction. Due to the low yield of the insulin-$Re(CO)_3^+$ crystallization experiments, IR spectroscopy was not performed, but IR experiments might shed light on the interaction between insulin and the $Re(CO)_3^+$ core.

CHAPTER VI

SUMMARY

^{99m}Tc is a mainstay of nuclear medicine. This nuclide has ideal clinical isotopic properties and can be widely available through the use of ^{99}Mo-^{99m}Tc generators. The development of a kit to reduce the pertechnetate eluted from the generator to $^{99m}Tc(CO)_3^+$ has sparked interest into radiopharmaceutical development based on the $^{99m}Tc(CO)_3^+$ core. The development of an analogous ^{188}W-^{188}Re generator and a similar reduction kit to produce $^{188}Re(CO)_3^+$ has made the pursuit of radiopharmaceuticals based on the $^{188}Re(CO)_3^+$ core a more practical endeavor. Rhenium tricarbonyl complex- based radiopharmaceuticals can serve as mimics for their ^{99m}Tc- based counterparts, since the chemistry of these two elements is very similar in their +1 oxidation states. Rhenium tricarbonyl complexes also have potential uses as therapeutic radiopharmaceuticals, especially with the incorporation of the beta emitting ^{188}Re isotope.

Herein, the syntheses and toxicity of tripodal tricarboyl rhenium complexes as radiopharmaceutical models are reported. Complexes of the type $[Re(CO)_3(TAME)]X$ (TAME = 1,1,1-trisaminomethylethane, X= Br^-, Cl^-, NO_3^-, ClO_4^-, and PF_6^-) were synthesized. $[Re(CO)_3(TAME)]Cl$ and $[Re(CO)_3(TAME)]Br$ were made by refluxing $Re(CO)_5Cl$ and $Re(CO)_5Br$, respectively, in methanol with the TAME ligand. The remaining three complexes were made via metathesis reactions of $[Re(CO)_3(TAME)]Cl$

with the corresponding silver salt ($AgNO_3$, $AgClO_4$, and $AgPF_6$). Full characterization, including X-ray diffraction analysis of the complexes, showed isostructural anions that differed only in the identity of the non-coordinating anion. The toxicity of these salts was investigated using two cell lines, the monoclonal HeLa-S3 cell line and a primary cell line harvested from the vascular smooth muscle cells of mice. None of the complexes were appreciably toxic in the HeLa-S3 cell line, even at the highest concentrations that the aqueous solubility limit of these complexes allowed. The common analgesics acetaminophen, acetylsalicylic acid, and ibuprofen were also tested at identical concentrations to further underscore the lack of toxicity displayed by these complexes. The bromide salt exhibited limited toxicity in the vascular smooth muscle cell line, which can likely be attributed to the cytotoxicity of the anion rather than the complex itself.

We also report the reaction of $Re(CO)_3(H_2O)_3^+$ with hen egg white lysozyme in aqueous solution. $Re(CO)_3(H_2O)_3^+$ was made according to the literature conditions by refluxing $Re(CO)_5Br$ in water for several days. We combined several stoichometries of $Re(CO)_3(H_2O)_3^+$ to lysozyme and observed the coordination of the two species via MALDI mass spectrometry. A peak corresponding to the mass of the lysozyme- $Re(CO)_3(H_2O)_3^+$ conjugate was observed as the concentration of $Re(CO)_3(H_2O)_3^+$ was increased. Crystallization of the lysozyme- $Re(CO)_3(H_2O)_3^+$conjugate was achieved via the hanging drop method, using a solution with a 50 mg mL^{-1} lysozyme concentration and a molar equivalent of lysozyme to $Re(CO)_3(H_2O)_3^+$ of 1:3. Single crystal X-ray diffraction analysis showed that the rhenium tricarbonyl cation binds to the His15 site of the lysozyme in two significantly populated rotamer conformations. The rotamer conformations were supported by the IR spectra of the lysozyme- $Re(CO)_3(H_2O)_3^+$ crystals, which showed one e and 2 a_1

v(CO) stretching bands resulting from the pseudo-C_{3v} symmetry of the facial $Re(CO)_3^+$ unit and the presence of multiple rotamers of the $Re(CO)_3^+$ adduct.

We continued our study of the lysozyme- $Re(CO)_3(H_2O)_3^+$ conjugate by first studying the binding of $Re(CO)_3^+$ to lysozyme through equilibrium dialysis and next through NMR experiments. The results of these experiments agreed with the crystallography experiments mentioned previously; namely, that the rhenium tricarbonyl cation binds to His 15 via replacement of one of the coordinated water molecules to result in a single covalent adduct. We soaked lysozyme- $Re(CO)_3(H_2O)_3^+$ crystals in a solution containing glyoxime in an attempt to replace the remaining two waters. The resulting crystals were also subjected to X-ray crystallographic analysis and no rhenium electron density was observed. This indicated that the glyoxime had leached the rhenium center away from the protein and that the bonding of the $Re(CO)_3(H_2O)_3^+$ complex to His 15 is reversible.

We further probed the interaction of $Re(CO)_3(H_2O)_3^+$ with two studies; the study of $Re(CO)_3(H_2O)_3Br$ as a potential X-ray contrast agent, and a study of the interaction of $Re(CO)_3(H_2O)_3^+$ and porcine insulin. The X-ray attenuation of $Re(CO)_3(H_2O)_3Br$ was compared to molar equivalents of sodium iodide by examining a radiograph of these compounds in ballistics gelatin. $Re(CO)_3(H_2O)_3Br$ attenuated X-rays at an rate equaling or exceeding that of sodium iodide, although further studies would be needed to determine the contribution of the bromide ion. The synthesis of an insulin- $Re(CO)_3^+$ was successful and mass spectra confirmed the formation of insulin-$Re(CO)_3^+$. The insulin-$Re(CO)_3^+$ conjugate was able to be crystallized via the hanging drop method and a novel buffer

system, but a structural solution of this conjugate has not been found. Further tests are needed to more completely probe the insulin-$Re(CO)_3^+$ interaction.

CHAPTER VII

ADDENDUM

Research in the area of tricarbonyl rhenium (I) based molecules is ongoing. This addendum has been prepared to better address the recent advances in this field in the time period between when this research was done and the publication of this manuscript. Additionally, this chapter will serve to better connect the author's work to the larger fields of $Re(CO)_3^+$ complex radiopharmaceutical development and organometallic protein complexes.

The field of radiopharmaceutical development based on the $M(CO)_3^+$ core (M= Re, Tc) continues to expand. In addition to the examples of examples of potential radiopharmaceuticals discussed in Chapter 1, several excellent reviews of these complexes have recently been published.[9, 34, 43, 115, 200, 201] Many of the synthetic and *in vitro* testing of the complexes were carried out in an analogous manner to the $[Re(CO)_3(TAME)]^+$ complexes discussed in Chapter 2 of this work and shown in Figure 7.1 (a), below.[202] Specific complexes used as examples to illustrate study commonalities and contrasts within the field of $Re(CO)_3^+$ radiopharmaceutical development in this section are also pictured in Figure 7.1 (b-d).[203-205]

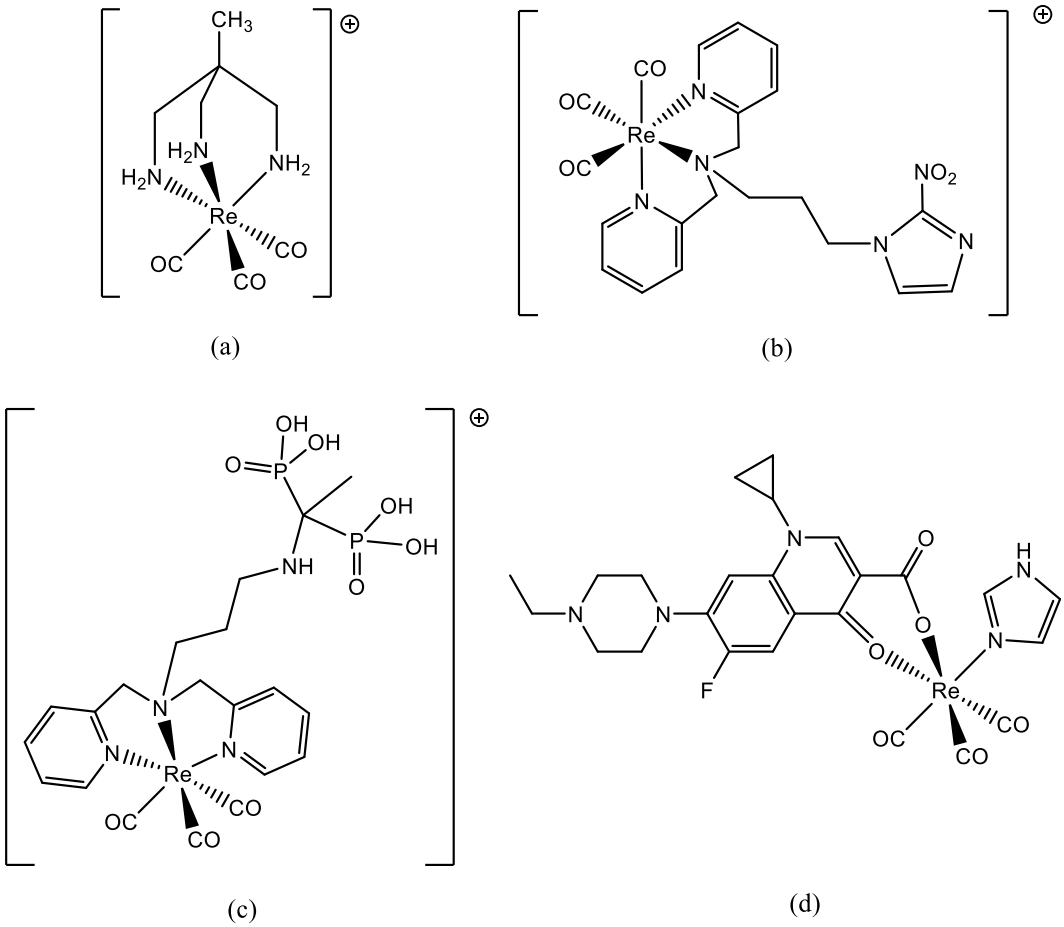

Figure 7.1: Novel $Re(CO)_3^+$ based complexes used to highlight the similarities in development and study of $Re(CO)_3^+$ based radiopharmaceuticals: (a) $[Re(CO)_3(TAME)]^+$, from Chapter 2 of this manuscript,[202] (b) rhenium analog of a potential $^{99m}Tc(I)(CO)_3$ hypoxia imaging agent,[203] (c) rhenium analog of a potential $^{99m}Tc(I)(CO)_3$ / $^{186/188}Re(I)(CO)_3$ bone-seeking imaging agent / metastatic bone pain palliative agent,[204] and (d) rhenium analog of a potential rhenium quinolone complex for infection imaging.[206]

The studies of the molecules above share many common features. One of the hallmarks of $^{99m}Tc(CO)_3$ based imaging agent development is that the synthesis and characterization is often accomplished using the non-radioactive $Re(CO)_3^+$ moiety. In addition to the standard characterizations, most potential rhenium tricarbonyl radiopharmaceuticals are characterized by their lipophilicity via a distribution coefficient or partition coefficient calculation. These can be determined using the shake flask method

containing two layers; an aqueous layer and an octanol layer, as described in Chapter 2. The differences in the distribution studies of these compounds arises from the detection method used to determine the concentration of the potential radiopharmaceutical in each layer. If the $^{99m}Tc(CO)_3$ analog of the compound was made, generally the determination is made using a gamma counter, as was the case with molecules (b) and (c) above.[203, 204] The partition coefficient of complex (d) was notable for its omission. However, in this case, distribution was actually determined by injecting the ^{99m}Tc analog into a mouse model and imaging the result.[206]

Another common thread in the studies of potential tricarbonyl rhenium (I) radiopharmaceuticals is the biological challenge study. The potential radiopharmaceutical is incubated in conditions simulating its target environment and then tested for degredation. The $Re(CO)_3(TAME)^+$ cation that was the basis of Chapter 2 was tested for stability via incubation in the presence of the competing biological ligands cysteine and histidine, mimicking the human serum environment, by Herrick *et al.*[67] In the Herrick study, the degredation of the complexes was monitored by ^1H NMR.[67] In the case of the tricarbonyl rhenium (I) bisphosphonate complex, (c), above, the ^{99m}Tc analog of the molecule was incubated with cysteine or histidine, separately, and degredation was monitored via HPLC. The stability of the resulting molecule was expressed as the percent of radiochemical purity.[204] The challenge study of the ^{99m}Tc analogs of (b) and (e) were also measured by HPLC, but the complexes were incubated in human blood serum[203] and standard phosphate buffer solution,[206] respectively.

The greatest variance in the studies of potential tricarbonyl rhenium (I) radiopharmaceuticals is in the cell proliferation, viability, and toxicity studies. One

possible explanation for these differences is that these studies are tailored to the target tissue of each potential radiopharmaceutical, with varying protocols based on the study goals and conditions required by each tissue culture. The toxicity of the complexes described in Chapter 2 were studied in an immortal cell line, human cervical cancer (He-La), and a primary cell culture (spontaneously hypertensive mouse vascular tissue). The primary cell culture was chosen because of the proposed use of the molecules as cardiac perfusion imaging agents and toxicity in the primary cell line was probed through trypan blue staining and direct counting. HeLa was chosen as a robust immortal cell line commonly used in the study of potential radiopharmaceutials and toxicity data from the HeLa line was obtained through the use of Invitrogen's LIVE/DEAD® Viability Assay.[207] In this assay, C_{12}-resazurin is reduced to red-fluorescent C12-resorufin by metabolically active cells while the cell impermeant SYTOX® Green stains cells with compromised plasma membranes. The resulting cells can then be directly counted or analyzed by flow cytometry. Complex (c) above was studied using a similarly designed cell study, in which toxicity was probed using the trypan blue staining / direct cell counting method and the MTT assay (Trevigen®) in the immortal PC-3 cell culture (human prostate adenocarcinoma derived from a metastatic bone site), which fits the target tissue of the potential bone imaging agents in this study.[204]

The MTT assay used in this study is certainly more commonly used than the LIVE/DEAD assay described previously.[201] The MTT assay measures cell proliferation rate by spectroscopically determining the amount of tetrazolium salt being reduced by metabolically active cells.[208] However, the authors of this study note that the reduction of the MTT measures cell proliferation indirectly, via the metabolism of the MTT, and thus

felt that a direct counting method was warranted to confirm the cell growth and toxicity of their complexes.[204] While it would be interesting to study the complexes in Chapter 2 with the MTT assay to see if there are any differences compared to the LIVE/DEAD assay, the inclusion of the direct counting typan blue staining method likely confirms their non-toxic nature.

The HeLa studies from Donnelly's group (molecule (b), above) were not designed to study toxicity, but instead to take advantage of the luminescent properties of some of their complexes to determine where the molecule would localize in the cell.[203] Further studies of the more stable complexes, including the one in Figure 7.1 (b), were carried out in a human neuroblastoma cell line. Instead of a staining technique to determine toxicity, ICP-MS was used to determine the concentration of the complexes inside the cytosol of the cell and was reported as a ratio to the amount of intracellular proteins.[203] In addition to the $Re(CO)_3^+$ complexes investigated by Donnelly's group, ICP-MS has been used to determine cellular uptake of platinum complexes[209] and ruthenium complexes[210] in the literature and could likely further the toxicity studies on the $[Re(CO)_3(TAME)]^+$ complexes described in Chapter 2. Since the complexes studied in Chapter 2 were largely non-toxic, an ICP-MS study of the intracellular matrix could provide evidence that these molecules could accumulate in the cytosol of the target tissue. The ^{99m}Tc version of complex (b) was subsequently studied in an animal model and the complex did indeed localize in the hypoxic tumor tissue of 1 of the 3 animals tested.[203]

The $Re(CO)_3$ - quinolone conjugate (d) developed by Psomas *et al*. was studied in a human erythroleukemia cell line (K-562).[206] Simlarly to Donnelly's study, cell culture was used to determine processing instead of toxicity of the complexes. In this case, the

^{99m}Tc analog of complex (d) was prepared and incubated with the K-562 cells. The cultures were then lyzed, sonicated, and centrifuged with a variety of buffers designed to separate cells into cytosol, nuclear, membrane, and mitochondria fractions. Each fraction was then analyzed with a γ-counter to determine the concentration of ^{99m}Tc.[206] An interesting follow up experiment to probe the processing of the molecules in Chapter 2 would be to combine the fractionation technique used by the Psomas group with the ICP-MS protocol in Donnelly's study to probe the location and concentration of the cold rhenium analogs in cell culture and to gain fundamental knowledge of the biological processing of these potential rhenium radiopharmaceuticals.

Biological processing of $[Re(CO)_3(H_2O)_3]^+$ is one of the focuses of Chapters 3-5 of this work; elucidating the interaction of this rhenium radiopharmaceutical precursor with proteins.[75, 76] As the above examples demonstrate, there are many tricarbonyl rhenium (I) and technetium (I) complexes with clinical potential, yet their specific interactions with their target biomolecules have yet to be characterized. The work described in Chapters 3 and 4 of this text describes the interaction of $[Re(CO)_3(H_2O)_3]^+$ with lysozyme as a model of $Re(CO)_3^+$ - protein interations. Part of Chapter 5 of this text describes preliminary studies of a $Re(CO)_3^+$ - insulin adduct as well.

This work builds upon the success of several groups who previously elucidated the structure of an organometallic protein adduct. The first $Re(CO)_3^+$ protein adduct was synthezised and structurally elucidated by Gray and coworkers to study the electron transfer properties of blue copper azurin.[74, 211] Gray and coworkers compared the electron transfer of Cu (I) to Ru (III), Os (III) or Re (I)*, complexes that were all bound to the His 83 position of azurin. Wild-type azurin has histidine residues at the above position and at

His 35, 46, and 117. With site directed mutagenesis, Gray and coworkers were able to introduce histidine residues at a variety of other positions, while eliminating native residues, to direct the metalation of their proteins.[77, 78, 114, 119] Strategic introduction of tryptophan and tyrosine residues demonstrated the importance of these residues in the multi-step electron transfers, termed "hopping," in proteins.[212]

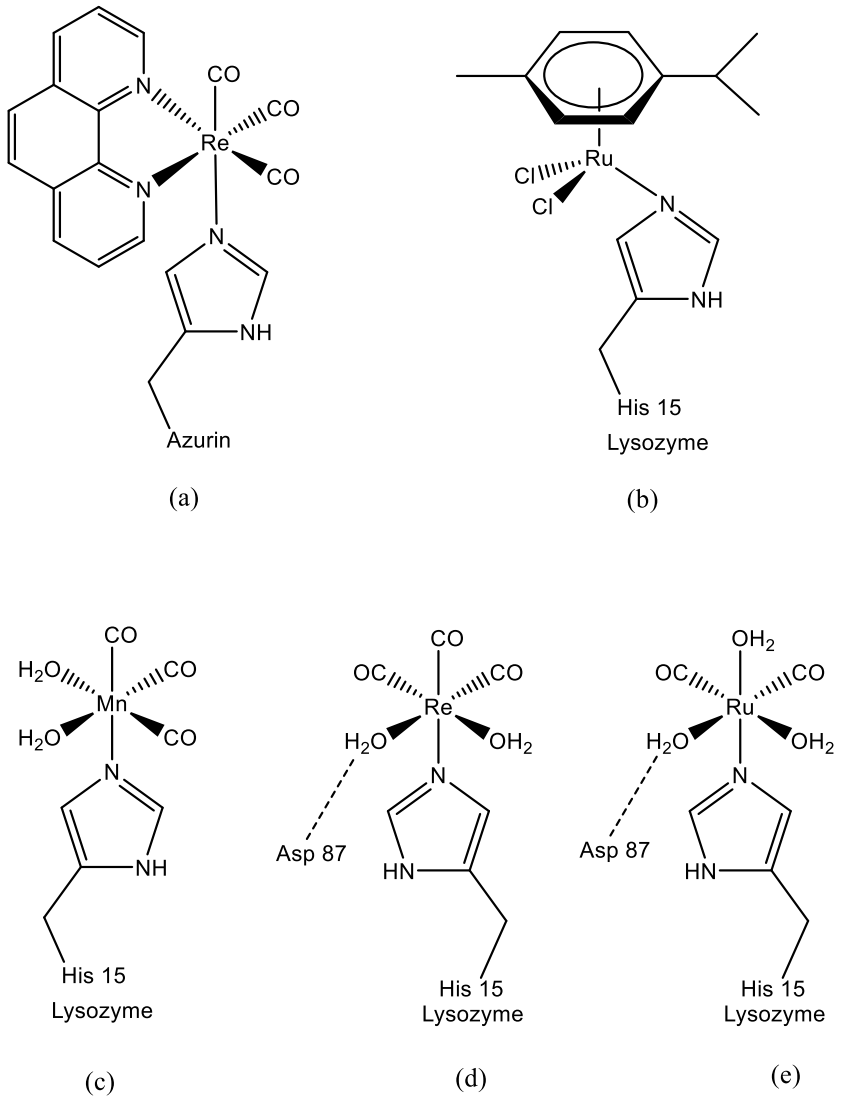

Figure 7.2: Coordination of organometallic complexes to proteins: (a) $Re(CO)_3$(phenanthroline)(His 83)$^+$ in the blue copper protein, azurin.[211] (b) (η^6-*p*-cymene)$RuCl_2(H_2O)$(His 15) lysozyme,[162] (c) $Mn(CO)_3(OH_2)_2$(His 15) lysozyme,[161] (d) $Re(CO)_3(OH_2)_2$(His 15) lysozyme,[76] and (e) $Ru(CO)_2(OH_2)_3$(His 15) lysozyme.{{190 Santos-Silva, Teresa 2011}}

The work in Chapters 3-5 focuses more on achieving a fundamental understanding of the $Re(CO)_3^+$-protein adduct. Thus, lysozyme was chosen as a well-characterized, easily crystallizable model protein for $Re(CO)_3^+$-protein interactions. Additionally, the structure of lysozyme with ruthenium[162] and manganese[161] complexes had previously been elucidated. In both cases, significant metalation was only observed at the His 15 residue. The structure of the bound ruthenium and manganese complexes are shown in Figure 7.2 (b) and (c) above.

The manganese tricarbonyl species, elucidated by Artero and coworkers is especially relevant to the work described in this manuscript. The synthesis, structural characterization, and study of $Re(CO)_3(OH_2)_2$-lysozyme described herein (Figure 7.2, (d)) was modeled in part after this work. Artero and coworkers attempted metalation with iron and ruthenium carbonyls in addition to the $Mn(CO)_3$ species described above, but were only able to observe the $Mn(CO)_3$ species in the crystallized lysozyme. The $Mn(CO)_3$-lysozyme adduct was characterized by IR spectroscopy, which exhibited pseudo-C_{3v} carbonyl stretches similar to those used to demonstrate metalation of lysozyme by $Re(CO)_3^+$ in the work described here. Additional similarities between these two studies were the less than 100% occupancy of the His 15 site and the lability of the metal carbonyl species. In the study described by Artero and co-workers, the $Mn(CO)_3$ fragment of the $Mn(CO)_3$-lysozyme complex was demetallated upon exposure to the nickel complex, [Ni(xbsms)] (H_2xbsms = 1,2-bis(4-mercapto-3,3-dimethyl-2-thiabutyl)benzene) to give $[Ni(xbsms)Mn(CO)_3(OH_2)]^+$ shown in Scheme 7.1 below.[161] Similar demetallation of $Re(CO)_3^+$-lysozyme was observed in the presence of glyoxime.[75]

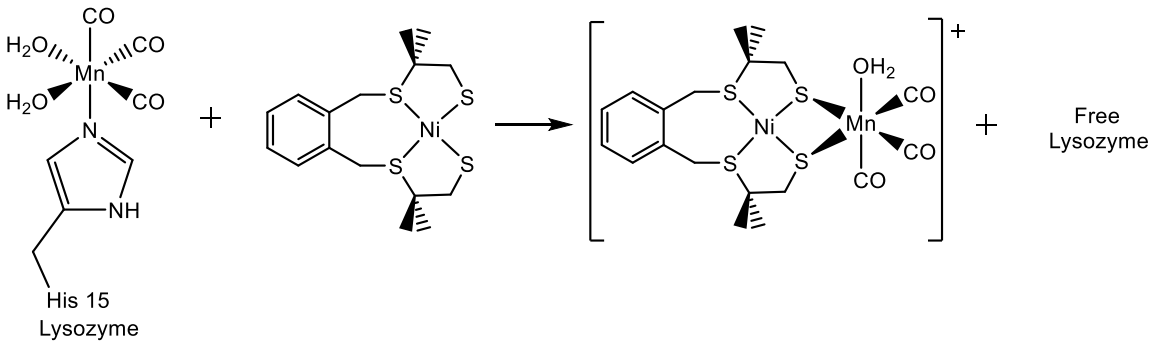

Scheme 7.1: Synthesis of $[Ni(xbsms)Mn(CO)_3(OH_2)]^+$ through reaction of $Mn(CO)_3$-lysozyme with [Ni(xbsms)].[161]

Zobi and Springler built upon the work described in Chapters 2 and 3 with a subsequently published study of the reaction of $Re(CO)_3(OH_2)_3^+$ with lysozyme.[177] By increasing the concentration of the cation, a $Re(CO)_3(OH_2)_2$(His 15)-lysozyme adduct, identical to the one shown in Figure 7.1 (d) was structurally characterized with 100% occupancy at the His 15 site. In subsequent reactions with imidazole (im), pyridine-2-carboxylic acid (pa), and L-serine (L-ser), the corresponding $Re(CO)_3(OH_2)$(im)(His 15) $Re(CO)_3$(pa)(His 15) and $Re(CO)_3$(L-ser)$_2$(His 15)-lysozyme adducts were observed. The (im) and (L-ser) versions were able to be structurally characterized by x-ray diffraction while the (pa) version was confirmed by LC-MS. Conversely, reactions of the $Re(CO)_3(OH_2)_2$(His 15)-lysozyme adduct with pyridine, 2-methylaminopyridine, and ethylenediamine demetallated the lysozyme.[177] This result is analogous to demetallation of $Re(CO)_3(OH_2)_2$(His 15)-lysozyme with glyoxime that we describe in the previous chapters.[75]

Lysozyme has also recently proved to be an excellent system for studying the interaction of carbon monoxide releasing molecules (CORMs) with proteins. Romão, et al reacted CORM-3 with horse myglobin, hen egg white lysozyme, and human hemoglobin,

albumin, and transferrin, and were able to structurally elucidate a Ru-lyzozyme adduct.[176] Lysozyme crystals were soaked with CORM-3, [*fac*-$Ru(CO)_3Cl(\kappa^2\text{-}H_2NCH_2CO_2)$], and the adduct $Ru(CO)_2(OH_2)_3$(His 15) was elucidated via X-ray diffraction with the metal modeled at 80% occupancy, as shown in Scheme 7.2 below. Two other sites, Asp 18 and Asp 52 contained metal density at lower occupancies. The same authors investigated the interaction of additional CORMs, $Ru(CO)_3Cl_2$(1,3-thiazole)[213] and *fac*-$[Mo(CO)_3$(histidinate)]Na,[214] with proteins, also shown in the figure below, but were only able to crystallize one additional covalent complex, the His 15, Asp 18 and Asp 119 adducts with $Ru(CO)(OH_2)_4$ from $Ru(CO)_3Cl_2$(1,3-thiazole). The molybdenum complex decomposed into a polyoxomolybdate cluster, $[PMo_{12}O_4]^{3-}$, that was hydrogen bonded to Arg 45 of lysozyme.

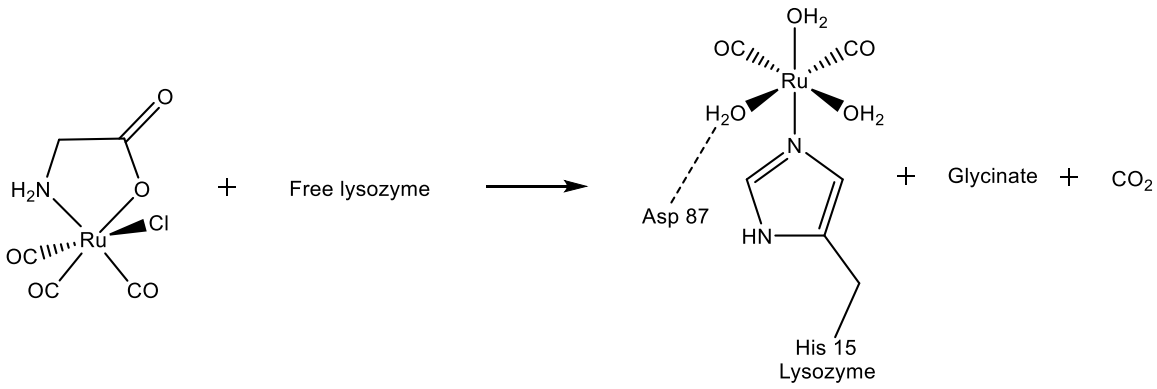

Scheme 7.2: The reaction of CORM-3 with lysozyme.[176]

In addition to the follow up work on the $Re(CO)_3(OH_2)_2$-(His 15) lysozyme adduct, another study from the University of Zurich, from Alberto and coworkers, was able to structurally elucidate a rhenium metallated carbonic anhydrase, specifically, human carbonic anhydrase IX.[215] Over expression of carbonic anhyrases are found in some hypoxic tumors, making them an attractive imaging target. Crystals of the carbonic

anhydrase protein were soaked in solutions containing an excess of $Re(CO)_3$cyclopentadienyl-based inhibitors of carbonic anhydrase like the one shown below in Figure 7.3. In the resulting crystal structure, the deprotonated amine terminus of the molecule was coordinated to a Zinc metal in the protein active site. The cyclopentadienyl moiety extended into a hydrophobic pocket. It would be interesting to see if zinc coordination could be exploited structurally elucidate a $Re(CO)_3^+$-insulin conjugate, like the ones described in Chapter 5, by X-ray diffraction. Insulin is traditionally crystallized with Zn^{2+},[157] and previous labeling attempts have taken place at the amine terminus.[13] Conversely, initial investigations of the $Re(CO)_3^+$ and $Tc(CO)_3^+$ interaction with metallothioeins show that the $[M(CO)_3(OH_2)_3]^+$ species replace the bound zinc metals, which could potentially be another route to a $Re(CO)_3$-protein conjugate, though no X-ray diffraction experiments were discussed in the metallothioein study.[216]

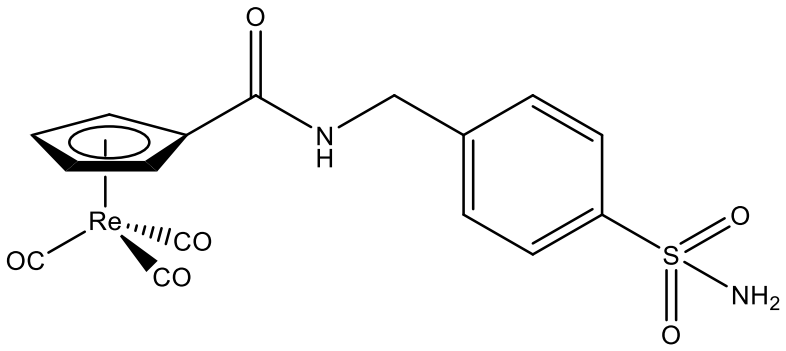

Figure 7.3: A $Re(CO)_3$cyclopentadienyl-based inhibitor of carbonic anhydrase.[215]

In conclusion, there are many connections between the work described in this manuscript and the work being done in the larger field. The $[Re(CO)_3(TAME)]^+$ complexes described in Chapter 2 of this manuscript were characterized and tested *in vitro* using methods that are paralleled in studies of other $Re(CO)_3^+$ potential radiopharmaceuticals.

The study of the $Re(CO)_3(OH_2)_2$-(His15) lysozyme conjugate, synthesized and characterized in Chapters 3 and 4, was modeled after previously published studies of organometallic protein conjugates and has since been expanded on by others using different metals and protein systems. Despite the numerous studies of these $M(CO)_3^+$ (M=Tc, Re) complexes and their potential radiopharmaceutical applications, there are currently no $M(CO)_3$ - based radiopharmaceuticals in clinical use.[201] Hopefully, this will change with continued exploration of the fundamental chemistry of these complexes and their biomolecule conjugates.

REFERENCES

1. World Health Organization. Fact sheet no. 297 – cancer. ; 2011. Report nr 297.

2. Bartholoma, M.; Valliant, J.; Maresca, K. P.; Babich, J.; Zubieta, J. *Chemical Communications* **2009**, *2009*(5), 493-512.

3. Larock, M.; Braat, S. H.; Sochor, H.; Maisey, M.; Rigo, P. *New developments in myocardial imaging technetium ^{99m}Tc sestamibi;* Martin Dunitz Ltd.: London, 1993.

4. Bhattacharyya, S; Dixit, M. *Dalton Transactions* **2011**, *40*(23), 6112-6128.

5. Bucerius, J.; Ahmadzadehfar, H.; Biersack, H. *^{99m}Tc-sestamibi Clinical Applications;* Springer-Verlag: Berlin, 2012.

6. Wester, H.; *Clinical Cancer Research* 2007, *13*, 3470-3481.

7. Mendes, F.; Paulo, A.; Santos, I. *Dalton Transactions* **2011**, *40*(20), 5377-5393.

8. Thorp-Greenwood, F.; Coogan, M. P. *Dalton Transactions* **2011**, *40*(23), 6129-6143.

9. Correia, J. D. G.; Paulo, A; Raposinho, P. D.; Santos, I. *Dalton Transactions* **2011**, *40*(23), 6144-6167.

10. Schibli, R.; Schubiger, A. P. *European Journal of Nuclear Medicine and Molecular Imaging* **2002**, *29*(11),1529-1542.

11. Liu, S; Chakraborty, S. *Dalton Transactions* **2011**, *40*(23), 6077-6086.

12. He, H.; Lipowska, M.; Xu, X.; Taylor, A. T.; Marzilli, L. G. *Inorganic Chemistry* **2007**, *46*(8), 3385-3394.

13. Sundararajan, C.; Besanger, T. R.; Labiris, R.; Guenther, K. J.; Strack, T.; Garafalo, R.; Kawabata, T. T.; Finco-Kent, D.; Zubieta, J.; Babich, J. W. *Journal of Medicinal Chemistry,* **2010**, *53*(6), 2612-2621.

14. Meszaros, L. K.; Dose, A.; Biagini, S. C. G.; Blower, P. J. *Dalton Transactions* **2011**, *40*(23), 6260-6267.

15. Leo, A.; Hansch, C.; Elkins, D. *Chemical Reviews* **1971**, *71*, 525-617.

16. Silverman, R. B. *The Organic Chemistry of Drug Design and Drug Action*; 2nd ed.; Elsevier Academic Press: Burlington, MA, **2004**.

17. Bartholoma, M. D.; Louie, A. S.; Valliant, J. F.; Zubieta, J. *Chemical Reviews* **2010**, *110*, 2903-2920.

18. Dilworth, J. R.; Parrott, S. J. *Chemical Society Reviews* **1998,** *27*(1), 43-55.

19. Pinkerton, T. C.; Desilets, C. P.; Hoch, D. J.; Mikelsons, M. V.; Wilson, G. M. *Journal of Chemical Educication* **1985**, *62*(11), 965.

20. Greenberg, J. H.; Lassen, N. A. *Journal of Cerebral Blood Flow and Metabolism* **1994**, *01*(14), Suppl 1:S1-3.

21. Boschi, A.; Uccelli, L.; Bolzati, C.; Duatti, A.; Sabba, N.; Moretti, E.; Di Domenico, G.; Zavattini, G.; Refosco, F.; Giganti, M. *Journal of Nuclear Medicine* **2003**, *44*(5), 806-814.

22. Liu, S. *Chemical Society Reviews* **2004**, *33*(7), 445-461.

23. Liu, S.; Edwards, D. S. *Chemical Reviews* **1999**, *99*(9), 2235-2268.

24. Alberto, R.; Schibli, R.; Waibel, R.; Abram, U.; Schubiger, A. P. *Coordination Chemistry Reviews* **1999**, *190-192*, 901-919.

25. Dabrowiak, J. C. *Metals in Medicine;* John Wiley and Sons Ltd.: West Sussex, UK **2009**.

26. Liu, S.; Edwards, D. S. *Bioconjugate Chemistry* **2001**, *12*(1), 7-34.

27. Jurisson, S. S.; Lydon, J. D. *Chemical Reviews* **1999**, *99*, 2205-2218.

28. Saha, G. B. *Fundamentals of Nuclear Pharmacy*, 6th ed.; Springer: New York, **2010**.

29. Lam, M. G. E. H; de Klerk, J. M. H.; van Rijk, P. P. *European Journal of Nuclear Medicine and Molecular Imaging* **2004** *31*, S162-70.

30. Bartholoma, M. D.; Vortherms, A. R.; Hillier, S.; Joyal, J.; Babich, J.; Doyle, R. P.; Zubieta, J. *Dalton Transactions* **2011**, *40*(23), 6116-6125.

31. Banerjee, S. R.; Maresca, K. P.; Francesconi, L.; Valliant, J.; Babich, J. W.; Zubieta, J. *Nuclear Medicine Biology* **2005,** *32*(1),1-20.

32. Peterson, T. E.; Furenlid, L. R. *Physics in Medicine and Biology* **2011**, 57(17), R145-182.

33. Qaim, S. M. *Nuclear Medicine Biology* **2000**, *27*(4), 323-328.

34. Donnelly, P. S. *Dalton Transactions* **2011**, *40*(5), 999-1010.

35. El-Mabhouh, A.; Mercer, J. R. *Applied Radiation and Isotopes* **2005**, *62*(4), 541-549.

36. Elder, R. C.; Yuan, J.; Helmer, B.; Pipes, D.; Deutsch, K.; Deutsch, E. *Inorganic Chemistry* **1997**, *36*(14), 3055-3063.

37. Blower, P. J.; Lam, A. S. K; O'Doherty, M. J.; Kettle, A. G; Coakley, A. J.; Knapp, Jr., F. F. *European Journal of Nuclear Medicine* **1998**, *25*, 613-621.

38. He, H.; Lipowska, M.; Xu, X.; Taylor, A. T.; Carlone, M.; Marzilli, L. G. *Inorganic Chemistry* **2005**, *44*(15), 5437-5446.

39. Dunzinger, A.; Hafner, F.; Schaffler, G.; Piswanger-Soelkner, J.; Brodmann, M.; Lipp, R. W. *European Journal of Nuclear Medicine and Molecular Imaging* **2008**, *35*(11), 2082-2087.

40. Goldenberg, D.M.; Abdel-Nabi, H.; Sullivan, C. L.; Serafini, A.; Seldin, D.; Barron, B.; Lamki, L.; Line, B.; Wegener, W. A. *Cancer* **2000,** *89*(1), 104-115.

41. Shih, W.; Hirschowitz, E.; Bensadoun, E.; Woodring, J.; Ryo, Y. U.; Kraman, S. *Annals of Nuclear Medicine* **2002**, *16*(3), 213-219.

42. Alberto, R.; Abram, U.; 99mTc: Labeling chemistry and labeled compounds. In: *Handbook of Nuclear Chemistry*; Vertes, A.; Nagy, S.; Klencsar, Z.; Rosch, F., Eds.; Kluwer Academic Publishers: Boston, **2003**.

43. Alberto, R. Organometallic Radiopharmaceuticals. In: *Topics in Organometallic Chemistry*; Springer-Verlag: Berlin, **2010**.

44. Häfliger, P.; Agorastos, N.; Spingler, B.; Georgiev, O.; Viola, G.; Alberto, R. *ChemBioChem* **2005**, *6*(2), 414-421.

45. Mundwiler, S.; Kündig, M.; Ortner, K.; Alberto, R. *Journal of the Chemical Society, Dalton Transactions* **2004**, *2004*(9), 1320-1328.

46. Agorastos, N.; Borsig, L.; Renard, A.; Antoni, P.; Viola, G.; Spingler, B.; Kurz, P.; Alberto, R. *Chemistry - A European Journal* **2007**, *13*(14), 3842-3852.

47. Howell, R. W. *Medical Physics* **1992**, *19*(6), 1371-1383.

48. Hom, R. K.; Katzenellenbogen, J. A. *Journal of Organic Chem* **1997**, *62*(18), 6290-6297.

49. Top, S.; Elhafa, M.; Vessieres, A.; Quivy, J.; Vaissermann, J.; Hughes, D. W.; McGlinchy; M. J.; Mornon, J. P.; Thoreau, E; Jaouen, G. *Journal of the American Chemical Society* **1995**, *117*, 8372.

50. Dozio, N.; Sarugeri, E.; Scavini, M.; Beretta, A.; Belloni, C.; Dosio, F.; Savi, A.; Fazio, F.; Sodoyez-Goffaux F.; Pozza, G. *Journal of Investigative Medicine* **2001**, *49*(1), 85-92.

51. Iozzo, P.; Osman, S.; Glaser, M.; Knickmeier, M.; Ferrannini, E.; Pike, V. W.; Camici, P. G.; Law. M. P. *Nuclear Medicine Biology* **2002**, *29*(1), 73-82.

52. Rissler, K.; Engelmann, P. *Journal of Chromatography B: Biomedical Sciences and Applications* **1996**, *679*(1-2), 21-29.

53. Guenther, K. J.; Yoganathan, S.; Garofalo, R.; Kawabata, T.; Strack, T.; Labiris, R.; Dolovich, M.; Chirakal, R.; Valliant J. F. *Journal of Medicinal Chemistry* **2006**, *49*(4), 1466-1474.

54. Jalilian, A. R; Garosi, J; Gholami, E.; Akhlaghi, M.; Saddadi, F.; Bolourinovin, F.; Karimian, A. *Nuclear Medicine Reveiews Central and Eastern Europe* **2007**, *10*(2), 71-75.

55. Awasthi, V.; Gambhir, S.; Sewatkar, A. B. Nuclear Medicine Biology **1994**, *21*(2), 251-254.

56. Kurtaran, A.; Li, S.; Raderer, M.; Leimer, M.; Müller, C.; Pidlich, J.; Neuhold, N.; Hübsch, P.; Angelberger, P.; Scheithauer, W. *Journal of Nuclear Medicine* **1995**, *36*(10), 1875-1881.

57. Schibli, R.; Schwarzbach, R.; Alberto, R.; Ortner, K.; Schmalle, H.; Dumas, C.; Egli, A.; Schubiger. P. A. Bioconjugate Chemistry, **2002**, *13*(4), 750-756.

58. Miessler, G. L.; Tarr, D. A. *Inorganic chemistry;* 3rd ed.; Pearson Education: Upper Saddle River, NJ, **2004**.

59. Alberto, R.; Ortner, K.; Wheatley, N.; Schibli, R.; Schubiger, A. P. *Journal of the American Chemical Society* **2001**, *123*(13), 3135-3136.

60. Alberto, R.; Schibli, R.; Egli, A.; Schubiger, A. P.; Abram, U.; Kaden, T. A. *Journal of the American Chemical Society* **1998**, *120*(31), 7987-7988.

61. Koźmiński, P.; Gniazdowska, E.; Fuks, L.; Kowalska, S. *Applied Radiation and Isotopes* **2011**, *69*(2), 436-442.

62. Herrick, R. S.; Ziegler, C. J.; Çetin, A.; Franklin, B. R. *European Journal of Inorganic Chemistry* **2007**, *2007*(12), 1632-1634.

63. Lazarova, N.; James, S.; Babich, J.; Zubieta, J. *Inorganic Chemistry Communications* **2004**, *7*(9), 1023-1026.

64. Pak, J. K.; Benny, P.; Spingler, B.; Ortner, K.; Alberto, R. *Chemistry - A European Journal* **2003**, *9*(9), 2053-2061.

65. Herrick, R. S. Group 6 and 7 Organometallic Bioconjugates Prepared from Amino Acids, Peptides or Proteins. In: *New Developments in Organometallic Chemistry Research;* Nova Science Publishers, Inc.: New York, **2006**.

66. Alberto, R. Radiopharmaceuticals. In: *Bioorganometallics*; Wiley-VCH: Weinheim **2006**.

67. Herrick, R. S.; Brunker, T. J.; Maus, C.; Crandall, K.; Cetin, A.; Ziegler, C. J. *Chemical Communications*, **2006**, *2006*(41), 4330-4331.

68. He, H.; Morley, J. E.; Twamley, B., Groeneman, R. H.; MacGillivray, L. R.; Benny, P. D. *Inorganic Chemistry* **2009**, *48*(22), 10625-10634.

69. Herrick, R. S.; Ziegler, C. J.; Gambella, A. *European Journal of Inorganic Chemistry* **2010**, *2010*(25), 3905-3908.

70. Costa, R.; Barone, N.; Gorczycka, C.; Powers, E. F.; Cupelo, W.; Lopez, J.; Herrick, R. S.; Ziegler, C. J. *Journal of Organometallic Chemistry* **2009**, *694*(14), 2163-2170.

71. Vitor, R. F.; Correia, I.; Videira, M.; Marques, F.; Paulo, A.; Costa Pessoa, J.; Viola, G.; Martins, G. G.; Santos, I. *ChemBioChem* **2008**, *9*(1), 131-142.

72. Fischman, A. J.; Babich, J. W.; Strauss, H. W. *Journal of Nuclear Medicine* **1993**, *34*(12), 2253-2263.

73. Amann, A.; Decristoforo, C.; Ott, I.; Wenger, M.; Bader, D.; Alberto, R.; Putz, G. *Nuclear Medicine Biology* **2001**, *28*(3), 243-250.

74. Bilio, A. J. D.; Crane, B. R.; Wehbi, W. A.; Kiser, C. N.; Abu-Omar, M.; Carlos, R. M.; Richards, J. H.; Winkler, J. R.; Gray, H. B. *Journal of the American Chemical Society* **2001**, *123*(13), 3181-3182.

75. Binkley, S. L.; Leeper, T. C.; Rowlett, R. S.; Herrick, R. S.; Ziegler, C. J. *Metallomics* **2011**, *3*(9), 909-916.

76. Binkley, S. L.; Ziegler, C. J.; Herrick, R. S.; Rowlett, R. S. *Chemical Communications* **2010**, ***46***(8), 1203-1205.

77. Blanco-Rodríguez, A. M.; Busby, M.; Gradinaru, C.; Crane, B. R.; Bilio, A. J. D.; Matousek, P.; Towrie, M.; Leigh, B. S.; Richards, J. H.; Vlcek, Jr., A; Gray, H. B. *Journal of the American Chemical Society* **2006**, *128*(13), 4365-4370.

78. Blanco-Rodríguez, A. M.; Busby, M.; Ronayne, K.; Towrie, M.; Gradinaru, C.; Sudhamsu, J.; Sýkora, J.; Hof, M.; Zális, S.; Bilio, A. J. D.; Crane, B. R.; Gray, H. B.; Vlcek, Jr., A. *Journal of the American Chemical Society* **2009**, *131*(33),11788-117800.

79. Biechlin, M.; d'Hardemare, A.; du Moulinet, Fraysse, M.; Gilly, F.; Bonmartin, A. *Journal of Labelled Compounds and Radiopharmaceuticals* **2005**, *48*(12), 873-85.

80. Park, S. H.; Jang, B. S.; Park, K. B. *Journal of Labelled Compounds and Radiopharmaceuticals* **2005**, *48*(1), 63-73.

81. Waibel, R.; Stichelberger, R.; Alberto, R.; Schubiger, P. A.; Chester, K. A.; Begent, R. H. J. *European Journal of Nuclear Medicine* **2000**, *2000*, S86.

82. Waibel, R.; Alberto, R.; Willuda, J.; Finnern, R.; Schibli, R.; Stichelberger, A.; Egli, A.; Abram, U.; Mach, J. P.; Plückthun, A.; *Nature Biotechnology* **1999**, *17*(9), 897-901.

83. Jurisson, S.; Berning, D.; Jia, W.; Ma, D. *Chemical Reviews* **1993**, *93*(3), 1137-1156.

84. Djokić, D.; Janković, D. *Journal of Labelled Compounds and Radiopharmaceuticals* **2007**, *50*(3), 155-163.

85. Sladkov, A. M.; Vasneva, N. A.; Johansson, A. A.; Derunov, V. V. *Inorganica Chimica Acta* **1977**, *25*, L100.

86. Schirrmacher, R.; Comagic, S.; Schirrmacher, E.; Rösch, F. *Journal of Labelled Compounds and Radiopharmaceuticals* **2004**, *47*(8), 477-483.

87. Zhang, J.; Vittal, J. J.; Henderson. W.; Wheaton, J. R; Hall, I. H.; Hor, T. S. A.; Yan, Y. K. *Journal of Organometallic Chemistry* **2002**, *650*(1-2), 123-132.

88. Herrick, R. S.; Wrona, I.; McMicken, N.; Jones, G.; Ziegler, C. J.; Shaw, J. *Journal of Organometallic Chemistry* **2004**, *689*(25), 4848-4855.

89. Zobi, F.; Blacque, O.; Schmalle, H. W.; Spingler, B.; Alberto, R. *Inorganic Chemistry* **2004**, *43*(6), 2087-2096.

90. Zobi, F.; Spingler, B.; Alberto, R. *ChemBioChem* **2005**, *6*(8), 1397-1405.

91. Zobi, F.; Spingler, B.; Fox, T.; Alberto, R. *Inorganic Chemistry* **2003**, *42*(9), 2818-2820.

92. Lippard, S. J.; Berg, J. M. *Principles of Bioinorganic Chemistry;* University Science Books: Mill Valley, California, **1994**.

93. Pil, P.; Lippard, S. J. *Science* **1992**, *256*, 234-237.

94. Sullivan, S. T.; Ciccarese, A.; Fanizzi, F. P.; Marzilli, L. G. *Inorganic Chemistry* **2000**, *39*, 836-842.

95. Schoellhorn, H.; Raudaschl-Sieber, G.; Mueller, G.; Thewalt, U.; Lippert, B. *Journal of the American Chemical Society* **1985**, *107*(21), 5932-5937.

96. Egli, A.; Alberto, R.; Tannahill, L.; Schibli, R. *The Journal of Nuclear Medicine* **1999**, *40*(11), 1913.

97. García-Garayoa, E.; Bläuenstein, P.; Bruehlmeier, M.; Blanc, A.; Iterbeke, K.; Conrath, P.; Tourwé, D.; Schubiger, P. A. *Journal of Nuclear Medicine* **2002**, *43*(3), 374-383.

98. Schottelius, M.; Wester, H. *Methods* **2009**, *48*(2), 161-177.

99. Rufini, V.; Calcagni, M. L.; Baum, R. P. *Seminars in Nuclear Medicine* **2006,** *36*(3), 228-247.

100. Du, J.; Hiltunen, J.; Marquez, M.; Nilsson, S.; Holmberg, A. R. *Applied Radiation and Isotopes* **2001**, *55*(2), 181-187.

101. Cantorias, M. V.; Howell, R. C.; Todaro, L.; Cyr, J. E.; Berndorff, D.; Rogers, R. D.; Francesconi, L. C. *Inorganic Chemistry* **2007**, *46*(18), 7326-7340.

102. Cyr, J. E.; Pearson, D. A.; Wilson, D. M.; Nelson, C. A.; Guaraldi, M.; Azure, M. T.; Lister-James, J.; Dinkelborg, L. M.; Dean, R. T. *Journal of Medicinal Chemistry* **2007**, *50*(6), 1354-1364.

103. Menda, Y.; Kahn, D.; *Seminars in Nuclear Medicine* **2002**, *32*(2), 92-96.

104. Bruehlmeier, M.; Garayoa, E. G.; Blanc, A.; Holzer, B.; Gergely, S.; Tourwé, D.; Schubiger, P. A.; Bläuenstein, P. *Nuclear Medicine Biology* **2002**, *29*(3), 321-317.

105. García-Garayoa, E.; Maes, V.; Bläuenstein, P.; Blanc, A.; Hohn, A.; Tourwé, D.; Schubiger, P. A. *Nuclear Medicine Biology* **2006**, *33*(4), 495-503.

106. Buchegger, F.; Bonvin, F.; Kosinski, M.; Schaffland, A. O.; Prior, J.; Reubi, J. C.; Bläuenstein, P.; Tourwé, D.; García-Garayoa, E.; Bischof Delaloye, A. *Journal of Nuclear Medicine* **2003**, *44*(10), 1649-1654.

107. Weiner, R.; Thakur, M. *BioDrugs* **2005**, *19*(3), 145-163.

108. Bella, R. L.; Garcia-Garayoa, E.; Bähler, M.; Bläuenstein, P.; Schibli, R.; Conrath, P.; Tourwé, D.; Schubiger, P. A. *Bioconjugate Chemistry* **2002**, *13*(3), 599-604.

109. La Bella, R.; Garcia-Garayoa, E.; Langer, M.; Bläuenstein, P.; Beck-Sickinger, A.; August Schubiger, P. *Nuclear Medicine Biology* **2002**, *29*(5), 553-560.

110. Lane, S. R.; Veerendra, B.; Rold, T. L.; Sieckman, G. L.; Hoffman, T. J.; Jurisson S. S.; Smith, C. J. *Nuclear Medicine Biology* **2008**, *35*(3), 263-272.

111. Smith, C. J.; Sieckman, G. L.; Owen, N. K.; Hayes, D. L.; Mazuru, D. G.; Kannan, R.; Volkert, W, A.; Hoffman, T. J. *Cancer Research* **2003,** *63*(14), 4082-4088.

112. Alves, S.; Correia, J. D. G.; Santos, I.; Veerendra, B.; Sieckman, G. L.; Hoffman, T. J.; Rold, T. L.; Figueroa, S. D.; Retzloff, L.; McCrate, J. *Nuclear Medicine Biology* **2006**, *33*(5), 625-634.

113. Kostić, N. M. *Comments on Inorganic Chemistry* **1988**, *8*(4):137-162.

114. Miller, J. E.; Di Bilio, A. J.; Wehbi, W. A.; Green, M. T.; Museth, A. K.; Richards, J. R.; Winkler, J. R.; Gray, H. B. *Biochimica Et Biophysica Acta (BBA)/Bioenergetics* **2004**, *1655*, 59-63.

115. Faulkner, S.; Long, N. J. *Dalton Transactions* **2011**, *40*(23), 6067.

116. Murray, A.; Scholfield, D. P.; Schibli, R.; Novak, I.; Waibel, R.; Vincent, R. M.; Perkins, A. C. *Journal of Labelled Compounds and Radiopharmaceuticals*, **2001**, *44*, S573-575.

117. Salmain, M.; Jaouen, G. *Comptes Rendus Chimie* **2003**, *6*(2), 249-258.

118. Tait, J. F.; Smith, C.; Gibson, D. F. *Bioconjugate Chemistry* **2002**, *13*(5), 1119-1123.

119. Shih, C.; Museth, A. K.; Abrahamsson, M.; Blanco-Rodriguez, A. M.; Di Bilio, A. J.; Sudhamsu, J.; Crane, B. R.; Ronayne, K. L.; Towrie, M.; Vlček, Jr., A.; Gray, H. *Science* **2008**, *320*, 1760.

120. Bolliger, Jr., M. J. *Science* **2008**, *320*, ,1760.

121. Abrams, M. J.; Davison, A.; Jones, A. G.; Costello, C. E.; Pang, H. *Inorganic Chemistry* **1983**, *22*(20), 2798-2800.

122. Alberto, R.; Ortner, K.; Wheatley, N.; Schibli, R.; Schubiger, A. P. *Journal of the American Chemical Society* **2001**, *123*(13), 3135-3136.

123. Pietzsch, H.; Gupta, A.; Reisgys, M.; Drews, A.; Seifert, S.; Syhre, R.; Spies, H.; Alberto, R.; Abram, U.; Schubiger, P. A. *Bioconjugate Chemistry* **2000**, *11*(3), 414-424.

124. Maria, L.; Cunha, S.; Videira, M.; Gano, L.; Paulo, A.; Santos, I. C.; Santos, I. *Dalton Transactions* **2007**, *2007*(28), 3010-3019.

125. Alberto, R. *Journal of Organometallic Chemistry* **2007**, *692*(6), 1179-1186.

126. Herrick, R. S.; Ziegler, C. J.; Jameson, D. L.; Aquina, C.; Cetin, A.; Franklin, B. R.; Condon, L. R.; Barone, N.; Lopez, J. *Dalton Transactions* **2008**, *2008*(27), 3605-3609.

127. Franklin, B. R.; Çetin, A.; Barone, N.; Condon, L. R.; Herrick, R. S.; Ziegler, C. J. *Inorganic Chemistry* **2008**, *47*(13), 5902-5909.

128. Banerjee, S.; Ambikalmajan Pillai, M. R.; Ramamoorthy, N. *Seminars in Nuclear Medicine* **2001**, *31*(4), 260-277.

129. Sheldrick, G. M. *SHELXTL, crystallographic software package version 6.10*. Madison, WI, USA: Brunker AXS Inc.; 2000.

130. Ross, R. *The Journal of Cell Biology* **1971**, *50*(1), 172-186.

131. Nobukawa, T.; Sanukida, S. *Water Research* **2001**, *35*(18), 4293-4298.

132. Qiao, Y.; Xia, S.; Ma, P. *Journal of Chemical & Engineering Data* **2007**, *53*(1):280-282.

133. Yunger, L. M.; Cramer, III, R. D. *Molecular Pharmacology* **1981**, *20*, 602-608.

134. Walter, A.; Gutknecht, J. *Journal of Membrane Biology* **1986**, *90*(3), 207-217.

135. Volkert, W. A.; Hoffman, T. J. *Chemical Reviews* **1999**, *99*(9), 2269-2292.

136. Heeg, M. J.; Jurisson, S. S. *Accounts of Chemical Research* **1999**, *32*(12), 1053-1060.

137. Puck, T. T.; Marcus, P. I.; Cieciura, S. J. *Journal of Experimental Medicine* **1956**, *103*(2), 272-283.

138. Neves, L. A. Dissertation. Akron, OH: The University of Akron; 1998. Available from: Ohio Link.

139. Strigul, N.; Koutsospyros, A.; Arienti, P.; Christodoulatos, C.; Dermatas, D.; Braida, W. *Chemosphere* **2005**, *61*(2), 248-258.

140. Zahir, F.; Rizwi, S. J.; Haq, S. K.; Khan, R. H. *Environmental Toxicology Pharmacology* **2005**, *20*(2), 351-360.

141. Sharma, S. K.; Goloubinoff, P.; Christen, P. *Biochemical and Biophysics Research Communications* **2008**, *372*(2), 341-345.

142. Koutsospyros, A.; Braida, W.; Christodoulatos, C.; Dermatas, D.; Strigul, N. *Journal of Hazardous Materials* **2006**, *136*(1), 1-19.

143. Alberto, R.; Egli, A.; Abram, U.; Hegetschweiler, K.; Gramlich, V.; Schubiger, P. A. *Journal of the Chemical Society, Dalton Transactions* **1994**, *1994*(19), 2815-2820.

144. Adams, K. M.; Marzilli, P. A.; Marzilli, L. G. Inorganic Chemistry **2007**, *46*(22), 9172-9181.

145. Zobi, F.; Blacque, O.; Sigel, R. K. O.; Alberto, R. *Inorganic Chemistry* **2007**, *46*(25), 10458-10460.

146. Zobi, F.; Blacque, O.; Schmalle, H. W.; Spingler, B.; Alberto, R. *Inorganic Chemistry* **2004**, *43*(6), 2087-2096.

147. Zobi, F.; Spingler, B.; Fox, T.; Alberto, R. *Inorganic Chemistry* **2003**, *42*(9), 2818-2820.

148. Stephenson, K. A.; Zubieta, J.; Banerjee, S. R.; Levadala, M. K.; Taggart, L.; Ryan, L.; McFarlane, N.; Boreham, D. R.; Maresca, K. P.; Babich, J. W.; Zubieta, J.; Valliant, J. F. *Bioconjugate Chemistry* **2004**, *15*(1), 128-136.

149. Stephenson, K. A.; Banerjee, S. R.; Sogbein, O. O.; Levadala, M. K.; McFarlane, N.; Boreham, D. R.; Maresca, K. P.; Babich, J. W.; Zubieta, J.; Valliant, J. F. *Bioconjugate Chemistry* **2005**, *16*(5), 1189-1195.

150. Agilent. Aglient. Yarnton, England: Agilent Technologies Ltd.; 2010.

151. McCoy, A. J.; Grosse-Kunstleve, R.; Adams, P. D.; Winn, M. D.; Storoni, L. C.; Read, R. J. *Journal of Applied Crystallography* **2007**, *40*(4), 658-674.

152. Murshudov, G. N.; Vagin, A. A.; Dodson, E. J. *Acta Crystallographica Section D: Biological Crystallography* **1997**, *53*, 240.

153. Emsley, P.; Cowtan, K. *Acta Crystallographica Section D* **2004**, *60*(12-1), 2126-2132.

154. Engh, R. A.; Huber, R. *Acta Crystallographica Section A* **1991**, *47*(4), 392-400.

155. Chen, V. B.; Arendall, W. B.; Headd, J. J.; Keedy, D. A.; *Acta Crystallographica Section D* **2010**, *66*(1), 12-21.

156. Jolles, P. *Lysozyme* In: *The Enzymes, Vol.4;* 2nd ed.; Academic Press: New York, **1960**, 431-445.

157. McPherson, A. *Crystallization of Biological Macromolecules*; Cold Spring Harbor Laboratory Press: Cold Spring Harbor, New York, **1999**.

158. Oxford Diffraction. Xcalibur CCD System, CrysAlisPro Software System, Version 1.171.33.48 ed.; Oxford Diffraction Ltd.; **2007**.

159. Casini, A.; Mastrobuoni, G.; Temperini, C.; Gabbiani, C.; Francese, S.; Moneti, G.; Supuran, C. T.; Scozzafava, A.; Messori, L. *Chemical Communications* **2006**, *2007*(2), 156-158.

160. Salmain, M.; Blais, J.; Tran-Huy, H.; Compain, C.; Jaouen, G. *European Journal of Biochemistry* **2001**, *268*(20), 5479-87.

161. Razavet, M.; Artero, V.; Cavazza, C.; Oudart, Y.; Lebrun, C.; Fontecilla-Camps, J.; Fontecave, M. *Chemical Communications* **2007**, *2007*(27), 2805-2807.

162. McNae, I. W.; Fishburne, K.; Habtemariam, A.; Hunter, T. M.; Melchart, M.; Wang, F.; Walkinshaw, M. D.; Sadler, P. J. *Chemical Communications (Cambridge)* **2004**, *2004*(16), 1786-1787.

163. Romao, C. C.; Royo, B. Rhenium compounds. In: *Comprehensive Organometallic Chemistry III; from Fundamentals to Applications*, III ed.; Elsevier: Oxford, **2007**.

164. Coursey, B. M.; Calhoun, J. M.; Cessna, J.; Hoppes, D. D.; Schima, F. J.; Unterweger, M. P.; Golas, A. P.; Callahan, A. P.; Mirzadeh, S.; Knapp, Jr., F. F. *Radioactivity and Radiochemistry* **1990**, *1*(38), 39-42.

165. Fuks, L.; Gniazdowska, E.; Kozminski, P.; Lyczko, M.; Mieczkowski, J.; Narbutt, J. *Applied Radiation and Isotopes* **2010**, *68*(1), 90-95.

166. Hawecker, J.; Lehn, J.; Ziessel, R. *Journal of the Chemical Society, Chemical Communications* **1983**, *1983*(9), 536-538.

167. Hawecker, J.; Lehn, J.; Ziessel, R. *Helvetica Chimica Acta* **1986**, *69*, 1990-2012.

168. Hassell, A. M.; An, G.; Bledsoe, R. K.; Bynum, J. M.; Carter, H. L.; Deng, S. J.; Gampe, R. T.; Grisard, T. E.; Madauss, K. P.; Nolte, R. T.; *et al*. *Acta Crystallographica Section D* **2007**, *63*(1), 72-79.

169. Grundler, P. V.; Helm, L.; Alberto, R.; Merbach, A. E. *Inorganic Chemistry* **2006**, *45*(25), 10378-10390.

170. Grundler, P. V. Salignac, B.; Cayemittes, S.; Alberto, R.; Merbach, A. E. *Inorganic Chemistry* **2004**, *43*(3), 865-873.

171. Salignac, B.; Grundler, P. V.; Cayemittes, S.; Frey, U.; Scopelliti, R.; Merbach, A. E.; Hedinger, R.; Hegetschweiler, K.; Alberto, R.; Prinz, U.; *et al. Inorganic Chemistry,* **2003**, *42*(11), 3516-3526.

172. Meier, U. C.; Scopelliti, R.; Solari, E.; Merbach, A. E. *Inorganic Chemistry,* **2000**, *39*(17), 3816-3822.

173. Bodenhausen, G.; Ruben, D. J. *Chemical Physics Letters* **1980**, *69*(1), 185-189.

174. Delaglio, F.; Grzesiek, S.; Vuister, G. W.; Zhu, G.; Pfeifer, J.; Bax, A. *Journal of Biomolecular NMR* **1995**, *6*(3), 277-293.

175. Salmain, M.; Caro, B.; Le Guen-Robin, F.; Blais, J.; Jaouen, G. *ChemBioChem* **2004**, *5*(1), 99-109.

176. Santos-Silva, T.; Mukhopadhyay, A.; Seixas, J. D.; Bernardes, G. J. L.; Romao, C. C.; Romao, M. J. *Journal of the American Chemical Society* **2011**, *133*(5), 1192-1195.

177. Zobi, F.; Spingler, B. *Inorganic Chemistry* **2012**, *51*(3), 1210-1212.

178. Wang, D.; Lippard, S. J. **2005,** *4*(4), 307-320.

179. Schwalbe, H.; Grimshaw, S. B.; Spencer, A.; Buck, M.; Boyd, J.; Dobson, C. M.; Redfield, C.; Smith, L. J. *Protein Science* **2001**, *10*(4), 677-688.

180. Helm, L. *Coordination Chemistry Reviews* **2008**, *252*(21-22), 2346-2361.

181. Kurz, P.; Probst, B.; Spingler, B.; Alberto, R. *European Journal of Inorganic Chemistry* **2006**, *2006*(15), 2966-2974.

182. Krasilnikova, A. A.; Shestopalov, M. A.; Brylev, K. A.; Kirilova, I. A.; Khripko, O. P.; Zubareva, K. E.; Khripko, Y. I.; Podorognaya, V. T.; Shestopalova, L. V.; Fedorov, V. E.; *et al. Journal of Inorganic Biochemistry* **2015**, *144*, 13-17.

183. Saladin, K. S. *Anatomy and Physiology; the Unity of Form and Function;* McGraw-Hill: Boston, **1998**.

184. Yu, S.; Watson, A. D. *Chemical Reviews* **1999**, *99*(9), 2353-2378.

185. Osborne, E. D.; Sutherland, C. G.; Scholl, A. J.; Rowntree, L. G. *Journal of the American Medical Association* **1923**, *1923*(80), 368.

186. Khan, D. A.; Solensky, R. *Journal of Allergy and Clinical Immunology* **2010**, *125*(2), S126-S137.

187. Seitz, C. S.; Pfeuffer, P.; Raith, P.; Bröcker, E.; Trautmann, A. *European Journal of Radiology* **2009**, *72*(1), 167-71.

188. Barrett, B. J.; Parfrey, P. S. *New England Journal of Medicine* **2006**, *354*(4), 379-386.

189. Feuerlein, S.; Roessl, E.; Proksa, R.; Martens, G.; Klass, O.; Jeltsch, M.; Rasche, V.; Brambs, H.; Hoffmann, M. H. K.; Schlomka, J. *Radiology* **2008**, *249*(3), 1010-1016.

190. Lide, D. R.; editor. *Handbook of Chemistry and Physics*, 72nd ed.;CRC Press: Boston, 1991.

191. Bloem, J. L.; Wondergem, J. *Radiology* **1989** *171*(2), 578-579.

192. Fobbe, F.; Wacker, F.; Wagner, S. *European Radiology* **1996,** *6*(2), 224-229.

193. Kahakachchi, C. L.; Moore, D. A. *Metallomics* **2010**, *2*(7), 490-497.

194. Yu, S.; Droege, M.; Segal, B.; Downey, S.; Sanderson, T.; Fellmann, J.; Watson, A. *Inorganica Chimica Acta* **1997**, *263*(1-2), 61-67.

195. Saltiel, A. R.; Kahn, C. R. *Nature* **2001** *414*, 799-806.

196. DeFronzo, R. A. Netherland Journal of Medicine **1997**, *50*(5), 191-197.

197. Kaaks, R.; Toniolo, P.; Akhmedkhanov, A.; Lukanova, A.; Biessy, C.; Dechaud, H.; Rinaldi, S.; Zeleniuch-Jacquotte, A.; Shore, R. E.; Riboli, E. *Journal of the National Cancer Institute* **2000**, 92(19), 1592-1600.

198. Fackler, M. L.; Malinowski, J. A. *American Journal of Forensic Medicine and Pathology* **1988,** *9*(3), 218-219.

199. Heinrich, M. C.; Häberle, L.; Müller, V.; Bautz, W.; Uder, M. *Radiology* **2009** *250*(1), 68-86.

200. Jürgens, S.; Herrmann, W. A.; Kühn, F. E. Development and recent advances. *Journal of Organometallic Chemistry* **2014**, *751*, 83-89.

201. Leonidova, A.; Gasser, G. *ACS Chemical Biology* **2014**, *9*(10), 2180-2193.

202. Binkley, S. L.; Barone, N. V.; Underwood, A. C.; Milsted, A.; Franklin, B. R.; Herrick, R. S.; Ziegler, C. J. *Journal of Inorganic Biochemistry* **2010**, *104*(6), 632-638.

203. North, A. J.; Hayne, D. J.; Schieber, C.; Price, K.; White, A. R.; Crouch, P. J.; Rigopoulos, A.; O'Keefe, G. J.; Tochon-Danguy, H.; Scott, A. M.; *et al. Inorganic Chemistry* **2015** *54*(19), 9594-9610.

204. Makris, G.; Tseligka, E. D.; Pirmettis, I.; Papadopoulos, M. S.; Vizirianakis, I. S.; Papagiannopoulou, D.; *Molecular Pharmaceutics* **2016,** *05*, 12.

205. Langdon-Jones, Symonds, N. O.; Yates, S. E.; Hayes, A. J.; Lloyd, D.; Williams, R.; Coles, S. J.; Horton, P. N.; Pope, S. J. A. *Inorganic Chemistry* **2014**, *53*(7), 3788-3797.

206. Kydonaki, T. E.; Tsoukas, E.; Mendes, F.; Hatzidimitriou, A. G.; Paulo, A.; Papadopoulou, L. C.; Papagiannopoulou, D.; Psomas, G. *Journal of Inorganic Biochemistry* **2016**, *160*(1), 94-105.

207. Molecular Probes. *LIVE/DEAD® Cell Vitality Assay Kit (L34951) Product Information*; Molecular Probes, Invitrogen Detection Technologies, **2004**.

208. ATCC. *MTT Cell Proliferation Assay Instruction Guide*; ATCC **2016**.

209. Samimi, G.; Kishimoto, S.; Manorek, G.; Breaux, J. K.; Howell, S. B. *Cancer Chemotherapeutics and Pharmacology* **2007**, *59*(3), 301-312.

210. Egger, A. E.; Rappel, C.; Jakupec, M. A.; Hartinger, C. G.; Heffeter, P.; Keppler, B. K. *Journal of Analytical Atomic Spectrometry*, **2009**, 24(1), 51-61.

211. Crane, B. R.; Bilio, A. J. D.; Winkler, J. R.; Gray, H. B. Journal of the American Chemical Society, **2001**, *123*(47), 11623-11631.

212. Warren, J. J.; Ener, M. E.; Vlcek, A.; Winkler, J. R.; Gray, H. B. *Coordination Chemistry Reviews*, **2012**, *256*(21-22), 2478-2487.

213. Santos, M. F. A.; Seixas, J. D.; Coelho, A. C.; Mukhopadhyay, A.; Reis, P. M.; Romao, M. J.; Romao, C. C.; Santos-Silva, T. *Journal of Inorganic Biochemistry* **2012**, *117*, 285-291.

214. Seixas, J. D.; Mukhopadhyay, A.; Santos-Silva, T.; Otterbein, L. E.; Gallo, D. J.; Rodrigues, S. S.; Guerreiro, B. H.; Gonçalves, A. M. L.; Penacho, N.; Marques, A. R. *et al. Dalton Transactions* **2013**, *42*(17), 5985-5998.

215. Can, D.; Spingler, B.; Schmutz, P.; Mendes, F.; Raposinho, P. *Angewandte Chemie International Edition* **2012**, *51*(14), 3354-3357.

216. Lecina, J.; Palacios, Ã.; Atrian, S.; Capdevila, M.; Suades, J.; *Journal of Biological Inorganic Chemistry* **2015**, *20*(3), 465-474.